2018

In search of new rare-earth rich intermetallics

Melissa Rhodehouse
Iowa State University

In search of new rare-earth rich intermetallics

by

Melissa L. Rhodehouse

A dissertation submitted to the graduate faculty

in partial fulfillment of the requirements for the degree of

DOCTOR OF PHILOSOPHY

Major: Inorganic Chemistry

Program of Study Committee:
Gerd H. Meyer, Co-major Professor
Gordon J. Miller, Co-major Professor
Patricia Thiel
Vitalij Pecharsky
Igor Slowing

The student author, whose presentation of the scholarship herein was approved by the program of study committee, is solely responsible for the content of this dissertation. The Graduate College will ensure this dissertation is globally accessible and will not permit alterations after a degree is conferred.

Iowa State University

Ames, Iowa

2018

DEDICATION

This work is dedicated to every person who saw potential in me and supported me in the pursuit of my goals- for my family, for my friends, for the McNair Program, and especially for Trail.

TABLE OF CONTENTS

Page

NOMENCLATURE v

ACKNOWLEDGMENTS vi

ABSTRACT vii

CHAPTER 1. INTRODUCTION 1

CHAPTER 2. EXPERIMENTAL TECHNIQUES 5
Structure analysis 6

CHAPTER 3. FROM THE NON-EXISTENT POLAR INTERMETALLIC Pt_3Pr_4 VIA $Pt_{2-X}Pr_3$ TO NOVEL Pt/Sn/Pr TERNARIES 9
Abstract 9
Introduction 10
Experimental section 12
Results and discussion 14
Conclusions 32
Associated content 39
Acknowledgments 39
References 39

CHAPTER 4. TERNARY POLAR INTERMETALLICS IN THE SYSTEMS Pt/Sn/*R* (*R* = La-Sm): STANNIDES OR PLATINIDES? 45
Abstract 45
Introduction 46
Experimental section 47
Results and discussion 48
Conclusions 59
Associated content 60
Acknowledgments 60
References 60

CHAPTER 5. AN OBSCURED OR NONEXISTENT BINARY INTERMETALLIC, Co_7Pr_{17}, ITS EXISTENT NEIGHBOR Co_2Pr_5, AND TWO NEW TERNARIES IN THE SYSTEM Co/Sn/Pr, $CoSn_3Pr_{1-x}$ AND $Co_{2-x}Sn_7Pr_3$ 63
Abstract 63
Introduction 64
Experimental section 65
Results and discussion 68
Conclusions 81
Associated content 86
Acknowledgments 86
References 86

CHAPTER 6. CONCLUSIONS 92
Conclusion 92
Future work 93

REFERENCES 94

APPENDIX: SUPPLEMENTARY TABLES AND FIGURES 97

NOMENCLATURE

R	Rare earth element
X	Halogen element
Z	Interstitial (Endohedral atom)
E	Main group element
T	Transition metal element
ROX	Rare earth metal oxide halide
R_2O_3	Rare earth metal(III) oxide
CN	Coordination number
f. u.	Formula unit
°C	Degree of Celsius
K	Degree of Kelvin
hr	Hour
μ	Absorption coefficient
SCXRD	Single crystal X-ray diffraction
PXRD	Powder X-ray diffraction
SEM	Scanning electron microscopy
EDS	Energy dispersive X-ray spectroscopy
SQUID	Superconducting Quantum Interference Device

ACKNOWLEDGMENTS

I would first like to thank my major professors, Dr. Gerd Meyer and Dr. Gordon Miller for their endless support and encouragement during my time as a graduate student. I would like to thank my committee members, Dr. Vitalij Pecharsky, Dr. Igor Slowing, and Dr. Patricia Thiel for taking the time to guide me through the course of this research. I would also like to say a special thank you Dr. Anja Mudring who has shared so much scientific knowledge with me with unwavering kindness and enthusiasm.

In addition, I would also like to give a special thank you to Volodymyr Smetana who spent countless hours training me from day one and has pushed me to succeed, not for anyone's benefit but my own.

Finally, I want to thank my friends and family whose love, patience, and humor kept me grounded throughout my years at Iowa State.

ABSTRACT

Our research efforts have focused on the investigation of novel intermetallic compounds containing transition metals with rare earth elements, specifically cobalt and platinum with praseodymium. The Co/Pr and Pt/Pr phase diagrams have been well explored. However, recent work has shown the existence of new binaries within these systems that are not present within the known phase diagrams. The binary Pt_3Pr_4 crystallizes in a new monoclinic structure type with six crystallographically independent Pt positions. Within the Co/Pr system, Co_7Pr_{17} (cubic) was characterized to crystallize in another new structure type consisting of eight and nine coordinated Co atoms. Most recently our investigation of the binary systems, including $Pt_{1.99}Pr_3$ as well as the ternary Pt/Pr/Sn and Co/Pr/Sn systems have yielded several new compounds including new structure types.

Through exploration of the binary Pt/Pr system using NaCl flux, single crystals of $Pt_{1.99}Pr_3$ were obtained. $Pt_{1.99}Pr_3$ adopts the Ga_2Gd_3 structure type where Pt atoms are coordinated by Pr atoms in chains of alternating cubes and square antiprism chains along the *c* axis. The remaining Pr positions form trigonal prisms and distorted tetrahedra around Pt atoms in 1:2 chains. The reported structure found for Pt_2Pr_3 is that of hexagonal Ni_2Ho_3. Subsequent loading of Pt_2Pr_3 in a Sn flux yielded two new ternaries in the Pt/Pr/Sn system: Single crystal analysis identified $Pr_4Pt_{12}Sn_{25}$ and $Pr_3Pt_4Sn_6$. The first is isostructural to $Gd_3Ni_8Sn_{16}$ while the latter is a new ternary in the $RE_3T_4E_6$ family (R = rare earth; T = Pt, Pd; E = Ge, Al, Sn, Si) where Pt and Sn form hexagonal and pentagonal nets.

Further investigation into the $R_3T_4E_6$ family led to the characterization of four new compounds within the family for T = Pt and R = La, Ce, Pr, and Nd. The neodymium compound forms a new high-temperature modification of the parent $R_3T_4E_6$ structure type ($Pr_3Pt_4Ge_6$)

where Pt atoms are seven coordinate in polyhedra that share edges and vertices. This new $R_3Pt_4Sn_6$ structure type is also orthorhombic with a slightly smaller volume, approximately 3%. Interestingly, $Pr_3Pt_4Sn_6$ forms both modifications as well, while La and Ce do not exhibit the high temperature modification.

Single crystal X-ray diffraction analysis of Co/Pr samples containing Sn as a flux revealed $CoSn_3Pr_{1-x}$ (x = 0.04) and $Co_{2-x}Sn_7Pr_3$ (x = 0.78), adding two new ternaries to the Co-Sn-Pr system. In the first, trigonal prisms of Sn around the Co atoms form vertex-sharing networks. The latter structure contains Co atoms surrounded by square prisms of Sn connected to $\{PrSn_{12}\}$ cuboctahedra to form slabs.

CHAPTER 1. INTRODUCTION

Metal-rich halides has been were first discovered in the 1960s by Corbett's group, beginning with the discovery of gadolinium sesquichloride, Gd_2Cl_3.[1] This structure contains gadolinium octahedra, $\{Gd_6\}$, connected via common *trans*-edges to infinite chains, $\{Gd_{4/2}Gd_{2/1}\}$, surrounded by halide ligands in the $\{Gd_6\}Cl_8$ fashion.[3,4]

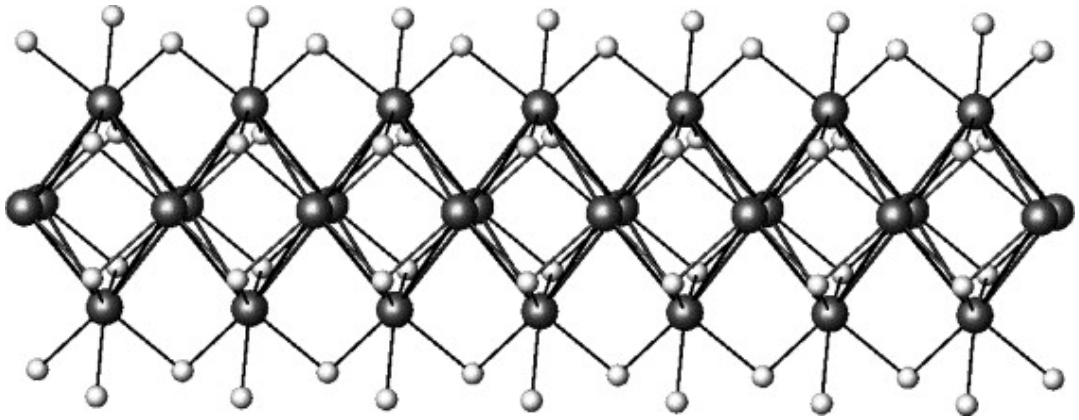

Figure 1. Side chain of Gd_2Cl_3 where black atoms are Gd. From Corbett, J.D. 2006.[2]

The many cluster complex halides that have since been synthesized differ from Gd_2Cl_3 in that either non- or semi-metal, *E*, or metal atom , *T*, occupy the octahedral, known as an interstitial atom, *Z*, which allows for phase stabilization. [5-7]

Cluster complex halides, $\{Z_zR_r\}X_x$ type,(*R* = rare-earth element; *X* = halide) are known with *z*, i.e. the coordination number (CN) of the endohedral atom ranging from 3-6 for smaller atoms like *E* = B, C, N, O and 6-8 for larger atoms like *T* = Os (and many other transition metal atoms).[6] Oligomers, chains, double chains, layers and finally three-dimensional structures form from condensation of clusters by face and edge sharing ultimately 'kicking off' the halide atoms and forming polar intermetallics. [5-7]

During the investigation of cluster complex halides with platinum as the endohedral atom, the Pt/Pr/*X* systems (*X* = Cl, Br, I) were studied. At the time no cluster complex chloride with Pt and Pr were know, however $\{PtPr_6\}I_{12}Pr$[8] and $\{PtPr_3\}I_3$[9] and, $\{PtPr_3\}Br_3$,[10] were reported. As the electronegativity of the halide increases cluster complex halide and intermetallic and salt compete to form. The intermetallic $\{Pt_3Pr_4\}$ was obtained. The most recent phase diagram[11] (1990) does not contain the Pt_3Pr_4 phase but reports seven binary Pt/Pr phases including Pt_3Pr_7, Pt_2Pr_3 (incongruently melting at 1340°C), PtPr (congruently melting out of a high-temperature modification at 1800°C), and the platinum-rich phases Pt_2Pr and Pt_5Pr.[6]

There is potential for many types of fluxes as observed when Pt_3Pr_4 formed from a melt of Pr, Pt, and $PrCl_3$, the last apparently working as the flux. In the last decade, much research has focused on flux synthesis methods as a means to lower reaction temperatures.[12] In the case of cobalt and platinum rare-earth binaries reaction temperatures in excess of 1500°C are required. Typical flux syntheses involve the addition of low melting metals, often tin or a salt (e.g. NaCl).

Use of NaCl and tin fluxes resulted in the formation of a new modification of Pt_2Pr_3 and a series of ternary Pt/Sn/Pr intermetallics. A reactive tin flux formed three new phases within the ternary Pt/Sn/Pr system, $Pt_4Sn_6Pr_3$, $Pt_4Sn_6Pr_{2.91}$, $Pt_{12}Sn_{24}Pr_{4.84}$, in which only one ternary phase has been reported, PtSnPr with the SiTiNi type of structure.[14] The first two are members of a the family $T_4E_6R_3$ (*T* = transition metal; *E* = p-block main group metal or metalloid; *R* = rare earth metal) with now seven known structure types: monoclinic $Pt_4Ge_6Y_3$ ($P2_1/m$)[14] and the disordered variant $Pt_4Yb_3Si_{5.7}$ ($P2_1/m$)[16] as well as five orthorhombic structures, slightly disordered $Pt_4Ge_6Ce_3$ (*Cmcm*),[17] $Pt_4Ge_6Pr_3$ (*Pnma*, *R* = Pr–Dy),[18] $Pd_4Sn_6Ce_3$ (*Pnma*, R = La-Pr),[19] $Pt_4Al_6Ce_3$ (*Pnma*)[20], and $Pt_4Sn_6Pr_{3-x}$ (*Pnma*, R = Pr).[13] These structures are made up of stacked pentagonal and hexagonal nets of mixed Sn and Pt atoms encapsulating the *R* atoms.

The newly synthesized series $Pt_4Sn_6R_3$, R = La–Nd crystallize in the $Pt_4Ge_6R_3$ type of structure (R = Pr–Dy) with Pr and Nd compounds forming a high temperature modification with reduced rare-earth content and clear structural differences.

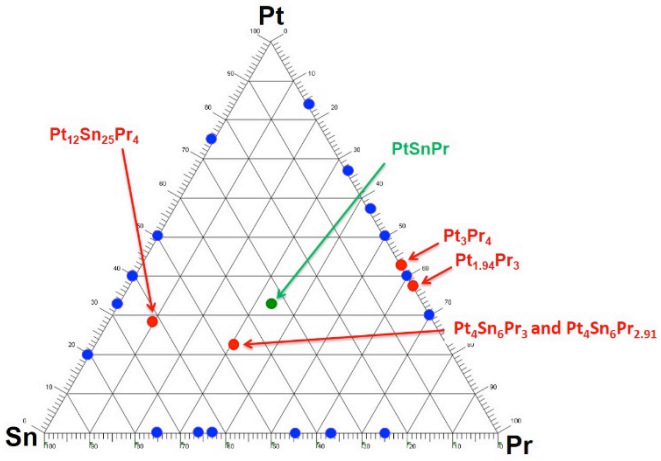

Figure 2. Ternary composition diagram of the system Pt/Sn/Pr

Another intermetallic was obtained as a minor phase from a melt of $PrBr_3$:Pr:Co = 1:2:1 molar mixture. Nine intermetallics are reported for this system: $CoPr_3$ (25 mol% Co), Co_2Pr_5 (28.6), $Co_{1.7}Pr_2$ (45.9), Co_2Pr (66.7), Co_3Pr (75), Co_7Pr_2 (77.8), $Co_{19}Pr_5$ (79.2), Co_5Pr (83.3), and $Co_{17}Pr_2$ (89.5).[21] The new Co_7Pr_{17} binary Co/Pr intermetallic is thought to be either nonexistent in thermodynamic equilibrium,[22,23] or obscured in the phase diagram as it is very close in composition to Co_2Pr_5 (28.6 mol% Co). Fluxes of NaCl and metallic Sn were also investigated for this system resulting in two new ternary Co/Sn/Pr intermetallics, $CoSn_3Pr_{1-x}$ (x = 0.044), $Co_{2-x}Sn_7Pr_3$ (x = 0.782).

$CoSn_3Pr_{1-x}$ (x = 0.04) crystallizes in the $RuSn_3La$ type exhibiting trigonal-prismatic {$CoSn_6$} clusters and {$Pr1Sn_{12}$} icosahedra while square pyramidal {$CoSn_5$} clusters and {$PrSn_{12}$} cuboctahedra highlight the crystal structure of $Co_{2-x}Sn_7Pr_3$ ($Ni_{2-x}Sn_{7-y}Ce_3$ type). This dissertation focuses on the investigation of these structures within the Co or Pt and Pr binary and

Co or Pt with Pr and Sn ternary systems using a variety of fluxes as well as arc melting synthesis techniques.

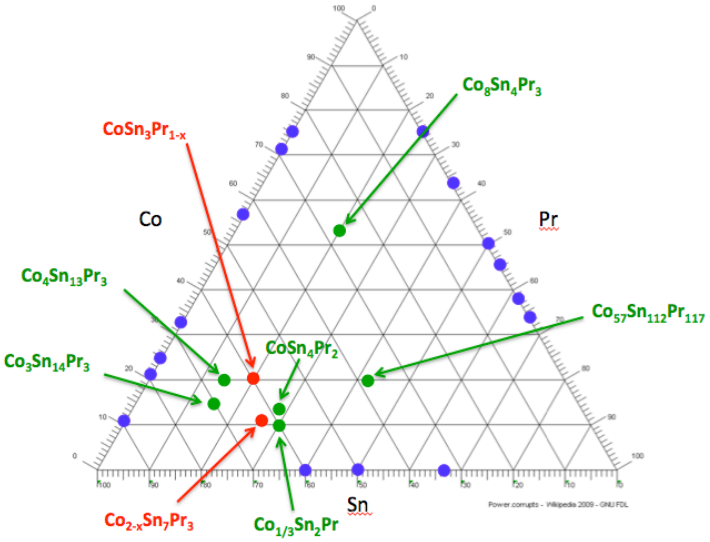

Figure 3. Ternary composition diagram of the Co/Sn/Pr system. Six compounds are reported in this system: $Co_8Sn_4Pr_3$ = $CoSn_{0.5}Pr_{0.375}$,[24] $Co_{57}Sn_{112}Pr_{117}$ = $CoSn_{1.96}Pr_{2.05}$,[25,26] $Co_4Sn_{13}Pr_3$ = $CoSn_{3.25}Pr_{0.75}$,[27] $CoSn_4Pr_2$,[28] $Co_3Sn_{14}Pr_3$ = $CoSn_{4.67}Pr$,[29] and $Co_{0.33}Sn_2Pr$ = $CoSn_6Pr_3$.[30]

CHAPTER 2. EXPERIMENTAL TECHNIQUES

Synthesis

Starting materials of rare earth metals, transition metals (Pt, 99.9%; Co, 99.9%) and Sn (99.9%), were provided by Materials Preparation Center, U.S. DOE Ames Laboratory and stored in an argon-filled glovebox (MBraun Labmaster dp) Sample materials were weighed within ±0.0005g inside a glovebox where they were then placed inside tantalum ampules or transported to another glovebox for arc melting. Samples ranged from 250mg-500mg. Due to the high melting points of the elements (822°C-1772°C), $PrCl_3$, NaCl, or Sn was used as a flux. Tantalum ampules were then evacuated and welded closed under argon. Ampules were then enclosed inside of evacuated fused silica tubes [Figure 4].

Figure 4. Tantalum ampule sealed in fused silica, left. Arc melted samples, right.

The rare earth metal halide, $PrCl_3$, was synthesized via the ammonium-halide route for use as a starting material.[31] The following reaction equation describes the synthesis of $PrCl_3$.

$$Pr_2O_3 + 6\ HCl + 6\ NH_4Cl \rightarrow 2\ (NH_4)_3PrCl_6 + 3\ H_2O$$

$$2\ (NH_4)_3PrCl_6 \rightarrow 6\ NH_4Cl + 2\ PrCl_3$$

Concentrated HCl was added to stoichiometric ratios of the rare earth metal oxide Pr_2O_3. The water was evaporated off and the ammonium halide was decomposed using special

decomposition equipment [Figure 5] by heating to 250°C quickly then to 350°C at a rate of 10°C/hr where it was held for 8 hours. The final product was confirmed by PXRD.

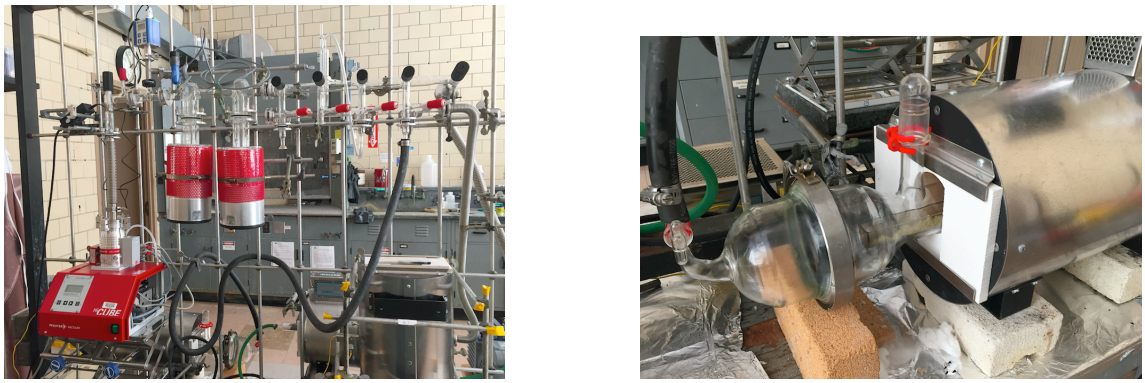

Figure 5. Schlenk line, left. Decomposition apparatus in furnace, right.

Alternatively, arc welding was used to melt samples. Weighed samples were placed on a copper hearth cleaned with diluted nitric acid and ethanol then arc melted with a tantalum electrode [FIGURE 6]. Melted beads were turned and re-melted three times to ensure homogeneity. Arc melted samples were wrapped in tantalum foil then sealed in evacuated fused silica before heating.

Heating treatments varied depending on the elements and flux used, and are detailed within the chapters. A typical heat treatment included placing the sealed sample in the tube furnace [FIGURE 6] (Mellen) with a programmer (Eurotherm) set to raise the temperature 500°C/hr until a temperature above the melting point of the lowest melting element. Temperature was held for 3-72 hours followed by either a quench or slow cooling at a rate of 10°C/hr to an annealing temperature.

Structure analysis

Samples were crushed and a portion ground for powder X-ray diffraction (PXRD) analysis (STOE STADI P diffractometer (STOE image plate, Cu $K_{\alpha 1}$; $\lambda = 1.54059$ Å))[32] or a Guinier X-ray camera detector (graphite monochromated Cu $K_{\alpha 1}$ radiation; Si as an internal

standard, a = 5.4308(1) Å))[33]. [FIGURE 4] Powder was placed on greased Mylar© sheets set between Al rings. For air sensitive samples an airtight sample holder was used. Data were analyzed using the WinXPow 3.0625 and LAZY PULVERIX software packages. Sample compositions were confirmed by scanning electron microscopy (SEM) equipped with electron microprobe (Energy Dispersive X-ray analysis, EDS). A Leica Cambridge 360 microscope, equipped with an Oxford X-Max 20 analyzer, was used with Oxford Aztec software, utilizing an extra high tension voltage of 20.0 kV and probe current 220 pA. EDS analyses were performed on at least three areas to (counting time of 60 sec) approximate atomic percentages for comparison and corroboration with single crystal refinement data.

Figure 6. Mellen tube furnace with Eurotherm temperature control, left, and arc welder, right.

Single crystals were selected from crushed bulk samples and affixed to glass fibers with grease. Crystals were tested at room temperature on either a Bruker APEX CCD diffractometer [FIGURE 7] or a 6 Bruker D8 VENTURE diffractometer (both with Mo K_α radiation; λ = 0.71073 Å) utilizing the APEX 2 and APEX 3 software suites, respectively, for data collection, integration, polarization, and empirical absorption correction.[34,35] Scans typically covered the 2θ range of ~5-63°. Structure refinement of atomic position, mixed side occupancy, and anisotropic displacement parameters was carried out with SHELXTL.[36]

Figure 7. Bruker APEX CCD diffractometer, left, and STOE STADI P diffractometer, right.

Physical Property Measurements

Phase-pure samples where tested for magnetic transitions. DC magnetic data was collected using a Quantum Design MPMS (Magnetic Property Measurement System) SQUID (Superconducting Quantum Interference Device) magnetometer. Approximately 20mg of powder was placed in a gas-tight fused silica sample holder, place inside the system and first tested in a DC field of 1 kOe over a temperature range of 2-250 or 300 K in order to determine critical temperature locations.

CHAPTER 3. FROM THE NON-EXISTENT POLAR INTERMETALLIC Pt_3Pr_4 VIA $Pt_{2-x}Pr_3$ TO NOVEL Pt/Sn/Pr TERNARIES

Melissa L. Rhodehouse,[†,‡] Thomas Bell,[§] Volodymyr Smetana,[‡,∥] Anja-Verena Mudring,[‡,∥,⊥] and Gerd H. Meyer,[*,†,‡,§]

[†]Department of Chemistry, Iowa State University, Ames, IA, 50011, USA
[‡]Ames Laboratory, USDOE, Iowa State University, Ames, IA 50011, USA
[§]Department of Chemistry, Universität zu Köln, Greinstraße 6, 50939 Köln, Germany
[∥]Department of Materials and Environmental Chemistry, Stockholm University, Svante Arrhenius väg 16 C, 10691 Stockholm, Sweden
[⊥]Department of Materials Science and Engineering, Iowa State University, Ames, IA 50011, USA

Abstract

Although the Pt–Pr phase diagram has been explored well, recent work on rare-earth metal cluster halides with endohedral transition metal atoms has provided a new binary intermetallic that is non-existent in the known phase diagram: The binary Pt_3Pr_4 (**1**) crystallizes in a new structure type (*mP*56, $P2_1/c$, a = 12.353(2) Å, b = 7.4837(9) Å, c = 17.279(2) Å, β = 118.003(7)°, Z = 8) with six crystallographically independent Pt as well as eight Pr positions. The subsequent detailed investigation has led to another previously unreported, binary phase with the Ga_2Gd_3 structure type, $Pt_{2-x}Pr_3$ (**2**, *tI*80, *I*4/*mcm*, a = 11.931(9) Å, c = 14.45(1) Å, Z = 16) that is practically overlapping with the rhombohedral Pt_2Pr_3 existing in the phase diagram. Application of different tin containing fluxes to reproduce the newly detected phases brought about two almost iso-compositional ternary compounds with Sn, $Pt_4Sn_6Pr_{2.91}$ (**3**) and $Pt_4Sn_6Pr_3$ (**4**), as well as $Pt_{12}Sn_{24}Pr_{4.84}$ (**5**). (**3**) is a representative of the $Pt_4Ge_6Ce_3$ type (*oP*52, *Pnma*, a = 7.2863(3) Å, b = 4.4909(2) Å, c = 35.114(2) Å) while (**4**) represents a new variant of the prolific $T_4E_6R_3$ family (T = transition metal, E = main group (semi-)metal, R = rare earth metal; $Pt_4Sn_6Pr_3$: *oP*52, *Pnma*, a = 27.623(1) Å, b = 4.5958(2) Å, c = 9.3499(5) Å). $Pt_{12}Sn_{24}Pr_{5-x}$ (**5**) crystallizes as a variant of the $Ni_8Sn_{16}Gd_3$ type (*cI*82, *Im*-3, a = 12.274(1) Å, Z = 2). Electronic

structure calculations provide hints on the origin of the structural changes (*pseudo*-polymorphism) for Pt_xPr_3 with $x = 1.97$ and 2.00, respectively) and reveal that heteroatomic Pt–Pr bonding strongly dominates in both binaries while the addition of the reactive metal tin leads to dominating Pt-Sn bonding interactions in the ternaries; Pt–Pt bonding interactions are strong but represent a minority in the binaries and are not present at all in the ternaries.

Figure A. The discovery of the non-existent intermetallic Pt_3Pr_4 from a $PrCl_3$ melt inspired a search for lower-temperature routes for binary and ternary intermetallics. $Pt_{1.97}Pr_4$ was obtained

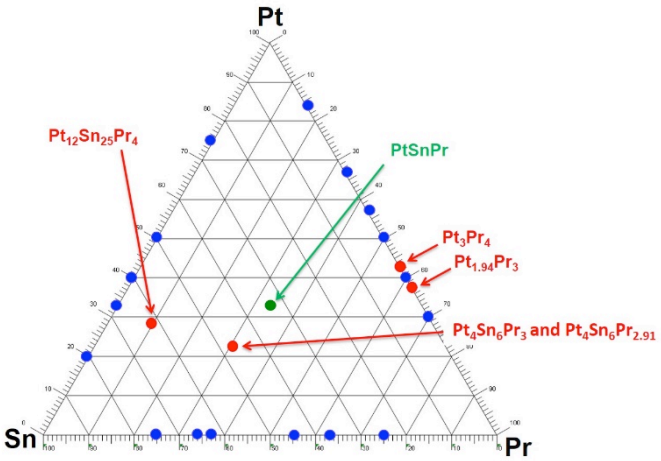

from a NaCl melt. A tin flux yielded three new Pt/Sn/Pr phases in the otherwise, except for PtSnPr, empty ternary phase field. The reactive tin flux substitutes the pure $\{PtPr_x\}$ clusters in the binaries by $\{PtSn_yPr_x\}$ clusters, all of which are connected to three-dimensional structures.

Introduction

A plethora of metal-rich halides has been synthesized and characterized in the aftermath of the first discovery of gadolinium sesquichloride, Gd_2Cl_3, in the 1960s.[1] Its crystal structure is made up of gadolinium octahedra, $\{Gd_6\}$ clusters, connected via common *trans*-edges to infinite chains, $\{Gd_{4/2}Gd_{2/1}\}$, surrounded by halide ligands in the $\{Gd_6\}Cl_8$ fashion.[2,3] To the best of our knowledge, the $\{Gd_6\}$ octahedra are empty, in contrast to almost all the other known cluster complex halides.[4-6] These afford an endohedral (interstitial) atom *Z*, either non- or semi-metal (*Z* = *E*) or metal atom (most importantly transition metal atom, *Z* = *T*) for heteroatom *Z*–*R* bonding

which is critical for phase stabilization. So far, $\{Z_zR_r\}X_x$ type compounds (R = rare-earth element; X = halide) are known with r, i.e. the coordination number (CN) of the endohedral atom, ranging from 3 to 8. Smaller atoms like E = B, C, N, O afford smaller CN's (3−6), while larger atoms like T = Os (and many other transition metal atoms) demand CNs of 6 to 8.[5]

Bonding in these cluster complex halides $\{Z_zR_r\}X_x$ is predominantly a symbiosis of polar, heteroatomic Z─R (intermetallic-like, multi-center covalent) and R─X (salt-like, ionic) character. Increasing cluster condensation pushes isolated clusters into oligomers, chains, double chains, then layers and, finally, three-dimensional structures.[4-6] Ultimate cluster condensation, at which end all the halide ligands are eliminated, constitutes polar intermetallics. Viewing at transition-metal (T)/rare-earth metal (R) intermetallics alone, the T atoms always have higher electron affinities (or electronegativities) than the R atoms, especially when it comes to the heavier 5*d* metals as from Os through Au.

In the pursuit of complementing our knowledge of cluster complex halides with platinum as the endohedral atom, we have also investigated the Pt/Pr/X systems (X = Cl, Br, I). Hitherto, there were only the iodides $\{PtPr_6\}I_{12}Pr$[7] and $\{PtPr_3\}I_3$[8] as well as the corresponding bromide, $\{PtPr_3\}Br_3$,[9] known, no cluster complex chloride with Pt and Pr. When the electronegativity of the halide increases, there is an increasing competition of cluster complex halide *versus* intermetallic and salt. When $\{PtPr_3\}Cl_3$ was targeted, the intermetallic $\{Pt_3Pr_4\}$ as well as remaining $PrCl_3$ was obtained, the latter apparently working as a flux for crystal growth. Although the system Pt/Pr seems to have been investigated thoroughly,[10] the new Pt_3Pr_4 does not exist in the phase diagram. Last modified in 1990, it presents seven binary Pt/Pr phases, Pt_3Pr_7, Pt_2Pr_3 (incongruently melting at 1340°C), PtPr (congruently melting out of a high-temperature modification at 1800°C), and the platinum-rich phases Pt_2Pr and Pt_5Pr.[5]

Other fluxes, such as sodium chloride instead of $PrCl_3$ or tin melts, resulted in the formation of what might be considered as a new modification of Pt_2Pr_3 and a number of ternary Pt/Sn/Pr intermetallics.

Experimental section

Synthesis. Starting materials were Pt beads (99.9%), Pr and Sn pieces (99.9%), and NaCl (99.9% purity). NaCl was dried in an oven at 80˚C overnight before placing inside an argon-filled glovebox. All samples, between 250-500 mg, were weighed and loaded into tantalum ampules inside an argon-filled glovebox. Pt/Pr binary samples were loaded with either NaCl or Sn (approx. 250 mg) as a flux. The NaCl excess could be removed with water. Ampules were sealed under argon with an He arc, followed by sealing in evacuated silica tubes with the aid of an H_2/O_2 torch. Samples were placed in a furnace at 1000˚C for 24 hours followed by slow cooling (-20˚C·hr^{-1}) to 850˚C or 700˚C for NaCl and Sn flux samples, respectively, and annealed for 72 hours.

Pt_3Pr_4 (1) single crystals were grown from a melt of Pt, Pr, and $PrCl_3$ in a 1:3:3 ratio. $PrCl_3$ was synthesized via the ammonium chloride route from the respective oxide.[11,12] The reactants were sealed in Ta ampules as described above, then heated to 1050˚C at a rate of 80˚C·hr^{-1} and held there for one week. The sample was cooled at a rate of -1˚C·hr^{-1} until 500˚C, followed by a rate of -10 ˚C·hr^{-1} until room temperature was reached.

$Pt_{1.97–1.99}Pr_3$ (2). The starting composition of Pt_3Pr_4 was weighed and loaded according to the above indicated method with NaCl as a flux. The resulting product was identified via powder X-ray diffraction to be multiphase containing also PtPr or Pt_3Pr_7. Small crystals of $Pt_{1.97}Pr_3$ were selected and characterized from the same sample. Additional crystals of $Pt_{1.99}Pr_3$ were detected in arc-melted samples of the same starting composition, Pt_3Pr_4. For comparison purposes, Pt_2Pr_3

was loaded into a tantalum ampule with a NaCl flux. The sample was sealed and heated according to the same scheme.

$Pt_4Sn_6Pr_{3-x}$ (3, 4), **$Pt_{12}Sn_{25}Pr_4$ (5).** A variety of stoichiometric loadings of Pt and Pr with Sn as a flux (150 mg) and NaCl (250 mg) as well, were weighed and placed inside tantalum tubes. Samples were sealed under the same conditions and placed in a tube furnace following the heating profile described above. (**3**) has been detected in the samples annealed at higher temperatures.

Structure analysis. Powder and single crystal X-ray diffraction were used to characterize products. Samples were crushed in air (as it was detected that even the ternaries are resistant to oxidation or hydrolysis in laboratory environment for extended periods) and a portion of the sample ground to a fine powder for phase analysis. Powders were sandwiched between greased Mylar sheets housed by an aluminum holder. Data was gathered on a STOE STADI P image plate diffractometer (Cu-Kα1 radiation, λ = 1.54178 Å; Si external standard, a = 5.4308(1) Å) and analyzed using WinXPow software.[13] Single crystal X-ray diffraction was performed on a Bruker APEX CCD and Bruker VENTURE diffractometer (both Mo-Kα radiation, λ = 0.71073 Å). The raw frame data were collected using the Bruker APEX3 program,[14] while the frames were integrated with the Bruker SAINT[15] software package using a narrow-frame algorithm integration of the data and were corrected for absorption effects using the multi-scan method (SADABS).[16] Initial models of the crystal structures were first obtained with the program SHELXT-2014[17] and refined using the program SHELXL-2014[18] within the APEX3 software package. All positions were refined anisotropically. Refinement details and structural parameters can be found in Tables 1–4.

Electronic structure calculations. DFT-based electronic structure calculations for Pt_3Pr_4, slightly idealized tetragonal Pt_2Pr_3 (with the fully occupied Pt4 site) and $Pt_4Sn_6Pr_3$ were accomplished according to the linear muffin–tin–orbital (LMTO) method in the atomic sphere approximation (ASA).[19,20] The Wigner–Seitz radii were automatically generated and empty spheres were included for better approximation of full potentials. Basis sets of Pr 6s, (6p), 5d and Pt 6s, 6p, 5d, (4f) and Sn 5s, 5p, (5d), (4f) were employed. 6p orbitals of Pr and 4f orbitals of Pt were downfolded as well as 5d and 4f orbitals of Sn.[21] Chemical bonding analysis was performed based on the crystal orbital Hamilton populations (COHP).[22] Total energy values for both modifications of Pt_2Pr_3 were obtained after full structural optimizations in non-magnetic regime using the projector-augmented wave method[23] and PBE–GGA potentials[24] in the VASP package.[25-29] Full structural optimizations (cell volume, shape and atomic coordinates) have been performed for both models with the convergence criteria 1 μeV. 8 × 8 × 8 *k*-point mesh was used to sample the first Brillouin zones for reciprocal space integrations with 500 eV energy cutoff.

Results and discussion

Two new praseodymium rich binary platinides, Pt_3Pr_4 (**1**, 42.9 mol% Pt) and $Pt_{1.97}Pr_3$ (**2**, 39.6 mol% Pt), have been observed during the exploration of rare-earth metal cluster complex halides with an endohedral transition metal atom and a subsequent more detailed analysis of the praseodymium rich side of the Pt/Pr system. Both compounds appear to have limited stability and can be obtained as minor products, so far only using flux methods, from excess $PrCl_3$ and NaCl melts, respectively. In an attempt to reproduce Pt_3Pr_4, stoichiometric loadings of the target compound were reacted, resulting, except for crystals of the neighboring phases PtPr and Pt_3Pr_7, in single crystals of a minor phase, $Pt_{1.97}Pr_3$. The stoichiometric Pt_2Pr_3, known since the 1970s,[30] has not been observed under these conditions at the investigated temperatures, suggesting

different stability ranges for both "polymorphs". Although the new phase exhibits a minor homogeneity range, no crystal has yet been detected with all Pt positions fully occupied.

Subsequent loading of Pt_2Pr_3 in a tin flux yielded three new ternaries in the Pt/Sn/Pr system. Single crystal X-ray diffraction analysis identified $Pt_{12}Sn_{25}Pr_4$ (**5**) and $Pt_4Sn_6Pr_3$ (**4**) with 29.2 and 30.8 mol% Pt, respectively. These are new representatives of the $Ni_8Sn_{16}Gd_3$ (= $Ni_{12}Sn_{24}Gd_{4.5}$) structure type[31] and of the $T_4E_6R_3$ family (T = Pt, Pd; R = rare earth element; E = Ge, Al, Sn, Si),[32-37] respectively. Throughout this family, which contains six known structure types, the transition and main group metal/metalloids exhibit complex polyanionic T-E nets around the R atoms forming tunnels along various directions.

Stoichiometric loadings of $Pt_4Sn_6Pr_3$ (**4**) with and without NaCl flux resulted in two different products, one isostructural with $Pt_4Ge_6Pr_3$, the other, $Pt_4Sn_6Pr_{2.91}$ (**3**) with a new structure type. It appears as if $Pt_4Sn_6Pr_{2.91}$ were a somewhat disordered high-temperature modification of $Pt_4Ge_6Pr_3$.

Crystal Structures. $Pt_{1.97}Pr_3$ (**2**, *tI*80, *I*4/*mcm*, a = 11.9444(7) Å, c = 14.488(1) Å) belongs to the Ga_2Gd_3 structure type[38] and is its first representative without a main group element. There are four crystallographically independent Pt positions in the structure of $Pt_{1.97}Pr_3$, as well as three Pr positions. The crystal structure is best described in terms of columns built of {Pt1Pr$_8$} clusters, i.e. square antiprisms with an endohedral Pt atom, and {Pt4Pr$_8$} clusters which come along as square prisms sharing faces along the c axis (Figure 1). While columns of square antiprisms (SAP) and square prisms (SP, almost cubes) are observed in cluster complex halides such as $\{OsSc_4\}Cl_4$[39] and in the structurally related telluride $\{SiTa_4\}Te_4$[40] (only SAP) as well as in $\{Ir_3Sc_{12}\}Br_{16}$ (ratio SAP:SP = 2:1) and $\{Os_5Lu_{20}\}I_{24}$[41] (SAP:SP = 4:1), a ratio of SAP:SP = 1:1 as in $Pt_{1.97}Pr_3$ is so far only known from polar intermetallics, i.e., Ga_2Gd_3 type. The space in

between the $PtPr_{8/2}$ columns is filled by $\{Pt2Pr_6\}$ trigonal prisms (equatorially capped by three additional Pr atoms in the second coordination sphere) and more complex $\{Pt3Pr_8\}$ clusters with the shape of strongly distorted tetragonal antiprisms or bicapped trigonal prisms (Figure 1a). The latter share tetragonal faces with identical units forming bicentric clusters.

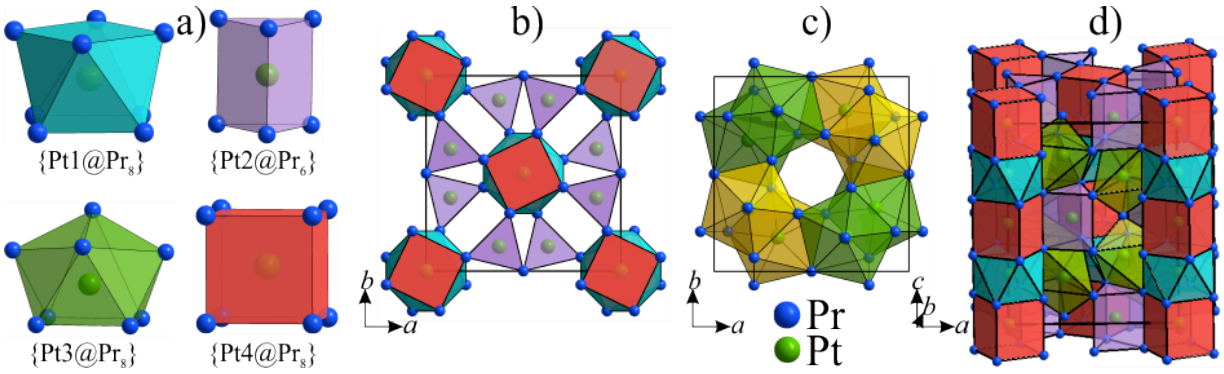

Figure 1. Coordination polyhedra and polyhedral packing in the crystal structure of $Pt_{1.97}Pr_3$.

In $Pt_{1.97}Pr_3$, the Pt atoms correspond to the positions of the Ga atoms in the prototype Ga_2Gd_3 while Pr occupies the positions of Gd. However, despite containing only two elements, this compound exhibits one distinct Pt position (Pt4) which is under-occupied to only 89%, which brings the structure closer to that of $InPt_7Ce_{12}$,[42] with a fully occupied In position. Interestingly, the under-occupied Pt4 position centers the largest void. Although rather unusual, the partial occupation of that Pt position is indirectly indicated by slightly elongated thermal ellipsoids of the Pr3 atoms surrounding it. Pt4−Pr3 contacts, at 3.286(1) Å, are on the upper edge of the Pt−Pr bonding range in the structure and are even longer than the sum of their atomic radii (1.35 + 1.85 = 3.20 Å). Such longer contacts for the current position are rather typical throughout this structure type and are followed by the largest thermal ellipsoid for the 4*c* position (Pt4 in $Pt_{1.97}Pr_3$), while its partial occupation has never been observed before. Of course, one could argue that the under-occupied position according to $Pt_{0.89}Pt_7Pr_{12}$ would rather be fully occupied

by a lighter and larger atom, for example an indium atom. However, indium metal was never near the experimental procedures and could not be detected by elemental analysis.

Pt_3Pr_4 (**1**, *mP*56, $P2_1/c$, a = 12.353(2) Å, b = 7.4837(9) Å, c = 17.279(2) Å, β = 118.003(7) °) crystallizes with the monoclinic crystal system in its own structure type (Figure 2). The entire structure can be described based on one polyhedron type, $\{PtPr_8\}$ clusters, with different degrees of distortion (Figure 2a). This cluster type includes six slightly different modifications of a tetragonal antiprism where one of the faces is not entirely planar or, alternatively, a bicapped trigonal prism similar to $\{Pt3Pr_8\}$ in $Pt_{1.97}Pr_3$ (above). Furthermore, due to significant distortions, the Pt5 and Pt6 coordination environments can more accurately be described as $\{PtPr_{7+1}\}$, as some of the Pr positions are situated slightly beyond the first coordination sphere. All Pt positions in the structure are at pairwise interatomic distances (2.871−3.030 Å) meaning that $\{PtPr_8\}$ polyhedra share square faces to form dimers, $\{Pt_2Pr_{12}\}$ (Figure 2b). These then share vertices, edges and faces with multiple similar neighboring units preventing clear separation of larger structural motifs and constructing a three-dimensional structure (Figure 2c).

It is worth noting that the same, although higher symmetric $\{Pt_2Pr_{12}\}$ cluster is the exclusive building unit in the crystal structure of the rhombohedral Pt_2Pr_3, the phase reported in the phase diagram.[5] However, the building principles are different due to the higher Pr proportion. Even though the polyhedral packing is efficient, tetrahedral voids are present in the crystal structures of Pt_3Pr_4, whereas plenty of both tetrahedral and octahedral voids have been observed in Pt_2Pr_3 resulting in a less dense packing.

Other examples of the T_3R_4 family include hexagonal Co_3R_4 for the smaller rare-earth elements, R = Gd-Lu and Y,[43] cubic Th_3P_4 *anti*-type Rh_3La_4,[44,45] and monoclinic Ru_3Ce_4.[46] While

the cubic Th_3P_4 type of structure is totally unrelated, the other two contain similarly fused clusters based on $\{TR_8\}$ bicapped trigonal prisms. In contrast to the $\{Pt_2\}$ dumbbells as evident in Pt_3Pr_4, Co_3R_4 as well as Ru_3Ce_4 exhibit Pt tetramers and chains, respectively. Also, $\{TR_8\}$ clusters are not the exclusive building blocks in the latter, similar to $Pt_{2-x}Pr_3$, where three different structural building units are present.

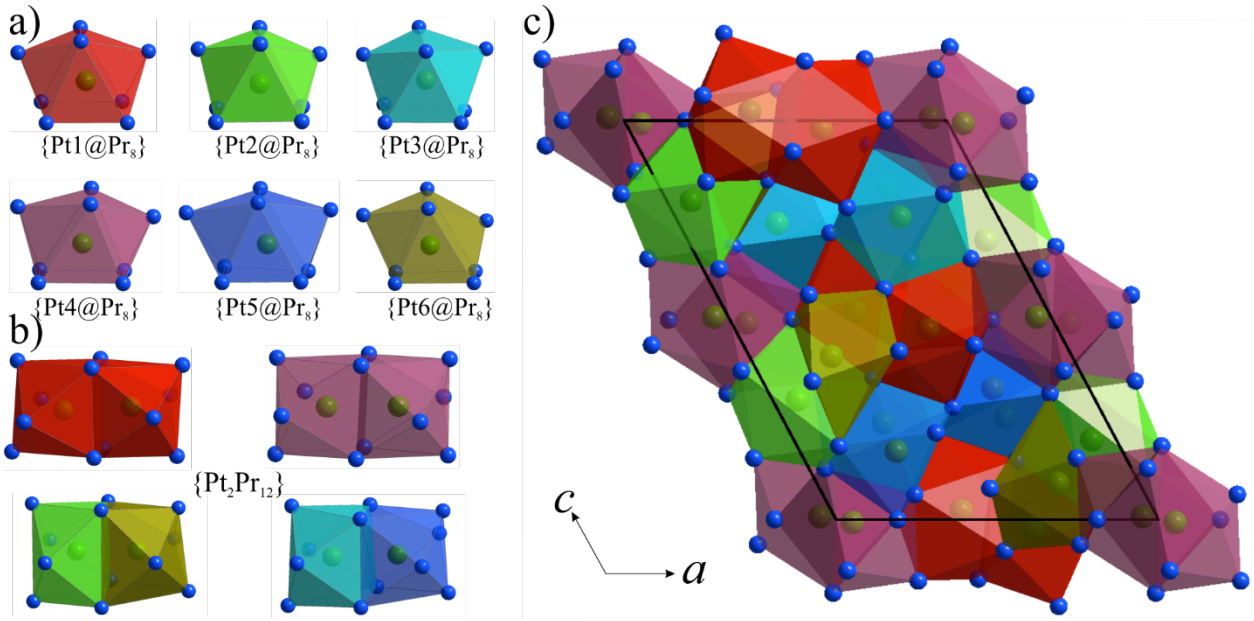

Figure 2. Coordination polyhedra and polyhedral packing in the crystal structures of Pt_3Pr_4.

The application of an obviously reactive flux to a mixture of platinum and praseodymium, a tin melt in the present case, results in ternary $Pt_xSn_yPr_z$ phases. The only ternary intermetallic that has been reported in this particular system is the equiatomic PtSnPr, which adopts the TiNiSi type of structure at ambient pressure (NP-PtSnPr) and the ZrNiAl-type at 10.5 GPa (HP-PtSnPr).[47,48]

On the other hand, ternary compounds containing a transition metal *T*, a rare-earth metal *R*, and a post-transition (main or *p* group) metal *E*, are numerous, including six structure types for the $T_4E_6R_3$ family, of which the $Pt_4Ge_6Ce_3$[30] type is highly prolific. $Pt_4Sn_6Pr_3$ (**4**, *oP*52, *Pnma*,

a = 27.623(1) Å, b = 4.5958(2) Å, c = 9.3499(5) Å) seems to be the first tin containing example of that type. $Pt_4Sn_6Pr_{2.91}$ (**3**, *oP*52, *Pnma*, a = 7.2863(3) Å, b = 4.4909(2) Å, c = 35.114(2) Å) appears to be a high temperature phase related to $Pt_4Sn_6Pr_3$ crystallizing in its own structure with some disorder and under-occupation.

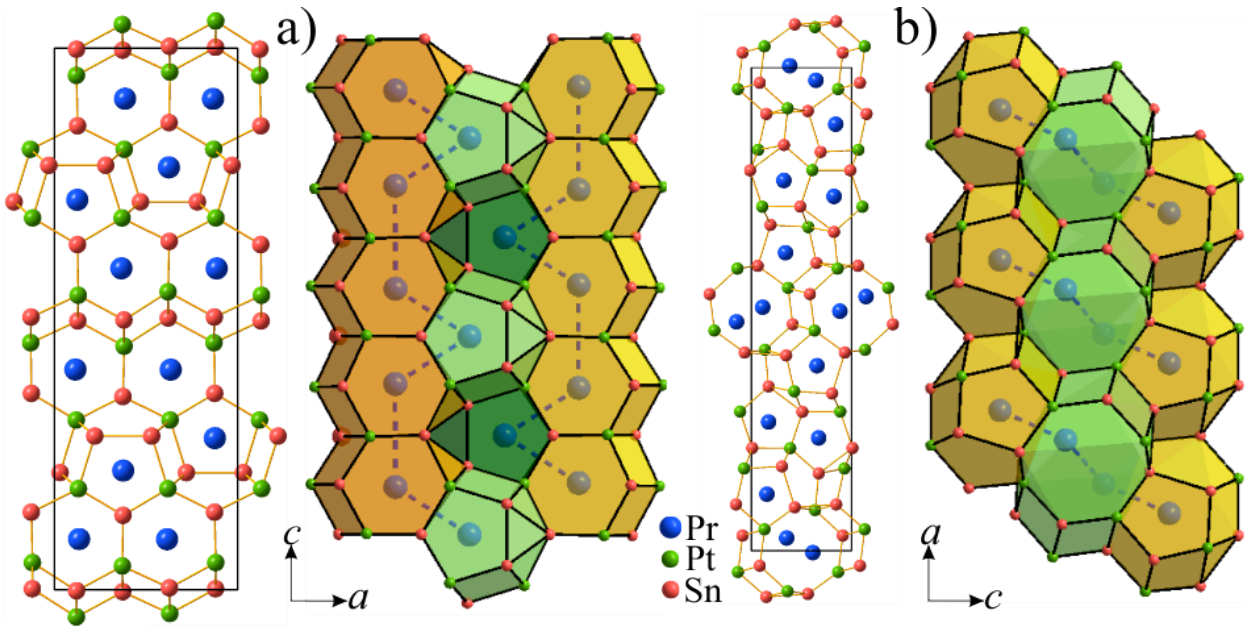

Figure 3. Projections of parts of the crystal structures of $Pt_4Sn_6Pr_3$ (left) and $Pt_4Sn_6Pr_{2.91}$ (right) exhibiting different zig-zag chains of praseodymium atoms (blue) in both structures.

Both phases, $Pt_4Sn_6Pr_3$ and $Pt_4Sn_6Pr_{2.91}$, may be described in terms of polyatomic networks of Pt and Sn atoms forming tunnels along [010] with encapsulated Pr atoms, see Figure 3. Such structural motifs are quite common in cation poor Au polar intermetallics and are represented in a few different variants.[49] Following this mode of description, basic building blocks in the crystal structure of $Pt_4Sn_6Pr_3$ (Figure 3, left) are $\{PrPt_7Sn_9\}$ and $\{PrPt_6Sn_9\}$ clusters with CNs of 16 and 15, respectively. Thus, cation, Pr^{3+}, centered polyhedra run parallel anionic $\{PtSn_x\}^{z-}$ 6/4/6 and 5/5/5 rings, respectively, along the b direction (Figure 4a). The mutual

location of the cation's positions leads to larger non-trigonal (as a rule 5-vertex truncated hexagons) shared faces, and formation of one-side branched tunnels along the *c* axis.

The situation in $Pt_4Sn_6Pr_{2.91}$ is way more complex due to relocation of the cation's positions and significant change of the anionic network (Figure 3, right). This compound contains elements of the tunnel structures observed in AAu_2Ga_2 or AAu_3Ga_2 (*A* = alkali metal),[50,51] i.e. octagonal channels with disordered cations and zigzag cationic chains (Figure 3b). Due to the disorder, Pr–Pr distances within these chains are in the range of 3.12–3.50 Å, significantly shorter compared with those in $Pt_4Sn_6Pr_3$ (4.1 Å and longer). There is a larger proportion of the pentagonal tunnels while the hexagonal tunnels are substituted by larger nonlinear channels. In contrast to $Pt_4Sn_6Pr_3$, the structure of $Pt_4Sn_6Pr_{2.91}$ exhibits preferable tunnel motifs only along one direction (*b*); however, fused pentagonal units (Pr@5/4/5, Figure 4c) form hexagonally shaped tunnels also along the *a* axis accommodating Pr zigzag chains. The octagonal channels can be described on the basis of zigzag Pr@4/7/4 units sharing large hexagonal faces with the building blocks of the other pentagonal tunnels Pr@5/7/5 and are therefore two side branched (Figs. 3b and 4c). Besides this fusion these structural elements are well separated from the identical ones and Pr@5/4/5 based tunnels sharing only smaller trigonal faces. Pr atoms inside octagonal tunnels are positionally disordered and the two different crystallographic sites are in fact not fully occupied in accordance with **2** and **5**. The total occupation of both disordered Pr positions reaches 91% and is in line with the disorder in the Pr–Pr zigzag chains that may lead to too short contacts (~2.81 Å). A large tunnel diameter together with big open faces leads to a large degree of freedom especially in the plane normal to the tunnel axis. Additionally, Pr3–Pr4 distances show a minor average shortening, 3.129(1) Å vs. 3.204(4) Å in $Pt_{1.97}Pr_3$ that may serve as an extra proof for their partial occupation.

An alternative description of the structures of $Pt_4Sn_6Pr_3$ and $Pt_4Sn_6Pr_{2.91}$ starts with coordination polyhedra surrounding the most electronegative atom, platinum, as utilized above for $Pt_{1.97}Pr_3$ and Pt_3Pr_4. In Pt_3Pr_4, the Pt atoms are surrounded by eight Pr atoms with Pt−Pr distances of, on the average, 3.082 Å, close to the sum of the atomic radii of Pt and Pr, 3.20 Å. These are considerably longer (8.4%) than the Pt−Pr distances in $\{PtPr_3\}Br_3$[9] (2.842 Å) which is reasonable, because the CN of Pt in $\{PtPr_3\}Br_3$ is only 6, and, furthermore, polyhedra in the intermetallic Pt_3Pr_4 are not isolated but intensely connected. However, it should be noted that the shortest Pt−Pr distances in Pt_3Pr_4 are about 2.9 Å being comparable to those in $\{PtPr_3\}Br_3$.

When moving from the binary Pt/Pr to the ternary Pt/Sn/Pr system, there is a completely new situation: platinum has by far the highest electron affinity (205.041(5) kJ/mol[52] of all bonding partners and both the smaller tin atoms (1.45 Å), with a $[Kr]4d^{10}5s^25p^2$ electron configuration, and the larger praseodymium atoms (1.85 Å), with a $[Xe]6s^25d^14f^2$ configuration, compete for the closest coordination to the central platinum atom. Tin wins. The average Pt−Sn distance over all the four crystallographically independent $\{PtSn_5\}$ square pyramids (Figure 4) is 2.66 Å, shorter than the sum of the atomic radii, 2.80 Å (with Pt−Sn distances ranging from 2.57 to 2.80 Å). We may call this the first coordination sphere surrounding the central Pt atom. Pr atoms, then constitute a second coordination sphere with an overall average Pt−Pr distance of 3.49 Å (ranging from 3.36 to 3.59 Å), considerably longer than the sum of the atomic radii, 3.20 Å. Summing up both coordination spheres, the central Pt atoms are surrounded by 5+4 atoms, respectively.

This situation is surprising because two sorts of atoms, Sn and Pr, of almost the same electron affinity (107.2984 kJ/mol[53] and 93(3) kJ/mol)[54] compete for the central atom, with the smaller atom (Sn, 1.45 Å) "winning" over the larger one (Pr, 1.85 Å). If we consider Pauling

electronegativities (Pt: 2.28, Sn: 1.96, Pr: 1.13),[55] the central atom and the ones in the first coordination sphere are both negative, only the ones in the second sphere are considerably more positive. Thus, bonding interactions between Pt and Sn must be much stronger than between Pt and Pr; one may consider rather covalent interactions between Pt and Sn, while Pr acts more or less like a Pr^{3+} cation (see below). The $\{PtSn_5\}$ polyhedra are connected with each other as Figure 5 shows and, thus, form a negatively charged three-dimensional network with the positive praseodymium atoms in interstices, which brings us back to the above description of the structure where the most positive atom (Pr) is considered central.

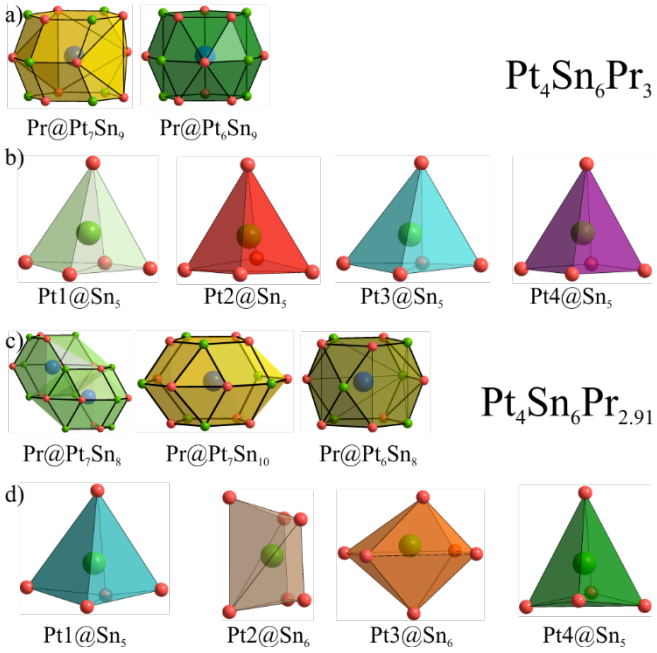

Figure 4. Coordination polyhedra around Pr and Pt atoms in the crystal structures of $Pt_4Sn_6Pr_3$ and $Pt_4Sn_6Pr_{2.91}$.

The situation in $Pt_4Sn_6Pr_{2.91}$ is similar but more complex (Figures 4 and 5). For example, instead of only $\{PtSn_5\}$ pyramids, there are still $\{PtSn_5\}$ and two different $\{PtSn_6\}$ polyhedra present. The latter remind strongly of distorted octahedron and trigonal prism. The diversity of such polyhedra, unsurprisingly, leads to a more complex negative three-dimensional network,

which is, on the other hand, a reflection of the cation disorder. Although, the mutual orientation and connection of the {$PtSn_x$} units reveal slabs of identical motifs for both structures.

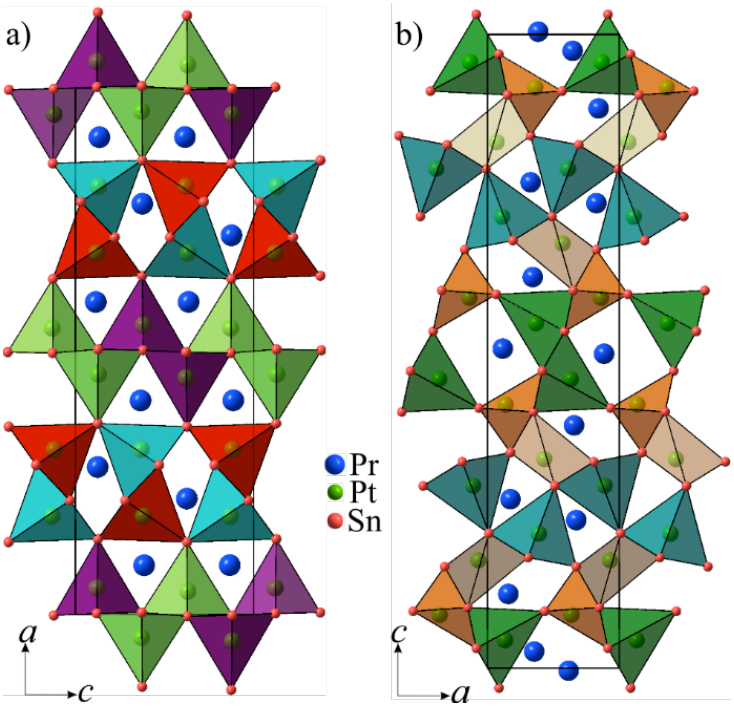

Figure 5. The packing of $Pt@Sn_x$ in the crystal structure of $Pt_4Sn_6Pr_3$ (a, {$PtSn_5$}) and $Pt_4Sn_6Pr_{2.91}$ (b, {$PtSn_5$}, {$PtSn_6$}).

It is interesting to note that despite significant structural changes both phases, which may be regarded as pseudo-polymorphs, have nearly the same unit cell volume and number of positions per atom type. The number of coincidences includes also coordination polyhedra of Pt positions, tricapped trigonal prisms {$Pt(Pr,Sn)_9$} in both structures in analogy with {$PtPr_8Pt$} in Pt_3Pr_4 and $Pt_{2-x}Pr_3$; however, Pr atoms are located in the second coordination sphere of Pt. Therefore, the coordination polyhedra around Pt are best described as slightly distorted Sn square pyramids for all positions in $Pt_4Sn_6Pr_3$ (Figure 4b) and significantly distorted Sn square pyramids, trigonal prisms and octahedra in $Pt_4Sn_6Pr_{2.91}$ (Figure 4d). From this point of view the crystal structure of $Pt_4Sn_6Pr_3$ consists strictly of various 2D and 1D units of the {$Pt@Sn_5$}

pyramids sharing edges within a unit and vertices between the units. Due to complexity, it is hard to separate such units in the crystal structure of $Pt_4Sn_6Pr_{2.91}$, while the building principles still remain identical – edge and vertex sharing polyhedra. No short Pt–Pt contacts are detected in any of the ternary compounds. On the other hand, various modification of the present structural motifs observed in both structures are quite common in *Ae*–Au–*Tr* systems (*Ae* = alkaline-earth metal, *Tr* = triel metals),[56-58] while exactly the same units (Figure 4a and c) have never been reported in Au polar intermetallics.[49]

$Pt_{12}Sn_{24}Pr_{4.84}$ (**5**) crystallizes in the $Ni_{12}Sn_{24}La_{4.87}$ structure type[59] and belongs to the $Gd_3Ni_8Sn_{16}$ (= $Ni_{12}Sn_{24}Gd_{4.5}$) structure family.[31] The most mysterious feature of that structure family, crystallizing with space group *Im*-3, is the peculiar occupation of the special position 2*a* in the center and the origin of the unit cell, (Figure 6a). Even though the position can ideally be refined as fully occupied with Sn, a number of hints suggest that this is actually partially occupied by Pr. Several compounds have been published with different rare-earth metals (*R*)[60] claiming all possible occupation options from fully occupied tin through mixed occupancies of *R* and Sn to partially occupied by *R*. With an occupation of 0.84 by Pr, the number of electrons would be just the same as tin's atomic number. A significant argument for the 2*a* position to be occupied with the rare earth element comes from the closely related structure of $EuRuSn_3$,[61] where the presence of two inequivalent Eu positions has been confirmed by means of Mössbauer spectroscopy.

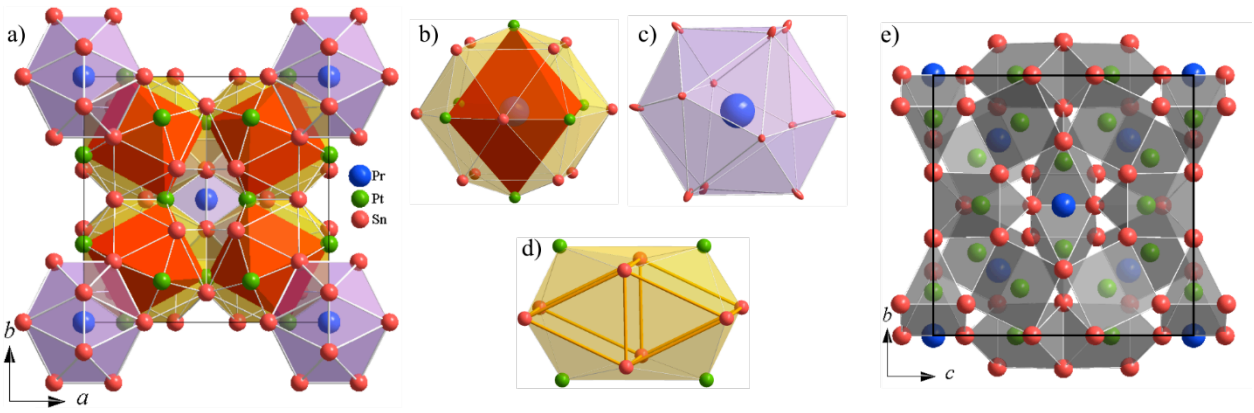

Figure 6. $Pt_{12}Sn_{24}Pr_{4.84}$: Projection of the crystal structure down [100] (a), $\{PrSn_{12}Pt_6\}$ tetrakis-cuboctahedra (b), $\{Pr_{0.84}Sn_{12}\}$ icosahedra (c), empty tetrakis-rhombic-prisms (d) and the packing of vertex-sharing $\{PtSn_6\}$ trigonal prisms.

The crystal structure of **5** may be described as a superpolyhedral variant of $PtHg_4$[62] with $\{PtSn_{12}\}$icosahedra taking the positions of Pt in $PtHg_4$ and $\{PrSn_{12}Pt_6\}$ tetrakis-cuboctahedra those of Hg. Such packing leaves plenty of voids centering each cell face and edge. The latter can be shown as strongly distorted icosahedra with offset poles along the fivefold axis, but more precisely they are Pt rhombic prisms tetracapped by Sn. This polyhedron also resembles the $\{Pt_2Pr_{12}\}$ unit from both Pt_3Pr_4 and $Pt_{2-x}Pr_3$, however without centering dumbbells. The $\{PrSn_{12}Pt_6\}$ tetrakis-cuboctahedra can simply be presented as interpenetrating Pt_6 octahedra and Sn_{12} cuboctahedra centered by Pr (Figure 6b), while the $\{PrSn_{12}\}$ icosahedra are slightly unusual showing a strong split of all Sn positions surrounding Pr. This results in a Pr–Sn distance range from 3.125 Å to 3.599 Å and serves as a proof that the center of the icosahedron is just partially occupied. The shortest distance occurs when the Pr atom is missing while the latter is close to the average Pr–Sn contact in the structure. Sn–Sn contacts within the icosahedron also vary from 2.8 Å, which is the sum of their covalent radii, to almost 4 Å when the central Pr position is occupied. In analogy with the two previous compounds the structrue can also be presented on the basis of $\{PtSn_x\}$ polyhedra (Figure 6e). In this case all Pt coordination polyhedra are trigonal prisms and a clear separation of the Pt environment is observed. Pt−Sn distances are in the range

2.60−2.77 Å, forming the first coordination sphere. The prisms are equatorially capped by two Pr and one Pt atoms with *d*(Pt−Pr) = 3.336(1) Å and *d*(Pt−Pt) = 4.105(1) Å, formally outside of the second coordination sphere.

Electronic structures. For simple molecules, for Werner-type coordination compounds as well as for compounds containing metal clusters of both early and late transition metals, for intermetallics as Hume-Rothery or Zintl phases, a number of simple electron counting rules are widely used as a very first approximation to their electronic structures. For example, for $K_2[PtCl_6]$ it would be the 18-electron rule, although not as decisive as for $[Fe(CO)_5]$ with strong ligands. For $K_4[\{Nb_6\}Cl_{18}]$ as well as for $K_2Zr[\{CZr_6\}Cl_{18}]$ there are 16 cluster-based electrons (CBEs) and for $Cs_2[\{Mo_6\}Cl_{14}]$ there are 24; these numbers are sometimes associated with eight three-center–two-electron and twelve two-center–two-electron bonds, respectively. For transition-metal centered rare-earth clusters in cluster-complex halides such as $[\{PtPr_6\}I_{12}]Pr$ or $\{PtPr_3\}Br_3$ the number of CBE's is 19 and 16, respectively. Roughly, the higher connected the clusters are—isolated in the former, edge-connected to chains in the latter—the lower the number of CBE's needs to be because they are shared between the connected clusters. When the same calculation is carried out for Pt_3Pr_4 and Pt_2Pr_3, now scaled to one Pt atom per formula unit, the numbers are 14 and 14.5, respectively, smaller than for the example of $\{PtPr_3\}Br_3$ (16) because the $\{PtPr_8\}$ clusters are three-dimensionally connected. For the tin-rich ternaries $Pt_4Sn_6Pr_3$ and $Pt_{12}Sn_{24}Pr_5$, the numbers, scaled to one Pt per formula unit with 10 valence electrons for Pt, 4 for Sn and 3 for Pr, are 18.25 and 19.25, respectively. Thus, the addition of a main group element, although less electronegative than the halogens, brings us back to the situation of the more isolated cluster-complex halides.

Of course, band structure calculations, the density of states (DOS) as well as overlap populations, as COOP (crystal orbital overlap population) or COHP (crystal orbital Hamilton population), are a much better means to evaluate the electronic structure of intermetallics. Electronic structure calculations have been performed on Pt_3Pr_4 (**1**) for a slightly idealized model of $Pt_{2.91}Pr_3$ (**2**) assuming all Pt positions fully occupied, and for $Pt_4Sn_6Pr_3$ (**3**). The DOS and associated PDOS (projected DOS) curves for the binaries (**1**) and (**2**) are qualitatively similar with broad regions extending 7 eV below the Fermi levels and large Pt 5*d* contributions located at 4.5–2 eV below E_F (Figure 7). The position of the latter allows the assignment of formally filled 5*d* orbitals in valence electron counting approaches and bonding schemes. Pt 6*s* states provide the largest contributions between –2 and –7 eV and dominate below –5 eV, though the contributions around E_F are rather negligible. Such situations are considerably different from *s*-*d* intermetallics with Pt, Cs_2Pt or Cs_9Pt_4H,[63,64] but are rather typical for Pt polar intermetallics with active and post-transition metals.[65-67] Pr 5*d* states dominate over 5*p* and 6*s* practically through the entire range. While Pr 5*p* and 6*s* states contribute to the DOS substantially in a region of 3–5 eV below E_F, their contributions at the Fermi level are rather insignificant. The sizable total DOS values at E_F, 1.3 and 4.9 states/eV·f.u. for Pt_2Pr_3 and Pt_3Pr_4, respectively, indicate metallic character. The DOS curves of Pt_2Pr_3 reveal a narrow but very deep pseudogap at the Fermi level, whereas those for Pt_3Pr_4 are on a sharp local maximum. In that case the shift in the Fermi level from that of the experimental composition lowers the DOS values significantly which is specifically achieved by adding valence electrons, i.e. partial substitution of Pt with a *p* block element. Total energy calculations performed for two different modifications of Pt_2Pr_3 revealed a rather small difference of about 5 meV/f.u., or 80 meV/cell with preference for the rhombohedral

variant. This may provide a hint why $Pt_{2-x}Pr_3$ cannot be obtained as a stoichiometric product in this structure type or it exists at higher temperatures only.

Distances and bonding analysis. Heteroatomic bonding dominates quantitatively throughout all structures including both binaries and all ternaries. Such interactions have been intensively studied in the ternary *A*–*T*–*E* systems (*A* = active metal, *T* = late transition metal, and *E* = *p* block element), but still binary systems are an interesting field for research due to the enhanced role of cation–anion bonding. The particular feature that makes many platinum and gold systems remarkable derives from substantial relativistic contributions to its bonding, chemically established by both increased binding via the more penetrating 6*s* orbitals and the relative elevation of the $5d^{10}$ states into greater mixing with higher energy valence states.

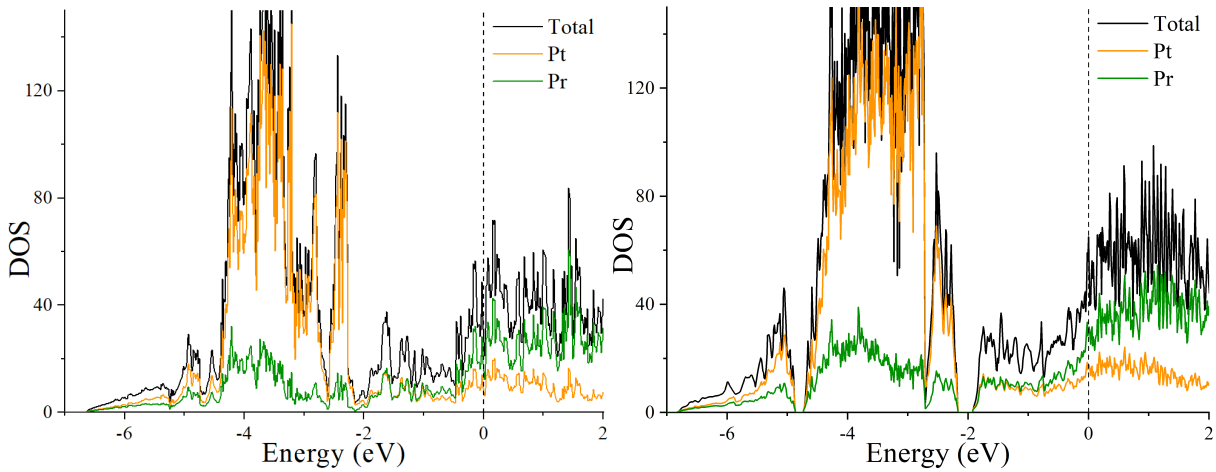

Figure 7. DOS and PDOS curves for the tetragonal $Pt_{1.97}Pr_3$ (left) and the monoclinic Pt_3Pr_4 (right).

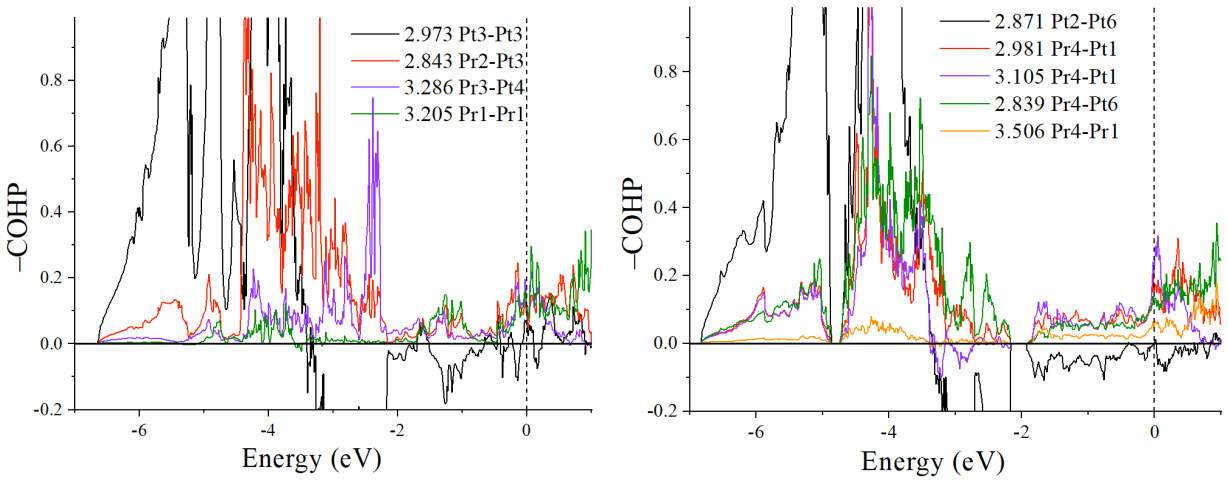

Figure 8. –COHP curves for selected interatomic interactions in the crystal structures of Pt_2Pr_3 (left) and Pt_3Pr_4 (right).

The electronegativity of Pt greatly exceeds that of the rare-earth elements, giving the more extreme polar distribution of Pr 5*d*. While some Pr states are certainly involved in bonding with Pt 5*d* at −2.0 to −4.5 eV, the effective oxidation of Pr affects the dislocation of some 5*d* states to higher energies similar to those observed in $Au_7Sn_3R_3$.[68]

Since the crystal structure of Pt_3Pr_4 exhibits basically variations of just one building unit based on Pt_2 dumbbells in $\{Pt_2Pr_{12}\}$, the most representative bonding interactions within and between such units were analyzed. Pt–Pt distances are in the range of 2.871−3.030 Å and appear to be quite normal for polar intermetallics, though being slightly longer than twice the atomic radius (2.70 Å).[69] The –COHP curve shows that the Pt2–Pt6 interaction is rather nonbonding at the Fermi level (Figure 8), while the –ICOHP (integrated COHP) value of 1.47 eV is still high. This allows us to consider these Pt–Pt contacts as bonding bridges for the cluster formation. Pr–Pt interatomic distances are widely spread from 2.83 to 3.51 Å, whereas unique separations may reach 3.87 Å, though providing much lower contributions to the bonding patterns. Two selected contacts connecting both Pt atoms in a dumbbell Pr4–Pt1 (2.981 and 3.105 Å) are strongly bonding at E_F and are highly populated: 0.82 and 0.69 eV/bond being practically inversely

proportional to their bond lengths. The shortest Pr–Pt contact in the structure, Pr4–Pt6 (2.839 Å) reveals the largest –ICOHP value of 0.98 eV/bond. This is due to the special location of that Pr position in between three Pr_2 dumbbells. Since Pt–Pr contacts represent over 50% of all bonds in the structure their contribution to total bonding exceeds 90%. Pr–Pr separations in the structure cover the range from 3.51 to 4.07 Å with a small fraction reaching even 4.71 Å. The shortest ones usually connect more than one Pt_2 dumbbell. Pr1–Pr4 contacts (3.506 Å) are also bonding at E_F with a –ICOHP value of 0.11 eV, and due to their relatively large number are comparable with the Pt–Pt ones in the total bonding contributions.

The bonding situation in $Pt_{2-x}Pr_3$ is slightly different due to the diversity of the structural elements and connected with them a redistribution of bonding interactions. The only Pt–Pt bonding distances are observed between Pt positions within $\{Pt_2Pr_{12}\}$ clusters identical to those in Pt_3Pr_4. These contacts are closer to the upper end of the Pt–Pt bonding spectrum (d(Pt3–Pt3) = 2.978(2) Å) in Pt_3Pr_4 and are all identical due to the high symmetry of the crystal structure. The major part of the Pr–Pr contacts in the structure range from 3.57 to 4.07 Å, but not without exclusions. This compound reveals short Pr5–Pr5 distances of 3.204 Å, which are well below the sum of the atomic radii. These contacts, however, do not show any indication of cation–cation repulsion leading to antibonding interactions and reveal an –ICOHP value of 0.16 eV. Furthermore, this distance can be explained by steric factors due to low bond saturation. These Pr positions are surrounded by just four Pt atoms with only two having bonding distances to each of them. This number is even lower than the one observed in $Na_8Au_{10}Ga_7$ for some Au–Ga contacts leading to their contraction well below the sum of the corresponding covalent radii.[70] On the other hand, this reduction was observed in all compounds throughout the Ga_2Gd_3 type.[71] Another extreme due to steric restrictions has been observed for some Pt–Pr contacts for Pt

positions inside of Pr_8 tetragonal prisms (d(Pt3–Pt3) = 3.286 Å) with a major part of those bonds being located around 2.85–3.07 Å. All the discussed contacts reveal bonding interactions at the Fermi level (Figure 8) including Pt–Pt pairs, found to be nonbonding in Pt_3Pr_4. It is interesting to note that E_F is located on the sharp slope for all interactions; removing up to 0.3 valence electrons per formula unit increases bonding interactions by a factor of up to two, while adding them leads to a significant decrease of the latter. This might serve as an extra explanation for the partial occupation of the Pt position. Quantitatively, the bonding contributions of different pairs do not differ significantly from those in Pt_3Pr_4, with the Pt–Pr component exceeding 90% of the total bonding, with the –ICOHP values for separate interactions ranging from 0.4 to 1.1 eV/bond. Pt–Pt contributions remain large but due to the limited number of contacts in the structure do not present any leading role.

A comparison of the overlap populations in Pt_2Pr_3 and $Pt_4Sn_6Pr_3$ (Figure 9) shows that Pt-Sn bonding interactions become the most dominant, reflected in the coordination polyhedra $\{PtSn_5\}$ with their relatively short internuclear distances. Both Pt−Pr and Sn−Pr bonding interactions play a role but to a lesser degree. Homoatomic Sn-Sn bonding and antibonding are pretty much balanced.

The cumulative integrated –COHP values (–ICOHPs) analysis (Table 5) for all interactions in Pt_2Pr_3 and $Pt_4Sn_6Pr_3$ revealed interesting tendencies on moving from the binary to the ternary phase. The lowest contributing Pt–Pt interactions in Pt_2Pr_3 (5.7%) are completely missing in $Pt_4Sn_6Pr_3$ and their role is taken over by Pr–Pr (1.9%) and Sn–Sn (5.7%) interactions. While heteroatomic Pt–Pr interactions in Pt_2Pr_3 provide over 85% in total, the Pt–Sn interactions in $Pt_4Sn_6Pr_3$ provide just 48.1% but accompanied with two other heteroatomic pairs Sn–Pr and Pt–Pr they reach nearly the same 92%. Interestingly Pr–Pr interactions in both compounds differ

slightly, however, with the considerable larger number of contacts in the binary phase such interactions are definitely more populated in the ternary compound.

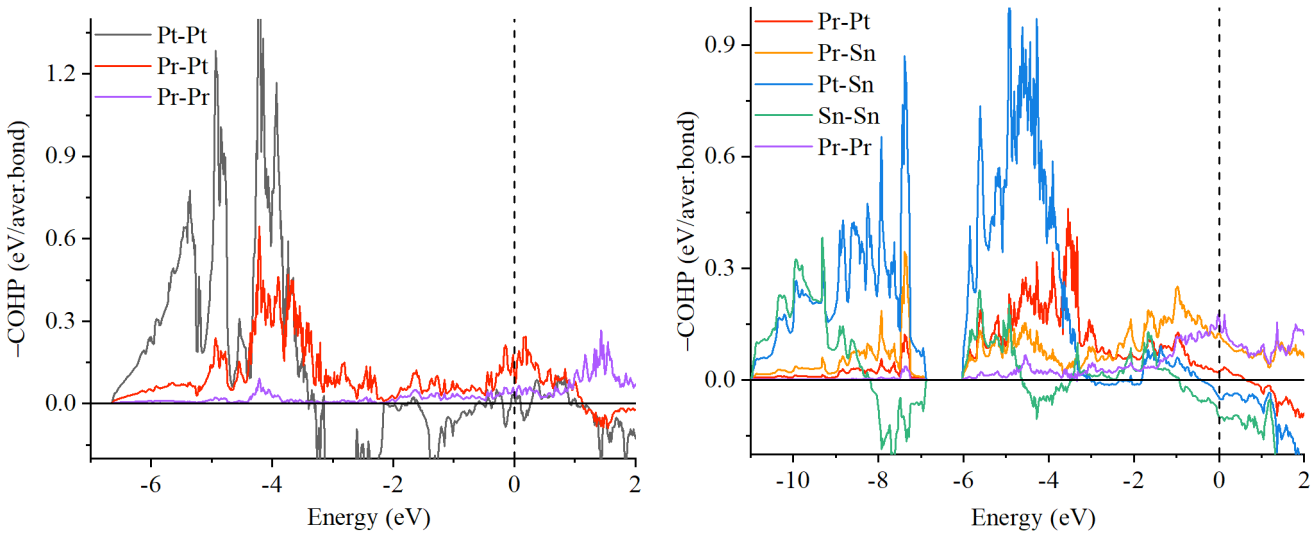

Figure 9. –COHP curves for different interatomic interactions in the crystal structures of Pt_2Pr_3 (left) and $Pt_4Sn_6Pr_3$ (right).

Conclusions

The central part of the Pt–Pr binary phase diagram has been augmented with two new representatives, Pt_3Pr_4 and $Pt_{2-x}Pr_3$. Both compounds can be obtained through high temperature reactions in $PrCl_3$ or NaCl fluxes, respectively, which apparently improve the quality of single crystal growth, especially for the low temperature phases. The application of a tin flux results in the formation of three new phases within the ternary Pt/Sn/Pr system, $Pt_4Sn_6Pr_3$, $Pt_4Sn_6Pr_{2.91}$, $Pt_{12}Sn_{24}Pr_{4.84}$. Both "modifications" of $Pt_4Sn_6Pr_3$, most likely existing at low and high temperatures, exhibit significant structural varieties although they crystallize in the same space group (*Pnma*) and have nearly identical unit cell volumes, with the difference being caused mainly by the partial deficiency of some Pr positions. Electronic structure calculations reveal that both compounds are metallic in nature with $Pt_{2-x}Pr_3$ showing a narrow but deep pseudogap at the Fermi level. The stoichiometric tetragonal Pt_2Pr_3 appears to have a higher total energy compared

to the rhombohedral Pt_2Pr_3 and is, therefore, thermodynamically unstable. Both electronic density of states and crystal orbital Hamilton populations (COHP) curves suggest that adding some valence electrons to the crystal structure of Pt_3Pr_4 decreases the DOS values and simultaneously enhances bonding interactions for all types of bonds. The overall bond populations in all structures are dominated by heteroatomic Pt–Pr interactions (in the binary Pt_3Pr_4 and $Pt_{2-x}Pr_3$) as well as Pt-Sn (and to a lesser degree Pt-Pr and Sn-Pr interactions) in $Pt_4Sn_6Pr_3$ while homoatomic bonding plays only a minor role. This is in striking consistency with the bonding schemes in rare-earth cluster complex halides with endohedral transition metal atoms, e.g. in $\{PtPr_3\}Br_3$ where Pt-Pr and Pr-Br bonding dominates.

Table 1. Crystallographic details and refinement parameters for $Pt_{1.97}Pr_3$ and Pt_3Pr_4.

Formula	$Pt_{1.97}Pr_3$	Pt_3Pr_4
Form. wt., g/mol	807.55	1148.91
Space group, *Z*	*I*4/*mcm* (no. 140), 16	$P2_1/c$ (no. 14), 8
a, Å	11.9444(7)	12.353(2)
b, Å		7.4837(9)
c, Å	14.488(1)	17.279(2)
β, °		118.003(7)
V, $Å^3$	2067.0(3)	1410.4(3)
Temperature, K	293(2)	293(2)
Density (calculated), g/cm^3	10.380	10.822
Absorption coefficient, μ, mm^{-1}	80.770	86.218
F (000)	5294	3760
θ range, °	2.4 to 24.4	1.9 to 27.3
Index ranges	$-12 < h < 13$	$-15 < h < 15$
	$-13 < k < 13$	$-9 < k < 9$
	$-16 < l < 16$	$-22 < l < 21$
Intensity data collected	6970	20998
Number of independent reflections	482 [R_{int} = 0.1195]	3123 [R_{int} = 0.1503]
Completeness, %	100	98.3
Data/ Restraints/ Parameters	482/0/33	3123/0/128
Goodness-of-fit (F^2)	1.051	1.055
R_1, ωR_2 [$I_0 > 2\sigma$ (I)]	0.0333; 0.0661	0.0560; 0.1326
R_1, ωR_2 (all data)	0.0509; 0.0719	0.0725; 0.1428
Largest diff. peak and hole [$e/Å^{-3}$]	2.329 and – 1.842	3.060 and – 4.182

Table 2. Crystallographic details and refinement parameters for $Pt_4Sn_6Pr_{3-x}$ (x = 0, 0.09) and $Pt_{12}Sn_{24}Pr_{4.84}$

Formula	$Pt_4Sn_6Pr_3$	$Pt_4Sn_6Pr_{2.91}$	$Pt_{12}Sn_{24}Pr_{4.84}$
Structure type	$Pt_4Ge_6Pr_3$	own	$La_{4.87}Ni_{12}Sn_{24}$
Form. Wt., g/mol	1915.23	1902.55	5871.43
Space group, *Z*	*Pnma* (no. 62), 4	*Pnma* (no. 62), 4	*Im*-3 (no. 204), 2
a, Å	27.623(1)	7.2863(3)	12.274(1)
b, Å	4.5958(2)	4.4909(2)	
c, Å	9.3499(5)	35.114(2)	
V, Å^3	1187.0(1)	1148.99(9)	1848.9(5)
Density (calculated) [g/cm^3]	10.717	10.998	10.547
μ, mm^{-1}	71.294	73.278	67.265
F (000)	3156	3135	4843
θ range, °	2.3 to 33.2	2.3 to 27.5	2.3 to 30.0
Index ranges	$-40 \le h \le 40$ $-7 \le k \le 7$ $-13 \le l \le 14$	$-9 \le h \le 9$ $-5 \le k \le 5$ $-45 \le l \le 40$	$-17 \le h \le 17$ $-17 \le k \le 17$ $-17 \le l \le 17$
Intensity data collected	22092	22001	20587
No.of independent reflections	2380 [R_{int} = 0.0757]	1481 [R_{int} = 0.0548]	516 [R_{int} = 0.1045]
Refinement method	Full-matrix least-squares on F^2		
Data/ Restraints/ Parameters	2380 / 0 / 80	1481 / 0 / 88	516/ 0/ 27
Goodness-of-fit (F^2)	1.050	1.079	1.129
R_1; ωR_2 [$I_0 > 2\sigma$ (I)]	0.0373; 0.0545	0.0311; 0.0631	0.0192; 0.0465
R_1; ωR_2 (all data)	0.0843; 0.0634	0.0411; 0.0654	0.0197; 0.0467
Largest diff. peak and hole [e·Å^{-3}]	3.577 and –4.413	4.146 and –4.306	1.685 and –1.066

Table 3. Atomic positions and equivalent thermal parameters of $Pt_{1.97}Pr_3$ and Pt_3Pr_4.

Atomic parameters					
Atom	Wyckoff site	*x*	*y*	*z*	U_{eq}
$Pt_{1.97}Pr_3$					
Pt1	4*a*	0	0	¼	0.0222(6)
Pt2	8*h*	0.6254(1)	0.1254(1)	0	0.0211(4)
Pt3	16*l*	0.17488(7)	0.67488(7)	0.30377(8)	0.0247(4)
Pt4*	4*c*	0	0	0	0.0320(11)
Pr1	8*g*	0	½	0.13943(15)	0.0232(6)
Pr2	8*h*	0.1737(1)	0.6737(1)	0	0.0264(6)
Pr3	32*m*	0.0705(1)	0.2045(1)	0.14020(9)	0.0294(4)
Pt_3Pr_4					
Pt1	4*e*	0.4029(1)	0.4527(2)	0.02239(8)	0.0302(3)
Pt2	4*e*	0.0762(1)	0.8055(2)	0.29976(8)	0.0328(3)
Pt3	4*e*	0.3043(1)	0.2009(2)	0.24252(8)	0.0292(3)
Pt4	4*e*	0.0458(1)	0.1824(2)	0.49255(8)	0.0304(3)
Pt5	4*e*	0.7013(1)	0.3291(2)	0.32874(9)	0.0350(3)
Pt6	4*e*	0.2539(1)	0.5466(2)	0.4090(1)	0.0415(3)
Pr1	4*e*	0.5476(1)	0.0131(2)	0.2825(1)	0.0256(3)
Pr2	4*e*	0.2847(1)	0.1505(2)	0.0628(1)	0.0256(3)
Pr3	4*e*	0.8098(1)	0.3419(2)	0.0003(1)	0.0246(3)
Pr4	4*e*	0.6569(1)	0.3400(2)	0.1487(1)	0.0273(3)
Pr5	4*e*	0.1534(1)	0.1951(2)	0.3462(1)	0.0293(4)
Pr6	4*e*	0.0498(1)	0.0066(2)	0.1281(1)	0.0277(4)
Pr7	4*e*	0.4716(1)	0.3190(2)	0.4219(1)	0.0276(4)
Pr8	4*e*	0.1299(1)	0.5114(2)	0.1841(1)	0.0280(4)

*site occupation factor, SOF = 0.893(9)

Table 4. Atomic positions, equivalent thermal parameters and site occupation factors (if other than 1.0) of $Pt_4Sn_6Pr_3$, $Pt_4Sn_6Pr_{2.91}$ and $Pt_{12}Sn_{24}Pr_{4.84}$

Atom	Wyckoff	*x*	*y*	*z*	U_{eq}	*SOF*
			$Pt_4Sn_6Pr_3$			
Pt1	4*c*	0.54385(2)	¼	0.6296(1)	0.0074(1)	
Pt2	4*c*	0.18660(2)	¼	0.1189(1)	0.0059(1)	
Pt3	4*c*	0.18654(2)	¼	0.6309(1)	0.0061(1)	
Pt4	4*c*	0.05015(2)	¼	0.3801(1)	0.0091(1)	
Pr1	4*c*	0.40665(2)	¼	0.6146(2)	0.0086(2)	
Pr2	4*c*	0.40641(2)	¼	0.1346(2)	0.0089(2)	
Pr3	4*c*	0.27999(2)	¼	0.37531(9)	0.0058(1)	
Sn1	4*c*	0.00358(3)	¼	0.1275(2)	0.0074(2)	
Sn2	4*c*	0.49826(3)	¼	0.8792(2)	0.0075(2)	
Sn3	4*c*	0.28370(4)	¼	0.0307(1)	0.0059(2)	
Sn4	4*c*	0.13746(3)	¼	0.8744(2)	0.0077(2)	
Sn5	4*c*	0.28374(4)	¼	0.7201(1)	0.0058(2)	
Sn6	4*c*	0.14329(3)	¼	0.3738(2)	0.0121(2)	
			$Pt_4Sn_6Pr_{2.91}$			
Pt1	4*c*	0.38949(8)	¼	0.21214(2)	0.0060(1)	
Pt2	4*c*	0.06991(9)	¼	0.82986(2)	0.0062(2)	
Pt3	4*c*	0.13717(8)	¼	0.41594(2)	0.0065(2)	
Pt4	4*c*	0.36766(9)	¼	0.54420(2)	0.0081(2)	
Pr1	4*c*	0.3265(1)	¼	0.76647(3)	0.0072(2)	
Pr2	4*c*	0.1570(1)	¼	0.11697(3)	0.0120(2)	
Pr3	4*c*	0.3849(3)	¼	0.00408(8)	0.0148(5)	0.44(1)
Pr4	4c	0.3539(3)	¼	0.02615(7)	0.0148(5)	0.47(1)
Sn1	4*c*	0.1928(1)	¼	0.67448(3)	0.0073(2)	
Sn2	4*c*	0.0105(1)	¼	0.21256(3)	0.0057(2)	
Sn3	4*c*	0.1735(1)	¼	0.34000(3)	0.0074(2)	
Sn4	4*c*	0.6513(1)	¼	0.59574(3)	0.0062(2)	
Sn5	4*c*	0.4140(2)	¼	0.46872(3)	0.0086(3)	
Sn6	4*c*	0.0656(4)	¼	0.5897(2)	0.0104(8)	0.69(1)
Sn7	4c	0.0533(9)	¼	0.5759(3)	0.0104(8)	0.31(1)
			$Pt_{12}Sn_{24}Pr_{4.84}$			
Pr1*	2*a*	0	0	0	0.0127(6)	0.84(1)
Pr2	8*c*	¼	¼	¼	0.0095(2)	
Pt1	24*g*	0	0.31828(2)	0.16722(2)	0.0072(1)	
Sn1	24*g*	0	0.37917(4)	0.37364(4)	0.0087(2)	
Sn2	24*g*	0	0.1286(1)	0.2635(2)	0.0134(3)	0.602(4)
Sn3	24*g*	0	0.1133(2)	0.2280(3)	0.0134(3)	0.398(4)

Table 5. Bond length ranges and average −ICOHP values as well as total contributions to bonding interactions in $Pt_{1.97}Pr_3$ (idealized as Pt_2Pr_3) and $Pt_4Sn_6Pr_3$.

Bond type	Length (Å)	−ICOHP (eV/bond)	no./cell	−ICOHP (eV/cell)	Contribution (%)
		"Pt_2Pr_3"			
Pt−Pr	2.843−3.795	0.73	264	193.4	85.6
Pt−Pt	2.973−3.622	0.81	16	12.9	5.7
Pr−Pr	3.205−3.906	0.11	178	19.7	8.7
		$Pt_4Sn_6Pr_3$			
Pt−Sn	2.590−2.815	2.28	68	155.1	48.1
Sn−Pr	3.229−3.623	0.82	104	85.0	26.4
Pt−Pr	3.380−3.584	0.80	72	57.6	17.9
Sn−Sn	2.914−3.461	0.42	44	18.4	5.7
Pr−Pr	4.182−4.615	0.26	24	6.24	1.9

Associated content

Supporting Information

Structural data as CIF files.

Accession Codes CCDC 1833515-1833519 contain the supplementary crystallographic data for this paper. These data can be obtained free of charge via www.ccdc.cam.ac.uk/data_request/cif, or by emailing data_request@ccdc.cam.ac.uk, or by contacting The Cambridge Crystallographic Data Centre, 12 Union Road, Cambridge CB2 1EZ, UK; fax: +44 1223 336033.

Author Information

Corresponding Author

*E-mail for GHM: ghmeyer@iastate.edu

ORCID

Volodymyr Smetana: 0000-0003-0763-1457

Anja-Verena Mudring: 0000-0002-2800-1684

Gerd H. Meyer: 0000-0003-1000-9001

Notes

The authors declare no competing financial interest.

Acknowledgments

Initial research by T. B. was supported by direct funds from the University of Cologne, Cologne, Germany. More recent research was supported by the Office of the Basic Energy Sciences, Materials Sciences Division, U. S. Department of Energy (DOE), and the Department of Chemistry at Iowa State University (ISU). Ames Laboratory is operated for DOE by ISU under contract No. DE-AC02-07CH11358.

References

(1) Lokken, D. A.; Corbett, J. D. *J. Am. Chem. Soc.* Gadolinium sesquichloride, an unusual example of metal-metal bonding **1970**, *92*, 1799-1800.

(2) Lokken, D. A.; Corbett, J. D. *Inorg. Chem.* Rare earth metal-metal halide systems. XV. Crystal structure of gadolinium sesquichloride. Phase with unique metal chains **1973**, *12*, 556-559.

(3) Simon, A.; Holzer, N.; Mattausch, H. *Z. Anorg. Allg. Chem.* Metallreiche Verbindungen der Seltenen Erden Gd_2Cl_3, Gd_2Br_3 und Tb_2Cl_3 **1979**, *456*, 207-216.

(4) Meyer, G. *Z. Anorg. Allg. Chem.* Cluster Complexes as anti-Werner Complexes **2008**, *634*, 2729-2736.

(5) Meyer, G. In *The rare earth elements: fundamentals and applications*; Arwood, D. A., Ed.; John Wiley & Sons, Inc., 2012.

(6) Meyer, G. In *Handbook on the Physics and Chemistry of Rare Earths*; Bünzli, J.-C. G.;Pecharsky, V. K., Eds.; Elsevier, 2014.

(7) Payne, M. W.; Corbett, J. D. *Inorg. Chem.* Encapsulation of the platinum and neighboring metals within cluster iodides of rare-earth elements **1990**, *29*, 2246-2251.

(8) Dorhout, P. K.; Payne, M. W.; Corbett, J. D. *Inorg. Chem.* Condensed metal cluster iodides centered by noble metals. Six examples of cubic R_3I_3Z phases (R = La, Pr; Z = Os, Ir, Pt) **1991**, *30*, 4960-4962.

(9) Llusar, R.; Corbett, J. D. *Inorg. Chem.* Reduced Praseodymium Cluster Bromides Stabilized by Transition Metals **1994**, *33*, 849-853.

(10) Massalski, T.; Okamoto, H.; Subramanian, P.; Kacprzak, L. Binary Alloy Phase Diagrams, ASM International, Materials Park, OH, 1990.

(11) Meyer, G.; Ax, P. *Mater. Res. Bull.* An analysis of the ammonium chloride route to anhydrous rare-earth metal chlorides **1982**, *17*, 1447-1455.

(12) Meyer, G.; Garcia, E.; Corbett, J. D. In *Inorg. Synth.*; John Wiley & Sons, Inc., 2007.

(13) WinXPow. Stoe & Cie GmbH, Darmstadt, Germany. **2004**.

(14) APEX3, Bruker AXS Inc., Madison, Wisconsin, USA, 2015.

(15) SAINT, Bruker AXS Inc., Madison, Wisconsin, USA, 2015.

(16) Krause, L.; Herbst-Irmer, R.; Sheldrick, G. M.; Stalke, D. *J. Appl. Crystallogr.* Comparison of silver and molybdenum microfocus X-ray sources for single-crystal structure determination **2015**, *48*, 3-10.

(17) Sheldrick, G. *Acta Crystallogr. Sect. A* SHELXT - Integrated space-group and crystal-structure determination **2015**, *71*, 3-8.

(18) Sheldrick, G. *Acta Crystallogr. Sect. C: Struct. Chem.* Crystal structure refinement with SHELXL **2015**, *71*, 3-8.

(19) Tank, R.; Jepsen, O.; Burkhardt, A.; Andersen, O. K. *TB-LMTO-ASA Program,* Max-Planck-Institut für Festkörperforschung, Stuttgart, Germany, 1994.

(20) Andersen, O. K.; Jepsen, O. *Phys. Rev. Lett.* Explicit, First-Principles Tight-Binding Theory **1984**, *53*, 2571-2574.

(21) Lambrecht, W. R. L.; Andersen, O. K. *Phys. Rev. B* Minimal basis sets in the linear muffin-tin orbital method: Application to the diamond-structure crystals C, Si, and Ge **1986**, *34*, 2439-2449.

(22) Dronskowski, R.; Bloechl, P. E. *J. Phys. Chem.* Crystal orbital Hamilton populations (COHP): energy-resolved visualization of chemical bonding in solids based on density-functional calculations **1993**, *97*, 8617-8624.

(23) Blöchl, P. E. *Phys. Rev. B* Projector augmented-wave method **1994**, *50*, 17953-17979.

(24) Perdew, J. P.; Burke, K.; Ernzerhof, M. *Phys. Rev. Lett.* Generalized Gradient Approximation Made Simple **1996**, *77*, 3865-3868.

(25) Kresse, G.; Marsman, M.; Furthmüller, J. *Vienna Ab Initio Simulation Package (VASP), The User Guide* **2010**.

(26) Kresse, G.; Furthmüller, J. *Comput. Mater. Sci.* Efficiency of ab-initio total energy calculations for metals and semiconductors using a plane-wave basis set **1996**, *6*, 15-50.

(27) Kresse, G.; Furthmüller, J. *Phys. Rev. B* Efficient iterative schemes for ab initio total-energy calculations using a plane-wave basis set **1996**, *54*, 11169-11186.

(28) Kresse, G.; Hafner, J. *Phys. Rev. B* Ab initio molecular dynamics for liquid metals **1993**, *47*, 558-561.

(29) Kresse, G.; Joubert, D. *Phys. Rev. B* From ultrasoft pseudopotentials to the projector augmented-wave method **1999**, *59*, 1758-1775.

(30) Le Roy, J.; Moreau, J.-M.; Paccard, D.; Parthe, E. *Acta Crystallogr. Sect. B: Struct. Sci.* R_3T_2 compounds (R = rare earth or Y; T = Rh, Pd, Pt) with the rhombohedral Er_3Ni_2 structure type **1977**, *33*, 2414-2417.

(31) Komarovskaya, L.; Skolozdra, R. *Dopovidi akademii nauk Ukrains'koi RSR, Seriya A* The crystal structure of $Gd_3Ni_8Sn_{16}$ and RNi_3Sn_2 (R = rare-earth element) compounds **1985**, *47*, 81-83.

(32) Flandorfer, H.; Rogl, P. *J. Solid State Chem.* The Crystal Structure of Two Novel Compounds: $CeAlSi_2$ and $Ce_3Al_4Si_6$ **1996**, *127*, 308-314.

(33) Tursina, A.; AV, G.; Bukhan'ko, N.; Rogl, P.; Seropegin, Y. *Chem. Met. Alloys* Crystal structure of the novel compound $Ce_3Pt_4Al_6$ **2008**, *1*, 62-66.

(34) Gribanov, A. V.; Sologub, O. L.; Salamakha, P. S.; Bodak, O. I.; Seropegin, Y. D.; Pecharsky, V. K. *J. Alloys Compd.* Crystal structure of the compound $Ce_3Pt_4Ge_6$ **1992**, *179*, L7-L11.

(35) Niepmann, D.; Pöttgen, R.; Künnen, B.; Kotzyba, G.; Mosel, B. D. *Chem. Mater.* The Stannides $La_3Pd_4Sn_6$, $Ce_3Pd_4Sn_6$, and $Pr_3Pd_4Sn_6$: A New Structure Type with a Complex Three-Dimensional $[Pd_4Sn_6]$ Polyanion **2000**, *12*, 533-539.

(36) Imre, A.; Hellmann, A.; Mewis, A. *Z. Anorg. Allg. Chem.* Neue Germanide mit geordneter $Ce_3Pt_4Ge_6$-Struktur – Die Verbindungen $Ln_3Pt_4Ge_6$ (Ln: Pr–Dy) **2006**, *632*, 1145-1149.

(37) Venturini, G.; Malaman, B. *J. Less Common Met.* Crystal structure of $Y_3Pt_4Ge_6$: An intergrowth of $BaAl_4$ and $YIrGe_2$ slabs **1990**, *167*, 45-52.

(38) Yatsenko, S. P.; Hladyschewsky, R. E.; Sitschewitsch, O. M.; Belsky, V. K.; Semyannikov, A. A.; Hryn, Y. N.; Yarmolyuk, Y. P. *J. Less Common Met.* Kristallstruktur von Gd_3Ga_2 und isotypen Verbindungen **1986**, *115*, 17-22.

(39) Zimmermann, S.; Brühmann, M.; Casper, F.; Heyer, O.; Lorenz, T.; Felser, C.; Mudring, A. V.; Meyer, G. *Eur. J. Inorg. Chem.* Eight-Coordinate Endohedral Rhenium, Osmium and Iridium Atoms in Rare-Earth Halide Cluster Complexes **2010**, *2010*, 2613-2619.

(40) Li, J.; Hoffmann, R.; Badding, M. E.; DiSalvo, F. J. *Inorg. Chem.* Electronic and structural properties of the novel chain compound tantalum telluride silicide, Ta_4Te_4Si **1990**, *29*, 3943-3952.

(41) Brühmann, M.; Mudring, A. V.; Valldor, M.; Meyer, G. *Eur. J. Inorg. Chem.* $\{Os_5Lu_{20}\}I_{24}$, the First Extended Cluster Complex of Lutetium with Eight-Coordinate Endohedral Osmium Atoms in Two Different Environments **2011**, *2011*, 4083-4088.

(42) Galadzhun, Y. V.; Zaremba, V. I.; Kalychak, Y. M.; Davydov, V. M.; Pikul, A. P.; Stępień-Damm, A.; Kaczorowski, D. *J. Solid State Chem.* $R_{12}Pt_7In$ (R=Ce, Pr, Nd, Gd, Ho)–new derivatives of the Gd_3Ga_2-type **2004**, *177*, 17-25.

(43) Lemaire, R.; Schweizer, J.; Yakinthos, J. *Acta Crystallogr. Sect. B* Structure cristalline des composes intermetalliques T_4Co_3 (T = Y, Gd, Tb, Dy, Ho, Er et Tm) **1969**, *25*, 710-713.

(44) Palenzona, A. *J. Alloys Compd.* The phase diagram of the La—Rh system **1992**, *190*, 13-15.

(45) Abdusalyamova, M. N.; Burnashev, O. R.; Mironov, K. Y. *J. Less Common Met.* The alloy systems Ln-Sb **1986**, *125*, 1-6.

(46) Fornasini, M.; Palenzona, A. *Z. Kristallogr.* The crystal structure of Ce_4Ru_3 **1992**, *200*, 57.

(47) Shoemaker, C. B.; Shoemaker, D. P. *Acta Crystallogr.* A ternary alloy with $PbCl_2$-type structure: TiNiSi(E) **1965**, *18*, 900-905.

(48) Riecken, J. F.; Rodewald, U. C.; Heymann, G.; Rayaprol, S.; Huppertz, H.; Hoffmann, R. D.; Poettgen, R. *Z. Naturforsch.* Synthesis, Structure and Properties of the High-pressure Modifications of the Ternary Compounds REPtSn (RE = La, Pr, Sm) **2006**, *61b*, 1477-1484.

(49) Smetana, V.; Rhodehouse, M.; Meyer, G.; Mudring, A.-V. *Acc. Chem. Res.* Gold polar intermetallics: structural versatility through exclusive bonding motifs **2017**, *50*, 2633-2641.

(50) Smetana, V.; Corbett, J. D.; Miller, G. J. *Inorg. Chem.* Four polyanionic compounds in the K-Au-Ga system: a case study in exploratory synthesis and of the art of structural analysis **2012**, *51*, 1695-1702.

(51) Smetana, V.; Miller, G. J.; Corbett, J. D. *Inorg. Chem.* Three alkali-metal-gold-gallium systems. Ternary tunnel structures and some problems with poorly ordered cations **2012**, *51*, 7711-7721.

(52) Bilodeau, R. C.; Scheer, M.; Haugen, H. K.; Brooks, R. L. *Physical Review A* Near-threshold laser spectroscopy of iridium and platinum negative ions: Electron affinities and the threshold law **1999**, *61*, 012505.

(53) Vandevraye, M.; Drag, C.; Blondel, C. *J. Phys. B-At., Mol. Opt. Phys.* Electron affinity of tin measured by photodetachment microscopy **2013**, *46*, 125002.

(54) Andersen, T. *Physics Reports* Atomic negative ions: structure, dynamics and collisions **2004**, *394*, 157-313.

(55) Allred, A. L. *J. Inorg. Nucl. Chem.* Electronegativity values from thermochemical data **1961**, *17*, 215-221.

(56) Dai, J.-C.; Corbett, J. D. *Inorg. Chem.* Transformation of $AeIn_4$ indides (Ae = Ba, Sr) into an $AeAu_2In_2$ structure type through gold substitution **2007**, *46*, 4592-4598.

(57) Liu, S.; Corbett, J. D. *Inorg. Chem.* Ba_2AuTl_7: An intermetallic compound with a novel condensed structure **2004**, *43*, 2471-2473.

(58) Palasyuk, A.; Dai, J.-C.; Corbett, J. D. *Inorg. Chem.* $SrAu_4In_4$ and $Sr_4Au_9In_{13}$: Polar intermetallic structures with cations in augmented hexagonal prismatic environments **2008**, *47*, 3128-3134.

(59) Zhuravleva, M. A.; Bilc, D.; Mahanti, S. D.; Kanatzidis, M. G. *Z. Anorg. Allg. Chem.* Single Crystal X-ray Structure Investigation and Electronic Structure Studies of La-Deficient Nickel Stannide $La_{4.87}Ni_{12}Sn_{24}$ Grown from Sn Flux **2003**, *629*, 327-334.

(60) Romaka, V. V.; Hlil, E. K.; Romaka, L.; Gignoux, D.; Fruchart, D.; Horyn, A.; Miraglia, S. *J. Alloys Compd.* Crystallographic, magnetic and electrical characteristics of some $R_{5-x}Ni_{12}Sn_{24+x}$ intermetallics **2010**, *493*, 35-40.

(61) Harmening, T.; Hermes, W.; Eul, M.; Pöttgen, R. *Solid State Sci.* Mixed valent stannide $EuRuSn_3$ – Structure, magnetic properties, and Mössbauer spectroscopic investigation **2010**, *12*, 284-290.

(62) Bauer, E.; Nowotny, H.; Stempfl, A. *Monatsh. Chem.* Roentgenographishce untersuchungen im System: Platin - Quecksilber **1953**, *84*, 692-700.

(63) Karpov, A.; Nuss, J.; Wedig, U.; Jansen, M. *Angew. Chem. Int. Ed.* Cs2Pt: A Platinide(-II) Exhibiting Complete Charge Separation **2003**, *42*, 4818-4821.

(64) Smetana, V.; Mudring, A.-V. *Angew. Chem. Int. Ed.* Cesium platinide hydride $4Cs_2Pt{\cdot}CsH$: an intermetallic double salt featuring metal anions **2016**, *55*, 14838-14841.

(65) Samal, S. L.; Corbett, J. D. *Z. Anorg. Allg. Chem.* Synthesis, structure, and bonding analysis of the polar Intermetallic phase Ca_2Pt_2Cd **2012**, *638*, 1963-1969.

(66) Samal, S. L.; Gulo, F.; Corbett, J. D. *Inorg. Chem.* Cluster chemistry in electron-poor Ae–Pt–Cd systems (Ae = Ca, Sr, Ba): $(Sr,Ba)Pt_2Cd_4$, $Ca_6Pt_8Cd_{16}$, and its known antitype $Er_6Pd_{16}Sb_8$ **2013**, *52*, 2697-2704.

(67) Gulo, F.; Samal, S. L.; Corbett, J. D. *Inorg. Chem.* Substantial Cd–Cd bonding in Ca_6PtCd_{11}: a condensed intermetallic phase built of pentagonal Cd_7 and rectangular $Cd_{4/2}Pt$ Pyramids **2013**, *52*, 10112-10118.

(68) Provino, A.; Steinberg, S.; Smetana, V.; Paramanik, U.; Manfrinetti, P.; Dhar, S. K.; Mudring, A.-V. *Cryst. Growth Des.* Gold in the layered structures of $R_3Au_7Sn_3$: from relativity to versatility **2016**, *16*, 5657-5668.

(69) Cordero, B.; Gomez, V.; Platero-Prats, A. E.; Reves, M.; Echeverria, J.; Cremades, E.; Barragan, F.; Alvarez, S. *Dalton Trans.* Covalent radii revisited **2008**, 2832-2838.

(70) Smetana, V.; Corbett, J. D.; Miller, G. J. *J. Solid State Chem.* $Na_8Au_{9.8(4)}Ga_{7.2}$ and $Na_{17}Au_{5.87(2)}Ga_{46.63}$: The diversity of pseudo 5-fold symmetries in the Na–Au–Ga system **2013**, *207*, 21-28.

(71) ICSD, FIZ-Karlsruhe, Karlsruhe, Germany, 2018.

CHAPTER 4. TERNARY POLAR INTERMETALLICS IN THE SYSTEMS Pt/Sn/*R* (*R* = La-Sm): STANNIDES OR PLATINIDES?

Melissa L. Rhodehouse,[†‡] Volodymyr Smetana,[‡§] Anja-Verena Mudring,[‡§⊥] and Gerd H. Meyer,[†‡*]

[†]Department of Chemistry, Iowa State University, Ames, IA, 50011, USA
[‡]Ames Laboratory, USDOE, Iowa State University, Ames, IA 50011, USA
[§]Department of Materials and Environmental Chemistry, Stockholm University, Svante Arrhenius väg 16 C, 10691 Stockholm, Sweden
[⊥]Department of Materials Science and Engineering, Iowa State University, Ames, IA 50011, USA

Abstract

Starting with a 4:6:3 molar ratio of Pt, Sn and *R* with *R* = La-Sm, with or without the application of a NaCl flux, seven ternary compounds were obtained as single crystals. The platinides $Pt_4Sn_6R_3$, *R* = La-Nd, crystallize with the $Pt_4Ge_6Pr_3$ type of structure (*oP*52, *Pnma*, *a* = 27.6–27.8 Å, *b* = 4.59–4.64 Å, *c* = 9.35–9.40 Å). With *R* = Pr and Nd, $Pt_4Sn_6R_{3-x}$ ternaries are obtained which are considered as high-temperature polymorphs with disorder on Sn and *R* sites and under-occupation at the *R* sites (x = 0.09 for Pr, and 0.11 for Nd; *oP*52, *Pnma*, *a* = 7.28–7.29 Å, *b* = 4.48–4.49 Å, *c* ≈ 35.1 Å). At this point in the lanthanide series, the composition $Pt_4Sn_6R_{3-x}$ seems to come to an end. With *R* = Sm $Pt_7Sn_9Sm_5$ (*oS*42, *Amm*2, *a* = 4.3289(5) Å, *b* = 28.798(4) Å, *c* = 7.2534(9) Å) is obtained under otherwise the same conditions. It exhibits the rare $Zr_5Pd_9P_7$ type of structure, linking polar intermetallics to metal phosphides, in accord with $P_7Pd_9Zr_5$ = $Pt_7Sn_9Sm_5$. All structures may be described in terms of either negative Pt/Sn networks encapsulating positive *R* atoms, or $\{PtSn_x\}$ clusters (x = 5, 6) sharing vertices and edges with *R* in the second coordination sphere and with considerable heterometallic Pt-*R* bonding contributions.

Introduction

Cluster complex halides such as $\{PtPr_6\}I_{10}$ with isolated $\{PtPr_6\}$ clusters or $\{PtPr_3\}Br_3$ with cluster chains constitute a symbiosis between intermetallic and salt.[1] Subsequent elimination of the halide ligands, i.e. successive cluster condensation, results in polar intermetallics, e.g. Pt_3Pr_4 with essentially heterometallic bonding features.[2] The addition of a reactive metal, e.g. as a tin melt, forces competition between the more electropositive metals Pr and Sn for the first coordination sphere of the most electron affine metal, Pt. Surprisingly, Sn wins although it has a larger electron affinity than Pr.

There was only one ternary phase known in the system Pt/Sn/Pr, the equiatomic PtSnPr with the SiTiNi type of structure, an *anti*-derivative of cottunite, $PbCl_2$, first reported in 1973.[3] We have recently added $Pt_4Sn_6Pr_3$ and $Pt_4Sn_6Pr_{2.91}$ as well as $Pt_{12}Sn_{25}Pr_4$.[2] The first two are members of a prolific family of intermetallics, $T_4E_6R_3$ (T = transition metal; E = p-block main group metal or metalloid; R = rare earth metal) with a growing number of structure types, sometimes with under-occupation and/or disorder: monoclinic $Pt_4Ge_6Y_3$ ($P2_1/m$)[4] and the disordered variant $Pt_4Yb_3Si_{5.7}$ ($P2_1/m$)[5] as well as five orthorhombic structures, slightly disordered $Pt_4Ge_6Ce_3$ (*Cmcm*),[6] $Pt_4Ge_6Pr_3$ (*Pnma*, R = Pr–Dy),[7] $Pd_4Sn_6Ce_3$ (*Pnma*, R = La-Pr),[8] $Pt_4Al_6Ce_3$ (*Pnma*)[9], and $Pt_4Sn_6Pr_{3-x}$ (*Pnma*, R = Pr).[2] The structures of this family are usually described as stacked pentagonal and hexagonal nets of mixed Sn and Pt atoms encapsulating the R atoms with high coordination numbers of 14-16. As $Pt_4Sn_6Pr_3$ and $Pt_4Sn_6Pr_{2.91}$ are closely related, the aim of this research was to figure out what the substitution of Pr by other lanthanides (R = La-Sm) would do to the existence and the crystal chemistry of these ternary intermetallics.

Experimental section

Synthesis. Starting materials were Pt beads (99.9%), La, Ce, Pr, Nd, Sm and Sn pieces (99.9%), and NaCl (99.9% purity). NaCl was dried in an oven at 80˚C overnight before placing inside an argon filled glovebox. All samples, between 250-500 mg, were weighed and loaded into tantalum ampules inside an argon-filled glovebox. Ampules were sealed under argon followed by sealing in evacuated silica tubes. Samples were placed in a furnace at 1000˚C for 24 hours followed by slow cooling (-20˚C·hr^{-1}) to 850˚C or 700°C and annealed for 72 hours. The NaCl flux was removed with water after the end of the reaction.

$Pt_4Sn_6R_3$ and $Pt_4Sn_6R_{3-x}$. Loadings of rare earth metals (R = La-Nd) with Pt and Sn pieces in molar ratios of Pt:Sn:R = 4:6:3 were weighed and placed inside tantalum tubes along with approximately 250 mg of NaCl. Samples were sealed under the same conditions and placed in a tube furnace following the heating profile described above. The somewhat disordered $Pt_4Sn_6R_{3-x}$ modification has been detected in the samples annealed at higher temperatures. No disordered variants have been detected in the samples with R = La and Ce.

$Pt_7Sn_9Sm_5$. The starting composition for $Sm_3Pt_4Sn_6$ was weighed and loaded according to the above indicated method with NaCl as a flux. The sample was sealed and heated according to the same scheme. The resulting product was identified via powder X-ray diffraction to be multiphase containing $Sm_5Pt_7Sn_9$ as the main product with further unknown phases. Small crystals of $Sm_5Pt_7Sn_9$ were selected and characterized by single-crystal X-ray diffraction.

Structure analysis. Powder and single crystal X-ray diffraction were used to characterize products. Samples were crushed in air and a portion ground to a fine powder for phase analysis. Powders were sandwiched between greased Mylar sheets housed by an aluminum holder. Data was gathered on a STOE STADI P image plate diffractometer (Cu Kα1 radiation, λ = 0.71073 Å; Si external standard, a = 5.4308(1) Å) and analyzed using WinXPow software.[10] Single crystal

X-ray diffraction was performed on a Bruker APEX CCD and Bruker VENTURE diffractometer (both Mo-Kα radiation, λ = 0.71073 Å), respectively. The raw frame data were collected using the Bruker APEX3 program,[11] while the frames were integrated with the Bruker SAINT[12] software package using a narrow-frame algorithm integration of the data and were corrected for absorption effects using the multi-scan method (SADABS).[13] All positions were refined anisotropically. Initial models of the crystal structures were first obtained with the program SHELXT-2014[14] and refined using the program SHELXL-2014[15] within the APEX3 software package. Crystallographic details and refinement parameters for $Pt_4Sn_6R_3$ and $Pt_4Sn_6R_{3-x}$ (*R* = La, Ce, Nd) and $Sm_5Pt_7Sn_9$ are summarized in Table 1; Table 2 contains atomic positions and equivalent thermal parameters of $Pt_4Sn_6Nd_3$, $Pt_4Sn_6Nd_{2.89}$ and of $Sm_5Pt_7Sn_9$. Further data have been deposited, see Supplemental Information.

Results and discussion

It is surprising that, until recently, the only ternary intermetallic compound known in the Pt/Sn/*R* systems have been the isocompositional PtSn*R* with *R* throughout the whole lanthanide series including yttrium.[3,16-17] The ambient pressure forms of PtSn*R* with *R* = Tb-Lu, Y[3] crystallize with the PtHoSn/NiZrAl type, an *anti*-derivative of Fe_2P, or with the SiTiNi type, an *anti*-derivative of cotunnite ($PbCl_2$), *R* = La-Eu.[16,17] In PtSnPr, Pr has twelve nearest neighbors from 3.130 to 3.596 Å, as heterometallic $\{PrPt_6Sn_6\}$ clusters, and Pt, the most electronegative of the three atom types, has four Sn (2.729-2.897 Å) as nearest and six Pr (3.130-3.596 Å) as second-nearest neighbors.

The reaction of binary Pt/Pr alloys, such as Pt_2Pr_3, with an, obviously reactive, tin flux yielded two new ternary intermetallics within the Pt/Sn/Pr system, $Pt_{12}Sn_{25}Pr_4$ and $Pt_4Sn_6Pr_3$ with 29.2 and 30.8 mol.% Pt, respectively.[2] Subsequent reactions with stoichiometric loadings of

$Pt_4Sn_6Pr_3$ with an unreactive NaCl flux, and without, resulted in two different products. First, stoichiometric $Pt_4Sn_6Pr_3$ crystallizing with the $Pt_4Ge_6Pr_3$ type of structure,[7] secondly, slightly sub-stoichiometric $Pt_4Sn_6Pr_{2.91}$, with a new structure type. Utilizing the same NaCl flux, single crystals of $Pt_4Sn_6R_3$ were grown for R = La, Ce, (Pr) and Nd, all of which adopt the reported $Pt_4Ge_6Pr_3$ type. The new $Pt_4Sn_6R_{3-x}$ type is obtained with R = Pr (x = 0.09) and Nd (x = 0.11). These slightly sub-stoichiometric ternary intermetallics appear to be the high-temperature "modifications" of the $Pt_4Ge_6R_3$ type. All attempts to produce the isocompositional $Pt_4Sn_6Sm_3$ or $Pt_4Sn_6Sm_{3-x}$ have failed.

Table 1. Crystallographic details and refinement parameters for $R_xPt_ySn_z$ (R = La, Ce, Nd, Sm).

Formula	$Pt_4Sn_6La_3$	$Pt_4Sn_6Ce_3$	$Pt_4Sn_6Nd_3$	$Pt_4Sn_6Nd_{2.89}$	$Pt_7Sn_9Sm_5$*
Structure type	$Pt_4Ge_6Pr_3$	$Pt_4Ge_6Pr_3$	$Pt_4Ge_6Pr_3$	$Pt_4Sn_6Pr_{3-x}$	$Zr_5Pd_9P_7$
Form. wt., g/mol	1909.23	1912.86	1925.22	1909.35	3185.59
Space group, Z	*Pnma* (no. 62), 4	*Pnma* (no. 62), 4	*Pnma (no. 62), 4*	*Pnma* (no. 62), 4	*Amm*2 (no. 38), 2
a, Å	27.787(5)	27.7018(7)	27.655(3)	7.2821(7)	4.3289(5)
b, Å	4.6380(9)	4.6149(1)	4.5851(4)	4.4782(5)	28.798(4)
c, Å	9.399(2)	9.3712(2)	9.342(1)	35.116(3)	7.2534(9)
V, Å^3	1211.3(4)	1198.02(5)	1184.6(2)	1145.2(2)	904.2(2)
Density (calculated) [g/cm^3]	10.469	10.605	10.795	11.075	11.700
μ, mm^{-1}	68.374	69.835	72.247	74.247	81.967
F (000)	3132	3144	3168	3142	2612
θ range, °	1.5 to 35.0	2.0 to 29.1	2.3 to 30.0	2.3 to 27.5	2.8 to 30.0
Index ranges	$-44 \le h \le 43$ $-7 \le k \le 7$ $-15 \le l \le 15$	$-38 \le h \le 38$ $-6 \le k \le 6$ $-13 \le l \le 13$	$-36 \le h \le 38$ $-4 \le k \le 6$ $-11 \le l \le 11$	$-9 \le h \le 7$ $-5 \le k \le 5$ $-45 \le l \le 32$	$-6 \le h \le 6$ $-40 \le k \le 35$ $-9 \le l \le 10$
Intensity data collected	22068	13338	6625	9282	4663
No. of independent reflections	2942 [R_{int} = 0.0649]	1956 [R_{int} = 0.0714]	1800 [R_{int} = 0.0554]	1479[R_{int} = 0.0964]	1956 [R_{int} = 0.0388]
Refinement method	Full-matrix least-squares on F^2				
Data/ Restraints/ Parameters	2942/ 0/ 80	1956 / 0 / 80	1800 / 0 / 80	1479 / 0 / 88	1394 / 0 / 68
Goodness-of-fit (F^2)	1.032	1.025	0.95	1.116	1.043
R_1; ωR_2 [$I_0 > 2\sigma$ (I)]	0.0389; 0.0812	0.0405; 0.0984	0.0442; 0.1005	0.0633; 0.1239	0.0224; 0.0438
R_1; ωR_2 (all data)	0.0610; 0.0875	0.0593; 0.1057	0.0838; 0.1125	0.0823; 0.1305	0.0243; 0.0441
Largest diff. peak and hole [e·Å^{-3}]	4.312 and –4.344	4.377 and –7.154	5.434 and –4.300	5.799 and –6.434	2.197 and –2.584

* Flack parameter = 0.036(13)

Table 2. Atomic positions and equivalent thermal parameters of $Pt_4Sn_6Nd_3$, $Pt_4Sn_6Nd_{2.89}$ and $Pt_7Sn_9Sm_5$.

Atom	Wyckoff site	*x*	*y*	*z*	U_{eq}	*SOF*
			$Pt_4Sn_6Nd_3$			
Pt1	4*c*	0.54411(2)	¼	0.1301(3)	0.0079(2)	
Pt2	4*c*	0.44962(3)	¾	0.3798(3)	0.0095(2)	
Pt3	4*c*	0.31348(2)	¾	0.1192(2)	0.0065(2)	
Pt4	4*c*	0.68647(3)	¼	0.3687(2)	0.0068(2)	
Sn1	4*c*	0.49638(5)	¾	0.1288(4)	0.0079(3)	
Sn2	4*c*	0.49838(5)	¼	0.3783(4)	0.0080(3)	
Sn3	4*c*	0.63755(4)	¼	0.1247(4)	0.0083(3)	
Sn4	4*c*	0.28345(5)	¼	0.2199(2)	0.0071(3)	
Sn5	4*c*	0.35654(5)	¾	0.3750(4)	0.0113(3)	
Sn6	4*c*	0.71658(5)	¾	0.4692(2)	0.0067(3)	
Nd1	4*c*	0.40650(4)	¼	0.1153(3)	0.0105(3)	
Nd2	4*c*	0.71982(3)	¾	0.1251(2)	0.0064(2)	
Nd3	4*c*	0.59387(4)	¾	0.3641(3)	0.0091(3)	
			$Pt_4Sn_6Nd_{2.89}$			
Pt1	4*c*	0.8900(2)	¾	0.71244(4)	0.0038(3)	
Pt2	4*c*	0.4310(2)	¼	0.67025(4)	0.0038(4)	
Pt3	4*c*	1.1381(2)	¾	0.58447(4)	0.0040(3)	
Pt4	4*c*	0.6330(2)	¼	0.54443(4)	0.0061(4)	
Sn1	4*c*	0.8081(4)	¼	0.67456(7)	0.0053(6)	
Sn2	4*c*	1.0104(4)	¾	0.78739(7)	0.0038(3)	
Sn3	4*c*	1.1733(4)	¾	0.66039(7)	0.0038(3)	
Sn4	4*c*	0.3498(4)	¼	0.59573(7)	0.0045(6)	
Sn5	4*c*	0.5863(4)	¼	0.46883(7)	0.0051(6)	
Sn6	4*c*	0.9350(5)	¼	0.58974(18)	0.0040(3)	0.73(1)
Sn7	4c	0.9460(15)	¼	0.5755(5)	0.0040(3)	0.27(1)
Nd1	4*c*	0.1744(3)	¼	0.73370(5)	0.0040(5)	
Nd2	4*c*	0.6570(3)	¾	0.61685(6)	0.0092(5)	
Nd3	4*c*	0.8849(11)	¾	0.5043(2)	0.0150(14)	0.366(8)
Nd4	4c	0.8625(7)	¾	0.52520(13)	0.0150(14)	0.52(1)
			$Pt_7Sn_9Sm_5$			
Pt1	2*a*	0	½	0.3897(2)	0.0048(2)	
Pt2	4*e*	½	0.92479(3)	0.3938(1)	0.0081(2)	
Pt3	4*e*	½	0.64679(3)	0.4415(1)	0.0063(2)	
Pt4	4*d*	0	0.79125(3)	0.4858(1)	0.0051(2)	
Sn1	4*e*	½	0.55556(6)	0.5255(2)	0.0049(3)	
Sn2	2*b*	½	0	0.6327(3)	0.0052(4)	
Sn3	4*e*	½	0.83999(6)	0.5624(2)	0.0046(3)	
Sn4	4*d*	0	0.70123(6)	0.3701(2)	0.0049(3)	
Sn5	4*d*	0	0.86855(6)	0.2296(2)	0.0076(3)	
Sm1	2*a*	0	½	0.7993(2)	0.0054(3)	
Sm2	4*d*	0	0.41027(4)	0.2013(2)	0.0059(2)	
Sm3	4*e*	½	0.72874(4)	0.6957(1)	0.0051(2)	

Crystal Structures. Polar intermetallics of the composition $Pt_4Sn_6R_3$ (**1**, 23.1 mol-% *R*) exist with *R* = La─Nd (*oP*52, *Pnma*, *a* = 27.6–27.8 Å, *b* = 4.59–4.64 Å, *c* = 9.35–9.40 Å). With *R* = Pr, Nd, a closely related composition exists, $Pt_4Sn_6R_{3-x}$, with a crystal structure only recently been reported for $Pt_4Sn_6Pr_{2.91}$ (**2**, 22.5 mol-% *R*, *oP*52, *Pnma*, *a* = 7.28–7.29 Å, *b* = 4.48–4.49 Å, *c* ≈ 35.1 Å). A stoichiometric loading of $Pt_4Sn_6Sm_3$ together with the same reaction conditions resulted in $Pt_7Sn_9Sm_5$ (**3**, 23.8 mol-% Sm, *oS*42, *Amm*2, *a* = 4.3289(5) Å, *b* = 28.798(4) Å, *c* = 7.2534(9) Å). The closely related $Pt_3Sn_5Eu_2$ (20 mol-% Eu) had already been reported with a similar unit cell (**4**, *oS*40, *Cmc*2_1, *a* = 4.533 Å, *b* = 26.629 Å, *c* = 7.318 Å).[18] Table S1 contains crystallographic details for all structures of compounds just mentioned except for $Pt_4Sn_6Pr_3$ and $Pt_4Sn_6Pr_{2.91}$ which have been reported in a preceding article.[2] Table S2 gives atomic parameters for $Pt_4Sn_6Nd_3$, $Pt_4Sn_6Nd_{2.89}$ and for $Pt_7Sn_9Sm_5$. Although the full picture of all phases that might exist in the ternary systems Pt/Sn/*R* is certainly not known to date, the close compositions of **1** = $PtSn_{1.50}R_{0.75}$, **2** = $PtSn_{1.50}R_{0.73}$, **3** = $PtSn_{1.29}Sm_{1.29}$, and **4** = $PtSn_{1.67}Eu_{0.67}$ and strong structural similarities may make a point for the strong influence of geometric factors in the variation within the greater structural family. Although being not directly related, $Pt_4Sn_6Nd_3$ and $Pt_7Sn_9Sm_5$ both show a direct group-subgroup relationship to $Pt_3Sn_5Eu_2$ through *Pmc*2_1.

The new ternary intermetallics $Pt_4Sn_6R_3$ (*R* = La–Nd, **1**) are isostructural with the analogous so-called germanides, $Pt_4Ge_6R_3$, which include *R* = Pr, Nd, Sm, Gd, Tb, Dy[7] while $Pt_4Ge_6La_3$ has never been reported and those with *R* = Ce[6] and Y[5] belong to closely related derivatives.

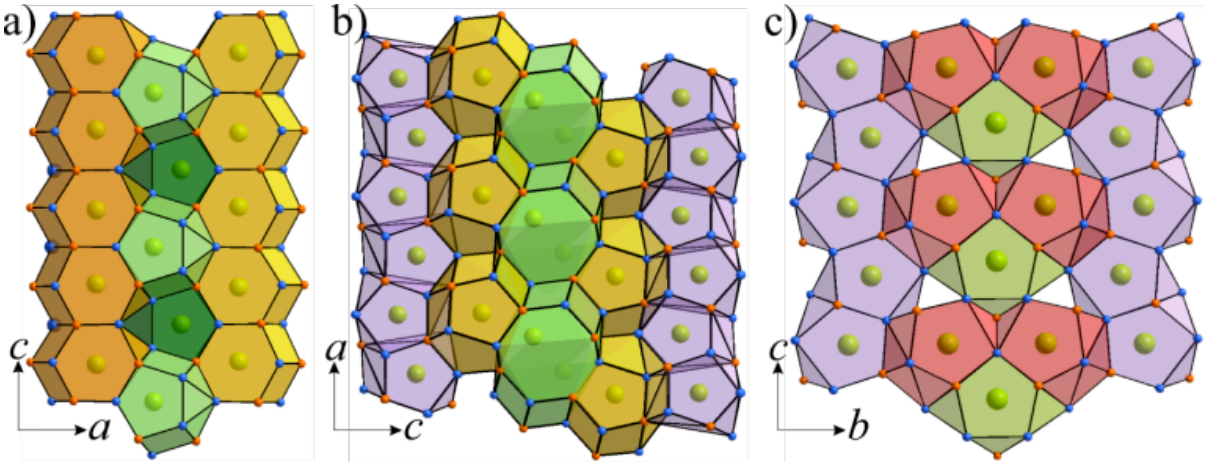

Figure 1. Projections of the crystal structures of $Pt_4Sn_6R_3$ (**1**, *R* = La-Nd), $Pt_4Sn_6R_{3-x}$ (**2**, *R* = Pr, Nd) and $Pt_7Sn_9Sm_5$ (**3**) onto equivalent planes.

There are usually alternative ways to describe crystal structures. In the present case, one can either start with, first, heteroatomic Pt and Sn clusters encapsulating endohedral *R* atoms, or secondly, with Pt centered Sn clusters which are surrounded, in the second coordination sphere, by *R* atoms. Either way, these building units, $\{RPt_xSn_y\}$ or $\{PtSn_y\}R_z$ (Fig. 1), are connected to three-dimensional structures. In the first description, a three-dimensional heteroatomic network of atoms with high electronegativities, 2.28 (Pt) and 1.96 (Sn) in the Pauling scale,[19] encapsulates electropositive lanthanide atoms *R* (EN = 1.13 for Pr). In the second way of description, the atom with the highest electron affinity, EA(Pt) = 205.3 kJ/mol, is surrounded by five or six Sn atoms, EA(Sn) = 116 kJ/mol, and additional *R* atoms at larger distances. Philosophically, we treat the structures of these polar ternary intermetallics as either Werner type coordination complexes, with the positive central atom (*R*) surrounded by negative ligands (Pt, Sn), $[RPt_xSn_y]$ or we consider them as *anti*-Werner type cluster complexes[20], $\{PtSn_y\}R_z$, with the atom of the highest electron affinity, Pt, as the central atom. The latter description paves a way to a better understanding of the condensation of clusters from cluster complexes like $\{PtPr_6\}I_{12}Pr$ via binary Pt_3Pr_4 (with $\{PrPr_x\}$ clusters) to ternaries like $Pt_4Sn_6Pr_3$.

Let us start with the perhaps more classical description. The crystal structures of all compounds in this article may be described in terms of network structures where the electronegative Pt and Sn atoms form tunnels along certain directions including the large *R* atoms which, viewed alone, form straight or zigzag chains (Fig. 1). Thus, the stoichiometric $Pt_4Sn_6R_3$ (**1**) with the $Pt_4Ge_6R_3$ type of structure exhibits linear one-side branched channels along the *b* and *c* axes. The structure is then formed of *R* centered heteroatomic clusters consisting of three parallel membered rings 6-4-6−{RPt_7Sn_9} forming the stem and 5-5-5−{RPt_6Sn_9} are responsible for the branches (Figs. 1a and 2a). On the other hand, these clusters can be represented as randomly equatorially capped hexagonal and pentagonal prismatic polyhedra. Each branch polyhedron has common pentagonal faces with two stem polyhedra and shares pentagonal faces with identical units along the *b* axis forming a parallel tunnel.

Although $Pt_4Sn_6R_{3-x}$ (*R* = Pr, Nd, **2**) have the same space group symmetry, almost identical compositions and unit cell volumes, the compounds show distinct differences in atomic packing (Fig. 1b) and exhibit disorder of both cationic (*R*) and anionic (Sn) sites. From the cationic point of view the structure contains three building units, 4-7-4−{RPt_7Sn_8}, 5-7-5−{RPt_7Sn_{10}} and 5-4-5−{RPt_6Sn_8}. The 4-7-4 units form two-side branched octagonal tunnels along the *b* (Fig. 1b), having large hexagonal faces shared with the 5-7-5 forming the branches. Similar tunnels were frequently observed for the *A*–Au–*Tr* intermetallics (*A* = active metal, *Tr* = triel)[21,22] including cationic zigzag chains and large positional disorders. A separate set of pentagonal tunnels along the *b* direction is observed in between forming cationic zigzag chains along the *a* axis through bigger shared hexagonal faces (Figs. 1b and 2c, violet). The packing of green, yellow and violet polyhedra (Fig. 2c) results in smaller voids in the form of tetrahedral stars that are, again, reminiscent of the active metal polar intermetallics, e.g. $A_{0.55}Au_2Ga_2$.[21]

$Pt_7Sn_9Sm_5$ (**3**) crystallizes with a slightly lower symmetric, well ordered representative of the series, though with slightly different atomic ratios, i.e. $PtSn_{1.29}Sm_{0.71}$ instead of $PtSn_{1.5}R_{0.75}$. The new $Pt_7Sn_9Sm_5$ belongs to the very rare $Zr_5Pd_9P_7$ structure type linking polar intermetallics to metal phosphides in accord with the formulation $P_7Pd_9Zr_5 = Pt_7Sn_9Sm_5$.

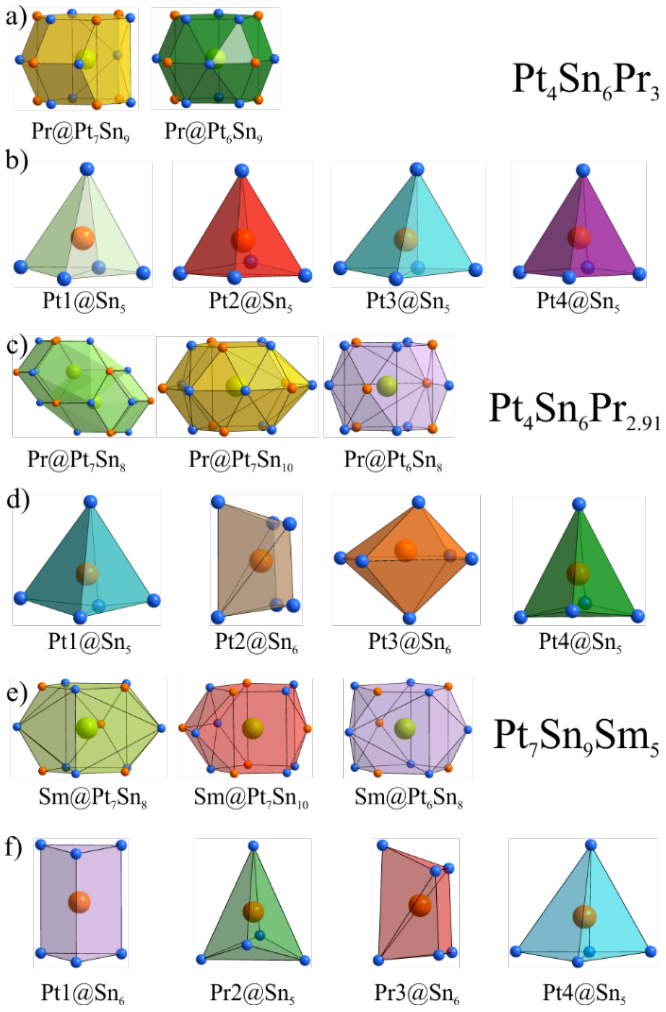

Figure 2. *R* and Pt centered clusters in the crystal structures of $Pt_4Sn_6R_3$ (**1**, *R* = La-Nd), $Pt_4Sn_6R_{3-x}$ (**2**, *R* = Pr, Nd) and $Pt_7Sn_9Sm_5$ (**3**).

Similar to **2**, three types of $\{SmPt_xPr_y\}$ polyhedra of similar architectures (Fig. 1c) build the entire structure. They are connected to form pentagonal channels along *a* with a different degree of fusion with the neighboring units. 5-3-5−$\{SmPt_5Sn_8\}$ clusters are responsible for the

zigzag chains along *b* sharing larger pentagonal faces with two identical polyhedra (Figs. 1c and 2e, violet).

5-4-5−{$SmPt_6Sn_8$} (red) together with 5-3-5−{$SmPt_5Sn_8$} (green) form fly-shaped trimers, separated in the *bc* plane. Green polyhedra share pentagonal faces with two red ones, while the latter have only a small trigonal face in common. The packing results in a limited number of small empty trigonal channels along the *a* axis. It is also worth noting that with the next *R* = Eu, $Pt_3Sn_5Eu_2$ exhibits similar cell parameters and zigzag chains of pentagonal 5-4-5−{$EuPt_6Sn_8$} clusters, but they are separated by more regular and well separated 5-8-5−{$EuPt_7Sn_{11}$} resulting in the compositional change from $Pt_7Sn_9Sm_5$ to $Pt_3Sn_5Eu_2$ = $PtSn_{1.67}Eu_{0.67}$.

In summary, the electropositive rare-earth element atoms *R* in $Pt_4Sn_6R_3$ (**1,** *R* = La-Nd), $Pt_4Sn_6R_{3-x}$ (**2**, *R* = Pr, Nd), $Pt_7Sn_9Sm_5$ (**3**) and $Pt_3Sn_5Eu_2$ (**4**) have high coordination numbers of 16 and 15 (**1**), 15, 17, 14 (**2**), and 13 (**3**) as well as 14, 18 (**4**) with heteroatomic "ligand" spheres of Pt and Sn atoms. As the atomic radii of Sn (1.45 Å) and Pt (1.35 Å)[23] are very similar, a mixed-ligand surrounding of the *R* atoms seems reasonable, which is actually obvious from the adoption of the (*anti*-)types of binary Fe_2P and $PbCl_2$, respectively, for the equiatomic PtSn*R* phases. For $Pt_4Sn_6Nd_3$, for example, with three crystallographically independent Nd positions, the average Nd-Pt/Sn distance is 3.538 Å (Table 1), with Nd-Sn distance ranges between 3.216 and 3.781 Å, as well as Nd-Pt 3.359 through 3.992 Å. The shortest distances are, therefore, close to the sum of the atomic radii of Pr (1.85 Å) and the average of Pt and Sn (1.40 Å), 3.25 Å. With the large coordination numbers of *R*, 16 and 15, respectively, the average distances have to be considerably longer. For the {RSn_9Pt_z} clusters they vary only little with the size of the rare-earth atoms, but there is a small lanthanide-contraction effect through the series $Pt_4Sn_6R_3$ (*R* = La-Nd), 3.489 (La)

to 3.465 Å (Nd). The average Sm-Sn/Pt distance in $Pt_7Sn_9Sm_5$ is much smaller (3.290 Å) which might be attributed to a coordination number of only 13 for all three Sm positions in the structure.

Table 3. Average distances and molar volumes[§] for ternary Pt/*E*/*R* intermetallics.

	$\{RSn_xPt_y\}$	$\{PtSn_xR_z\}$	Pt/Sn/*R*	Pt/Ge/*R*	
	R−Sn+Pt	Pt−Sn	Pt−*R*	V_m	V_m
$Pt_4Sn_6La_3$	3.487	2.675	3.536	182.4	
$Pt_4Sn_6Ce_3$	3.474	2.666	3.523	180.4	153.5
$Pt_4Sn_6Pr_3$	3.464	2.658	3.512	178.7	152.5
*$Pt_4Sn_6Nd_3$	3.463	2.657	3.511	178.3	151.0
$Pt_4Sn_6Pr_{2.91}$	3.381			173.0	
$Pt_4Sn_6Nd_{2.89}$	3.373			172.4	
$Pt_7Sn_9Sm_5$	3.290	2.816	3.122	272.3	
$Pt_3Sn_5Eu_2$	3.402	2.778	3.485	133.0	

[§]The molar volume, V_m, is calculated from the cell volume, V_E, via: $V_m = (V_E \times N_A)/Z$; with N_A Avogadro's constant and Z the number of formula units in the unit cell.
*The distances for this compound are curiously similar to that of the Pr analog and needs to be further investigated before submission.

In the second, the anti-Werner way to describe the crystal structures of these ternary phases, we take the atom with the highest electronegativity, or electron affinity, platinum, as the central atom. Then, in all of the structures discussed in this article, Pt is the central atom of a Sn polyhedron/cluster, $\{PtSn_x\}$ with x = 5, 6, see Fig. 2. All structures, $Pt_4Sn_6R_3$ (**1**, *R* = La-Nd), $Pt_4Sn_6R_{3-x}$ (**2**), $Pt_7Sn_9Sm_5$ (**3**) and $Pt_3Sn_5Eu_2$ (**4**) exhibit $\{PtSn_5\}$ square pyramids, whereas their proportion is changing from 100% in **1** to 50% in **2** and **3** and to 33% in **4**. **2**, **3** and the **4** further exhibit polyhedra close to trigonal prisms but show a slope of up to 30° between the horizontal faces. Finally, each of the latter contains one $\{PtSn_x\}$polyhedron atypical for any other structure, $\{PtSn_6\}$ octahedra in **2**, regular trigonal prisms in **3** and monocapped trigonal prisms in **4**. From this point of view, it becomes clear that the structure of **2** is at a transition point between those with *R* = La-Nd and *R* = Sm, Eu, the latter of which have not yet been obtained with $Pt_4Sn_6R_3$

stoichiometry. All the structures do, however, exhibit identical building principles forming chains through the edge and vertex sharing of the common {$PtSn_5$} pyramids and {$PtSn_6$} prisms. Average Pt-Sn distances in $Pt_4Sn_6R_3$ are close to 2.66 Å (Table 1) and reflect somewhat the lanthanide contraction which seems surprising. The {$PtSn_{5-6}$} clusters need to be connected via common Sn atoms, in accord with the compositions of **1** = $PtSn_{1.50}R_{0.75}$, **2** = $PtSn_{1.50}R_{0.73}$, **3** = $PtSn_{1.29}Sm_{1.29}$, which happens in rather different ways, see Fig. 3. All of them form chains through edge and vertex sharing of {$PtSn_5$} pyramids and {$PtSn_6$} prisms.

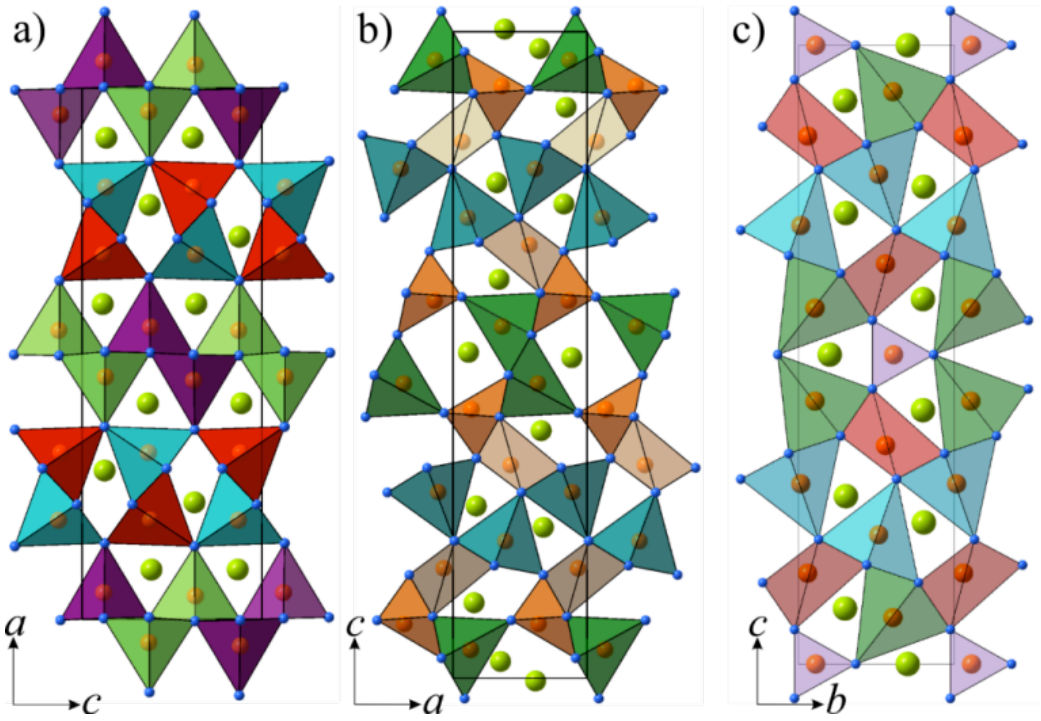

Fig. 3 The packing/connection of {$PtSn_x$} polyhedra in the crystal structures of $Pt_4Sn_6R_3$ (**1**, *R* = La-Nd), $Pt_4Sn_6R_{3-x}$ (**2**, *R* = Pr, Nd) and $Pt_7Sn_9Sm_5$ (**3**).

In the second coordination sphere, Pt is surrounded by *R* atoms with average distances around 3.5 Å (Table 1) with a stronger reflection of the lanthanide contraction. This is only surprising when one considers whether there is Pt-*R* bonding. The sum of the atomic radii of Pt (1.35 Å) and Pr (1.85 Å), i.e. 3.20 Å, suggests that there are no significant bonding interactions.

Then, the obvious influence of the lanthanide contraction on the Pt-*R* distances would simply be a packing effect. However, integrated crystal orbital Hamilton populations show a value of -0.80 eV/bond for Pt-Pr bonding, much less than the 2.28 eV/bond for Pt-Sn bonding, but it adds up to 18% of the overall bonding for $Pt_4Sn_6Pr_3$.[2]

Nevertheless, as Pt has a higher electronegativity/electron affinity than Sn, we are, strictly speaking, dealing with platinides, not stannides, and thus, may finally remove the question mark from the title!

Conclusions

The series $Pt_4Sn_6R_3$ has been observed for the light rare earth elements, R = La–Nd; they are isostructural and crystallize with the $Pt_4Ge_6R_3$ type of structure (*R* = Pr–Dy), so-called germanides. These are in fact platinides like the corresponding "stannides", subject to the higher electronegativity/electron affinity of Pt than Sn. The respective Pr and Nd compounds could be thought dimorphic with $Pt_4Sn_6R_{3-x}$ as the high temperature modification with a slightly reduced *R* content, x = 0.09 (Pr) and x = 0.11 (Nd); they crystallize in the same space group (*Pnma*) and with nearly identical unit cell volumes. However, the crystal structures of $Pt_4Sn_6R_3$ and $Pt_4Sn_6R_{3-x}$ are distinctly different and show, besides under-occupation of Pr sites, disorder of both Sn and Pr sites. All attempts to synthesize $Pt_4Sn_6Sm_3$ and $Pt_4Sn_6Sm_{3-x}$ have failed. Instead, $Pt_7Sn_9Sm_5$ was obtained, a new example for the rare $Zr_5Pd_9P_7$ type of structure linking polar intermetallics to metal phosphides in accord with the formulation $P_7Pd_9Zr_5 = Pt_7Sn_9Sm_5$. Bonding in all these compounds is predominantly heterometallic, Pt-Sn, Sn-*R*, and Pt-*R* bonding contributions decrease in this sequence.

Associated content

Supporting Information

Structural data as CIF files.

Accession Codes CCDC 1833491−1833495 contain the supplementary crystallographic data for this paper. These data can be obtained free of charge via ww.ccdc.cam.ac.uk/data_request/cif, or by emailing data_request@ccdc.cam.ac.uk, or by contacting The Cambridge Crystallographic Data Centre, 12 Union Road, Cambridge CB2 1EZ, UK; fax: +44 1223 336033.

Author Information

Corresponding Author

*E-mail for GHM: ghmeyer@iastate.edu

ORCID

Volodymyr Smetana: 0000-0003-0763-1457

Anja-Verena Mudring: 0000-0002-2800-1684

Gerd H. Meyer: 0000-0003-1000-9001

Notes

The authors declare no competing financial interest.

Acknowledgments

This research was supported by the Office of the Basic Energy Sciences, Materials Sciences Division, U. S. Department of Energy (DOE), and the Department of Chemistry at Iowa State University (ISU). Ames Laboratory is operated for DOE by ISU under contract No. DE-AC02-07CH11358.

References

(1) Meyer, G. Symbiosis of Intermetallic and Salt: Rare-Earth Metal Cluster Complexes with Endohedral Transition Metal Atoms, *Handbook on the Physics and Chemistry of Rare Earths*, Vol. 45, Chapter 264, Elsevier, 2014.

(2) Rhodehouse, M. L.; Bell, T.; Smetana, V.; Mudring, A.-V.; Meyer, G. H. From the non-existent polar intermetallic Pt_3Pr_4 via $Pt_{2-x}Pr_3$ to novel Pt/Sn/Pr ternaries, *Inorg. Chem*. **2018**, revised.

(3) Dwight, A. E.; Harper, W. C.; Kimball, C. W. HoPtSn and other intermetallic compounds with the Fe_2P-type structure. *J. Less-Common Met.* **1973**, *30*, 1-8.

(4) Venturini, G.; Malaman, B. Crystal structure of $Y_3Pt_4Ge_6$: An intergrowth of $BaAl_4$ and $YIrGe_2$ slabs. *J. Less-Common Met.* **1990**, *167*, 45-52.

(5) Gribanov, A.; Rogl, P.; Grytsiv, A.; Seropegin, Y.; Giester, G. Novel intermetallic $Yb_{\sim 3}Pt_{\sim 4}Si_{6-x}$ (x = 0.3) – A disordered variant of the $Y_3Pt_4Ge_6$-type. *J. Alloys Compd.* **2013**, *571*, 93-97.

(6) Gribanov, A.V.; Sologub, O. L.; Salamakha, P. S.; Bodak, O. I.; Seropegin, Y. D.; Pecharsky, V. K. Crystal structure of the compound $Ce_3Pt_4Ge_6$. *J. Alloys Compd.* **1992**, *179*, L7–L11.

(7) Imre, A.; Hellmann, A.; Mewis, A. New Germanides with an Ordered Variant of the $Ce_3Pt_4Ge_6$ Type of Structure – The Compounds $Ln_3Pt_4Ge_6$ (Ln: Pr–Dy). *Z. Anorg. Allg. Chem.* **2006**, *632*, 1145–1149.

(8) Niepmann, D.; Pöttgen, R.; Künnen, B.; Kotzyba, G.; Mosel, B. D. The Stannides $La_3Pd_4Sn_6$, $Ce_3Pd_4Sn_6$, and $Pr_3Pd_4Sn_6$: A New Structure Type with a Complex Three-Dimensional $[Pd_4Sn_6]$ Polyanion. *Chem. Mater.* **2000**, *12*, 533–539.

(9) Tursina, A. I.; Gribanov, A.V.; Bukhan'ko, N.G.; Rogl, P.; Seropegin, Y.D. Crystal structure of the novel compound $Ce_3Pt_4Al_6$. *Chem Met. Alloys* **2008**, *1*, 62–66.

(10) WinXPow. Stoe & Cie GmbH, Darmstadt, Germany, **2004**.

(11) APEX3, Bruker AXS Inc., Madison, Wisconsin, USA, 2015.

(12) SAINT, Bruker AXS Inc., Madison, Wisconsin, USA, 2015.

(13) Krause, L.; Herbst-Irmer, R.; Sheldrick, G. M.; Stalke, D. Comparison of silver and molybdenum microfocus X-ray sources for single-crystal structure determination. *J. Appl. Crystallogr.*, **2015**, *48*, 3-10.

(14) Sheldrick, G. M. SHELXT - Integrated space-group and crystal-structure determination. *Acta Cryst.* **2015,** *A71*, 3-8.

(15) Sheldrick, G. M. Crystal structure refinement with SHELXL. *Acta Cryst.* **2015**, *C71*, 3-8.

(16) Brink Shoemaker, C.; Shoemaker, D. P. A Ternary Alloy with $PbCl_2$-type Structure: TiNiSi(*E*), Acta Cryst. **1965**, *18*, 900-905.

(17) Riecken, J. F.; Rodewald, U. Ch.; Heymann, G.; Rayaprol, S.; Huppertz, H.; Hoffmann, R.-D.; Pöttgen, R. Synthesis, Structure and Properties of the High-pressure Modifications of the Ternary Compounds REPtSn (RE = La, Pr, Sm), *Z. Naturforsch*. **2006**, *61b*, 1477 – 1484.

(18) Harmening, T.; Hermes, W.; Eul, M.; Schappacher, F. M.; Pöttgen, R. Structure and properties of $Eu_2Pt_3Sn_5$. *Z. Kristallogr.*, **2009**, *224*, 351-357.

(19) Emsley, J. The Elements, 2nd ed., Clarendon Press, Oxford 1991.

(20) Meyer, G. Cluster Complexes as *anti*-Werner Complexes. *Z. Anorg. Allg. Chem.* **2008**, *634*, 2729-2736.

(21) Smetana, V.; Miller, G. J.; Corbett, J. D. Three alkali-metal-gold-gallium systems. Ternary tunnel structures and some problems with poorly ordered cations. *Inorg. Chem.* **2012**, *51*, 7711-7721.

(22) Smetana, V.; Miller, G. J.; Corbett, J. D. Four polyanionic compounds in the K-Au-Ga system: a case study in exploratory synthesis and of the art of structural analysis. *Inorg. Chem.* **2012**, *51*, 1695-1702.

(23) Slater, J. C. Atomic Radii in Crystals. *J. Chem. Phys*., 1964, **41**, 3199-3204.

CHAPTER 5. AN OBSCURED OR NONEXISTENT BINARY INTERMETALLIC, Co_7Pr_{17}, ITS EXISTENT NEIGHBOR Co_2Pr_5, AND TWO NEW TERNARIES IN THE SYSTEM Co/Sn/Pr, $CoSn_3Pr_{1-x}$ AND $Co_{2-x}Sn_7Pr_3$

Melissa L. Rhodehouse,[†,‡] Thomas Bell,[§] Volodymyr Smetana,[‡,I] Anja-Verena Mudring,[‡,I,⊥] and Gerd H. Meyer,[*,†,‡,§]

[†]Department of Chemistry, Iowa State University, Ames, IA, 50011, USA
[‡]Ames Laboratory, USDOE, Iowa State University, Ames, IA 50011, USA
[§]Department of Chemistry, Universität zu Köln, Greinstraße 6, 50939 Köln, Germany
[I]Department of Materials and Environmental Chemistry, Stockholm University, Svante Arrhenius väg 16 C, 10691 Stockholm, Sweden
[⊥]Department of Materials Science and Engineering, Iowa State University, Ames, IA 50011, USA

Abstract

Four compounds are reported in this study: Co_7Pr_{17} (**10**, *cP*96, $P2_13$, a = 13.4147(8) Å, Z = 4), either non-existent or obscured in the phase diagram has been obtained from a $PrBr_3$ flux. With 29.2 mol% Co, it is close to Co_2Pr_5 (28.6 mol% Co, **2**, C_2Mn_5 type of structure, *mC*28, *C*2/*c*, a = 16.5471(7) Å, b = 6.5107(3) Å, c = 7.1067(3) Å, β = 96.230(3)˚, Z = 4), existent in the Co/Pr phase diagram, produced by arc-melting of a stoichiometric mixture of the metals. The addition of the reactive tin to Co/Pr mixtures yielded two new ternary polar intermetallics, $CoSn_3Pr_{1-x}$ (x = 0.04, **11**, $RuSn_3La$ type, *cP*40, *Pm*-3*n*, a = 9.587(3) Å, Z = 8) and $Co_{2-x}Sn_7Pr_3$ (x = 0.78, **12**, $Ni_{2-x}Sn_{7-y}Ce_3$ tape, *oC*24, *Cmmm*, a = 4.5043(4) Å, b = 27.227(2) Å, c = 4.5444(3) Å, Z = 2). Electronic structure calculations exhibit extensive heteroatomic Co-Pr interactions in the binaries with little homoatomic contributions. With tin as the third component in the ternaries, heteroatomic Co–Sn and Sn–Pr bonding interactions are dominant in $CoSn_3Pr$, following the succession of coordination spheres around Co.

Introduction

With roughly 70 elements of the periodic table having metallic properties under ambient conditions, there are n!/(n-k)!k! = 70!/68!2! = (70x69)/2 = 2415 binary systems possible, and with each system containing statistically certainly more than one compound, and more modifications at higher temperatures and/or pressures, the number of possible compounds is virtually infinite, already under thermodynamic equilibrium. Off equilibrium, there are an unforeseeable number of further compounds. Moving to ternary or even higher systems, the number of possible compounds is endless, with for example, 54740 ternary systems for 70 metals.

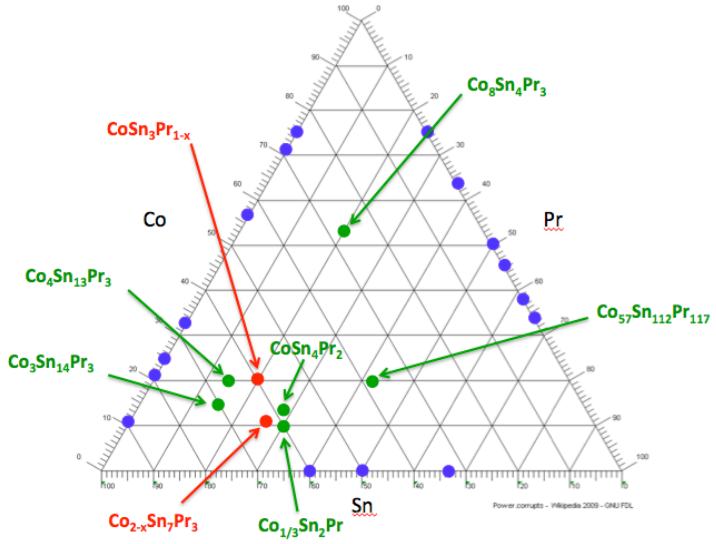

Figure 1. The Co/Sn/Pr compositional triangle.

The most recent compilation of the Co/Pr system exhibits nine intermetallic compounds, $CoPr_3$ (**1**, 25 mol% Co), Co_2Pr_5 (**2**, 28.6), $Co_{1.7}Pr_2$ (**3**, 45.9), Co_2Pr (**4**, 66.7), Co_3Pr (**5**, 75), Co_7Pr_2 (**6**, 77.8), $Co_{19}Pr_5$ (**7**, 79.2), Co_5Pr (**8**, 83.3), and $Co_{17}Pr_2$ (**9**, 89.5), some of which have low- and high-temperature modifications (**2**, **6**, **9**), one exists only at high temperatures (**8**, 854-1232°C).[1] We hereby add a new binary compound, either nonexistent in thermodynamic equilibrium,[2,3] or obscured in the phase diagram, Co_7Pr_{17} (**10**, 29.2 mol% Co) very close in composition to **2** (28.6 mol% Co). This new intermetallic was obtained in the pursuit of cluster

complex halides such as $\{CoPr_3\}Br_3$ in minor yields from a $PrBr_3$:Pr:Co = 1:2:1 molar mixture. Attempts to reproduce **10** in a classic arc-melting procedure yielded **2**. As the interpretation of these results was that **10** had been produced essentially from a $PrBr_3$ melt, other fluxes such as NaCl and metallic Sn were used. As a NaCl melt was un-reactive, providing a temperature above 800°C and some chance for the precipitation of an intermetallic from an over-saturated solution, the Sn melt is reactive and provided two new ternary Co/Sn/Pr intermetallics, **$CoSn_3Pr_{1-x}$ (x = 0.044, 11), $Co_{2-x}Sn_7Pr_3$ (x = 0.782, 12)**. Ternary Co/Pr/Sn intermetallics have been largely underexplored since the last published ternary, $Co_{57}Pr_{117}Sn_{112}$, in 2010. Currently, six compounds are reported in this system: $Co_8Sn_4Pr_3 = CoSn_{0.5}Pr_{0.375}$ (**13**),[4] $Co_{57}Sn_{112}Pr_{117} = CoSn_{1.96}Pr_{2.05}$ (**14**),[5,6] $Co_4Sn_{13}Pr_3 = CoSn_{3.25}Pr_{0.75}$ (**15**),[7] $CoSn_4Pr_2$ (**16**),[8] $Co_3Sn_{14}Pr_3 = CoSn_{4.67}Pr$ (**17**),[9] and $Co_{0.33}Sn_2Pr = CoSn_6Pr_3$ (**18**),[10] see Figure 1.

Experimental section

Synthesis. Starting materials were Co beads (99.9%), Pr and Sn pieces (99.9%), and NaCl (99.9% purity). NaCl was dried in an oven at 80˚C overnight before placing inside an argon filled glovebox. $PrBr_3$ was prepared from the oxide following the ammonium bromide route.[11] All samples, between 250-500 mg, were weighed and loaded into tantalum ampules inside an argon-filled glovebox. Co/Pr binary samples were arc melted or loaded with either NaCl or Sn (approx. 250 mg) as a flux. The NaCl excess could be removed with water. Ampules were sealed under argon with an He arc, followed by sealing in evacuated silica tubes with the aid of an H_2/O_2 torch. Samples with NaCl as a flux were placed in a furnace at 1000˚C for 24 hours followed by slow cooling (-10˚C·hr^{-1}) to 850˚C and annealed for 3 days. Samples with Sn as a flux were placed in a furnace at 500˚C for 48 hours, then quenched.

Co_7Pr_{17} (10). The starting composition for $\{CoPr_3\}Br_3$, $PrBr_3$ + 2Pr + Co, was weighed and loaded according to the above indicated method. The mixture was pre-reacted at 800 ˚C for 7 days, cooled at 1 ˚C·hr^{-1} to 400 ˚C and finally cooled to room temperature at 10 ˚C·hr^{-1}. The resulting product was multiphase containing a new intermetallic compound in minor quantities. Small crystals of Co_7Pr_{17} were selected and characterized from that sample. Attempts to prepare Co_7Pr_{17} from a stoichiometric mixture of the metals resulted in the formation of Co_2Pr_5.

Co_2Pr_5 (2). The starting composition of Co_2Pr_5 was weighed, pressed into a pellet and arc melted. The resulting button was annealed at 500 ˚C for a week. According to powder X-ray diffraction the sample was found to be phase pure. Small crystals of Co_2Pr_5 of good quality could be selected and tested from the same sample; however, the crystals for structural investigation were selected from additional nonstoichiometric samples obtained in Ta ampule with NaCl flux using slow cooling according to the above described scheme.

$CoSn_3Pr_{1-x}$ (x = 0.044, 11), $Co_{2-x}Sn_7Pr_3$ (x = 0.782, 12). Starting compositions of Co_7Pr_{17} and Co_2Pr_5 with excess Sn as a flux were weighed and placed inside tantalum tubes. Samples were sealed under the same conditions and placed in a tube furnace following the heating profile described above. Single crystals of (**11**) were obtained as minor phase (**12**) was obtained from an initial attempt to reproduce the reported **$CoSn_4Pr_2$** from the stoichiometric loading with a NaCl flux.

Structure analysis. Single crystal and powder X-ray diffraction were used to characterize products. Samples were crushed in air due to low sensitivity to oxidation and hydrolysis for extended periods. A portion of the respective sample was ground to a fine powder for purity check and phase analysis. Powders were sandwiched between greased Mylar sheets housed by an aluminum holder. Data was gathered on a STOE STADI P image plate diffractometer (Cu-$K_{\alpha 1}$ radiation, λ = 1.54178 Å; Si external standard, a = 5.4308(1) Å) and analyzed using WinXPow

software.[12] Single crystal X-ray diffraction was performed on a Bruker APEX CCD and Bruker VENTURE diffractometer (both Mo-Kα radiation, λ = 0.71073 Å). The raw frame data were collected using the Bruker APEX2/APEX3 programs,[13] while the frames were integrated with the Bruker SAINT[13] software package using a narrow-frame algorithm integration of the data and were corrected for absorption effects using the multi-scan method (SADABS).[14] All positions were refined anisotropically. Initial models of the crystal structures were first obtained with the program SHELXT-2014[15] and refined using the program SHELXL-2014[16] within the APEX3 software package. Refinement details and structural parameters can be found in Tables 1–3.

Differential thermal analysis has been performed on ~0.1g sample cut from the as cast button. It was sealed in a Mo crucible (outgassed under a vacuum by induction heating) by arc welding and subjected to heating (20 °C/min) and cooling (5−10 °C/min) runs (accuracy of ± 5 °C) in a Netzsch 404 thermoanalyzer.

Electronic structure calculations. DFT-based electronic structure calculations for $Pr_{17}Co_7$ and slightly idealized $PrCoSn_3$ (with the fully occupied Pr sites) were performed according to the linear muffin–tin–orbital (LMTO) method in the atomic sphere approximation (ASA).[17,18] The Wigner–Seitz radii were automatically generated and empty spheres were included for better approximation of full potentials. They were determined to be 1.87, 1.81, 1.77, 1.76, 1.74, 1.79 and 1.81 Å for Pr1–Pr7; 1.53, 1.51 and 1.50 Å for Co1–Co3 in (**1**); 2.26, 2.20, 1.43 and 1.59 for Pr1, Pr2, Co and Sn, respectively, in (**3**). Basis sets of Pr 6s,(6p),5d and Co 4s,4p,3d and Sn 5s,5p,(5d),(4f) were employed. 6p orbitals of Pr were downfolded as well as 5d and 4f orbitals of Sn.[19] Chemical bonding analysis was performed based on the crystal orbital Hamilton populations (COHP).[20]

Results and discussion

The cobalt atom with its nine valence electrons appears to be perfect as an endohedral atom *T* in cluster complex halides, *X* = Cl, Br, I, in both octahedral or trigonal-prismatic rare-earth metal (*R*) clusters: [{$CoPr_6$}I_{12}]Pr with isolated octahedra and {Co_2Pr_2}I with condensed trigonal prisms may serve as only two examples,[21] of which more than 30 have been synthesized and characterized over the years.[22] Another compound, {$CoPr_3$}Br_3,[23] subject to powder X-ray diffraction studies crystallizing with a defect NaCl-type of structure, also known from Gd_3CCl_3 (cubic, Ca_3PI_3 type),[24] was the target within the pursuit of getting deeper knowledge of the {TR_3}X_3 family which comes about in 6 structural varieties.[22] Single crystals of the intermetallic Co_7Pr_{17} were obtained instead. Apparently, $PrBr_3$ served as a flux for the crystallization of this hitherto nonexistent intermetallic.

In the praseodymium rich part of the Co/Pr phase diagram, there are three compounds, $CoPr_3$, "$Co_{1.7}Pr_2$", and Co_2Pr_5 (28.6 mol-% Co) which melts incongruently at 544°C.[1] It is very close in composition to Co_7Pr_{17} (29.2 mol-% Co) which has now been obtained through annealing of a $PrBr_3$/2Pr/Co synthesis at 400°C, originally heated up to 800°C. Attempts to reproduce Co_7Pr_{17} via the conventional arc-melting procedure all failed and produced Co_2Pr_5 as single crystals. With the heavier rare-earth metals, phases of the composition T_3R_7 (30 mol-% *T*) are also frequently seen.

The application of the non-reactive NaCl flux to the binary Co/Pr compositions did not yield any new results other than Co_2Pr_5. The reactive tin flux led into an already existing gold mine with the addition of three new Co/Sn/Pr ternaries to the already reported six. As tin was used in excess, these three compounds, **$CoSn_3Pr_{1-x}$ (x = 0.044, 11), $Co_{2-x}Sn_7Pr_3$ (x = 0.782, 12)**, exist in the tin-rich part of the ternary system where all the others except $Co_8Sn_4Pr_3$ were found.

Crystal structures. It is amazing that two compounds that are very close in composition, $CoPr_{2.43}$ (Co_7Pr_{17}, **10**, *cP*96, $P2_13$, a = 13.4147(8) Å, Z = 4) and $CoPr_{2.5}$ (Co_2Pr_5, **2**, *mC*28, *C*2/*c*, a = 16.5471(7) Å, b = 6.5107(3) Å, c = 7.1067(3) Å, β = 96.230(3)°, Z = 4) crystallize with extremely different structures. In the first, there are three crystallographically independent Co positions surrounded by 8, 9, and 9 Pr atoms, respectively, with overall averaged Co-Pr distances of 2.973 Å, see Figure 2. In the second, there are exclusively trigonal-prismatic {$CoPr_x$} clusters present with d(Co-Pr) = 3.008 Å. The (calculated) density of Co_7Pr_{17} is considerably higher than that of Co_2Pr_5, 7.726 vs. 7.149 g/cm^3.

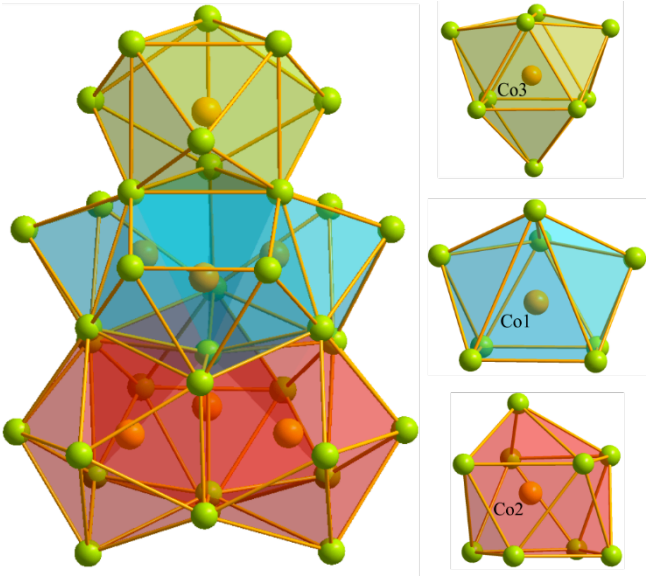

Figure 2. The three crystallographically independent {$CoPr_x$} clusters (with x = 8, 9, 9) in Co_7Pr_{17} and the connection of three light blue {$Co1Pr_8$} clusters with three red {$Co2Pr_9$} and one green {$Co3Pr_9$} cluster to a {Co_7Pr_{35}} supercluster.

Co_7Pr_{17} crystallizes cubic in the non-centrosymmetric space group $P2_13$. All positions are fully occupied and there no elemental disorder on any site. Phases of similar to equal compositions have been reported with T = Pd more than four decades ago and either addressed as $Pd_{28}R_{64}$ or so called Pd_2R_{5-x} (x = 0.14) with R = Tb, Dy, Ho, Er, Tm, Lu, Y.[25] The structure was determined for $Pd_{28}Dy_{64} = Pd_7Dy_{17}$ in space group $Fd\bar{3}m$ and is related to the structure of

perfectly ordered $NiTi_2$.[26] There are two out of three Dy sites as well as the only Pd site under-occupied. As we have recently obtained Pd_7Er_{17} which turns out to be isotypic with Co_7Pr_{17} with a = 13.365(2) Å, which is almost identical with Fornasini's a = 13.368 Å for "Pd_2Er_5",[25] we have reason to believe that this is the ordered low temperature modification of the reported phase.[27]

The structure of Co_7Pr_{17} may be described in different ways. One is to connect the $\{CoPr_x\}$ clusters of Figure 2 to a supercluster $\{Co_7Pr_{35}\}$, Figure 2 (left), which are further connected to a three-dimensional structure, in accord with space group symmetry. Another way is to edge-share tetramers of centered trigonal prisms $\{CoPr_6\}$ around empty $\{Pr_4\}$ tetrahedra, $\{Co_4Pr_{16}\}$ (green) and trimers of interpenetrating $\{CoCo_2Pr_{10}\}$ icosahedra, $\{Co_3Pr_{20}\}$ (blue), Figure 3. All faces of the former are capped by additional Pr atoms forming a distorted Pr_6 octahedron around the central $\{Co_4Pr_4\}$ tetrahedral star. The sequence $A_4B_4A_6$ is a well-known structure of the clusters in gamma brasses.[28] $\{TR_6\}$ trigonal prisms and their clusters are frequently observed in other binaries. The most prominent examples include face-sharing dimers as single building units in Pt_3Pr_4 or Pt_2Pr_3,[29,30] edge- and vertex sharing trimers and polymers in two compositionally related Pd_3R_7,[31,32] Pd_2R_5[33,34] and Co_2R_5.[35]

The second group of polyhedra (Figure 3, left, blue) belongs to the anti-Mackay type of clusters.[36] Anti-Mackay clusters are polytetrahedral formations; the most stable consist strictly of interpenetrating icosahedra and those observed in (**10**) satisfy this condition. The $Pd_{1-x}R_2$ phases contain similar units built around the T_4 tetrahedron, thereby containing four interpenetrating icosahedra in contrast to the three as observed in Co_7Pr_{17}. Among the most stable anti-Mackay type oligomers, tetramers are the most popular due to the wide spread of the gamma brasses.[37] Homoatomic dimers and tetramers have been observed in Li intermetallics,[38-41] while hetero-diatomic dimers, tetramers, pentamers and tridecamers have been detected in e.g. Mn_3Al_{10},[42] in

the La–Ni–Mg system,[43] and the Bergman type quasicrystal approximants.[44] Co_7Pr_{17} is the first representative of a structure with anti-Mackay type trimers.

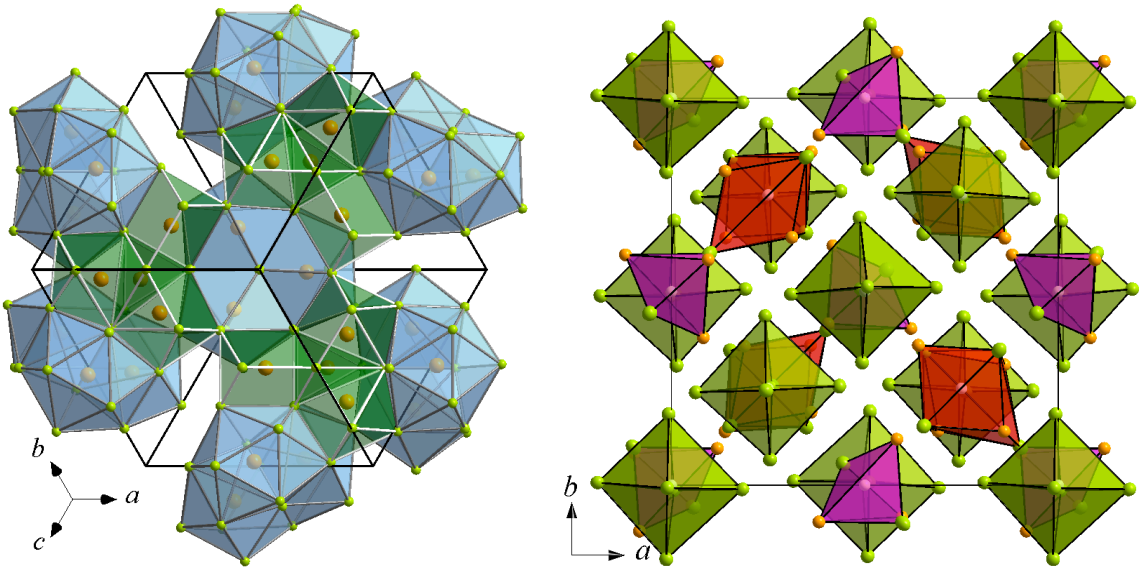

Figure 3. Left: Edge-shared tetramers of centered trigonal prisms $\{CoPr_6\}$ around empty $\{Pr_4\}$ tetrahedra, $\{Co_4Pr_{16}\}$ (green) and trimers of interpenetrating $\{CoCo_2Pr_{10}\}$ icosahedra, $\{Co_3Pr_{20}\}$ (blue) in the crystal structure of $Pr_{17}Co_7$. Right: $\{Pr_6\}$ octahedra (green), $\{Co_4Pr_4\}$ tetrahedral stars (red) and $\{Co_3Pr_2\}$ trigonal bipyramids (violet) in a Heusler type arrangement.

An alternative elegant description of the structure of Co_7Pr_{17} is based on a Heusler type packing (Figure 3, right). The centers of $\{Pr_6\}$ octahedra, $\{ Co_3Pr_2\}$ trigonal bipyramids and $\{Co_4Pr_4\}$ tetrahedral stars are identical with the atoms of the Hg_2CuTi type,[45] the *F*-43*m* variant of the most common Cu_2AlMn-*Fm*3*m* arrangement.[46] Thus, $\{Pr_6\}$ octahedra are located as the atoms of a cubic densest packing of spheres (4*a*; 0,0,0 in *F*-43*m*) and fill one half of the tetrahedral holes (4c, ¼¼¼) with $\{ Co_4Pr_4\}$ tetrahedral stars occupying the other half of the tetrahedral holes (4d, ¼¾¾) and the $\{Co_3Pr_2\}$ trigonal bipyramids are in 4b, ½½½.

A phase labelled Co_3Pr_7 was discovered in an early phase diagram determination (1974) and found to be **Co_2Pr_5** (**2**) by powder X-ray diffraction in analogy with Co_2Sm_5 whose structure was determined by single crystal X-ray diffraction.[35] These crystallize with the C_2Mn_5 type of

structure where, so far, Co_2R_5 with R = Pr, Nd, Sm are the only representatives with a 3d-T metal; other T_2R_5 phases with R = Eu, Dy, Er, Yb, Lu are known with 4d- and 5-d noble metals centering the $\{R_6\}$ trigonal prisms. The crystal structure of **Co_2Pr_5 (2)** was refined from single-crystal X-ray data. $\{CoPr_6\}$ trigonal prisms share edges and vertices forming formally separated layers parallel to the *bc* plane (Figure 4). The prisms form two phase-shifted sinusoidal chains through edge-sharing along the *c* direction forming a checkered pattern being a one-dimensional analogy of the $HfCuSi_2$ type.[47] These connect to identical units along the *b* direction through vertex-sharing. In spite of the low symmetry the space in between the layers is filled by pretty regular empty $\{Pr_4\}$ tetrahedra and $\{Pr_5\}$ square pyramids, though there are no larger polytetrahedral motifs as observed in Co_7Pr_{17}.

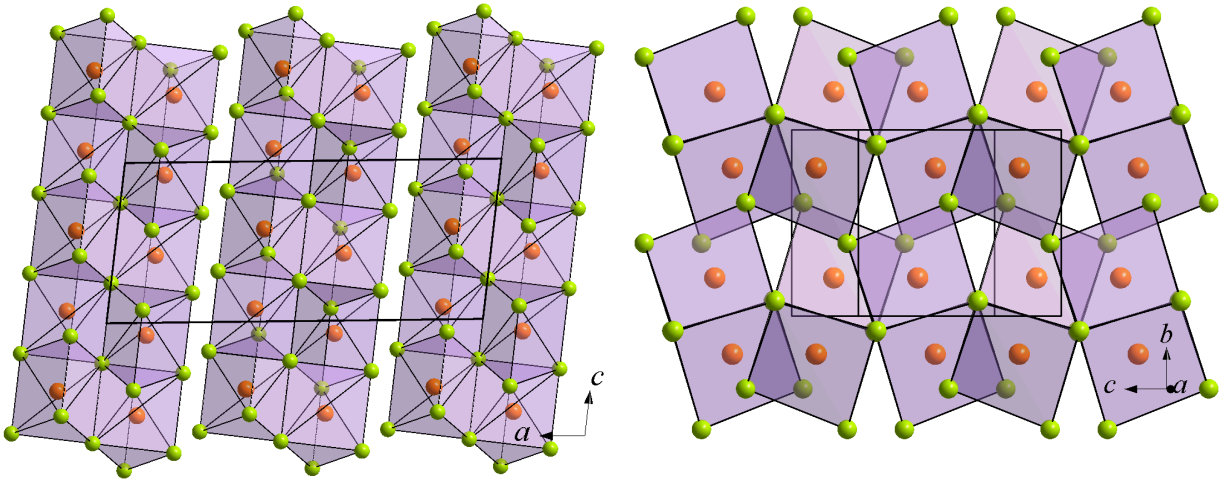

Figure 4. Packing motifs based on edge- and vertex-sharing $\{CoPr_6\}$ trigonal prisms in the crystal structure of Co_2Pr_5.

The crystal structure of **$CoSn_3Pr_{1-x}$ (x = 0.044, 11,** *cP*40, $Pm\bar{3}n$, a = 9.587(3) Å, Z = 8, $RuSn_3La$[48] type) consists of a vertex-sharing network of trigonal-prismatic $\{CoSn_6\}$ clusters, d(Co-Sn) = 2.608 Å, $CoSn_{6/2} = CoSn_3$ that incorporates the Pr atoms (Figure 5, left). These occupy two crystallographically independent sites, (Pr1, 2*a*; Pr2, 6*c*) corresponding to $\{Pr1Sn_{12}\}(Co_4)$ icosahedra, d(Pr1-Sn) = 3.274(1) Å, with 4 Co atoms at a distance of 3.390(1) Å

and {Pr2Sn_{12}}Co_4 tetracapped cuboctahedra with the Co atoms in the same coordination sphere as Sn, with distances of 3.329(1) (Pr2-Sn), 3.390(1) (Pr2-Co), and 3.401(1) Å (Pr2-Sn). The {Pr1Sn_{12}} icosahedra, form a body-centered arrangement and share smaller trigonal faces resulting in a relatively dense packing with only small tetrahedral voids (Figure 5, right).

The peculiar problem of this, and a number of related, structures is the under-occupation of one Pr site, Pr1, 85.2%. With this, the thermal displacement factor has a reasonable value (U_{11} = U_{22} = U_{33} = 0.0147), close to that for site 6c (Pr2, U_{11} = 0.0124(3), U_{22} = U_{33} = 0.0088(2)).

For **$RuSn_3Eu$**, with the same structure, full occupation of both Eu sites is assumed although U_{eq}'s are then 0.0243(4) and 0.0060(2), respectively.[49] However, there are a number of interpretations in the literature for *T*/*E*/*R* ternary intermetallics claiming full or partial occupation of a position by *E* or *R*, or mixed occupation by *E*/*R* or *T*/*E*. In the Co/Sn/Pr system, $Co_4Sn_{13}Pr_3$ = $CoSn_{3.25}Pr_{0.75}$ (**15**) has been reported,[7] with estimations on the basis of isostructural behavior with no refinement or analysis. In $Pt_{12}Sn_{24}Pr_{4.84}$[29] as well as in the isostructural $Ni_{12}Sn_{24}La_{4.87}$[50] one R site is under-occupied; they both belong to the $Gd_3Ni_8Sn_{16}$ (= $Ni_{12}Sn_{24}Gd_{4.5}$) structure family.[51] Another work suggested mixed *R*/Sn occupation for $Pt_{12}Sn_{24+x}R_{5-x,}$ assuming full occupation of the 2*a* site.[52] Mixed Ca/Sn and Sn/Co occupations have been proposed for $Co_8Sn_{25}Ca_7$[53] and $Co_{4.3}Sn_{12.7}Yb_3$.[54]

$Co_{2-x}Sn_7Pr_3$ (x = 0.782, 12, *oC*24, *Cmmm*, *a* = 4.5043(4) Å, *b* = 27.227(2) Å, *c* = 4.5444(3) Å, *Z* = 2) belongs to a not so popular family, the $Ni_{2-x}Sn_{7-y}Ce_3$ type of structure, although with unique features. It remains unclear why the Sn content in the prototype is given as 7−y as all the other compounds exhibit fully occupied Sn positions.

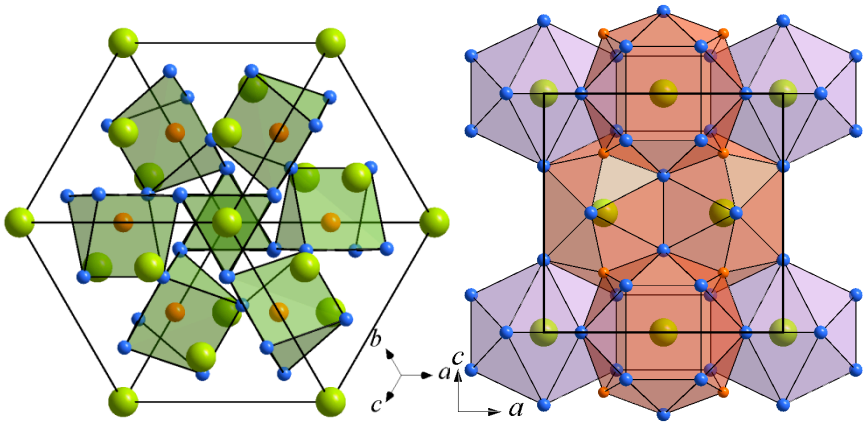

Figure 5. {$PrSn_{12}$} (blue), {$PrSn_{12}$}Co_4 (reddish) and {$CoSn_6$} polyhedra in the crystal structure of **$CoSn_3Pr_{1-x}$ (x = 0.044) = $Co_4Sn_{12}Pr_{3.82}$.**

(**12**) follows the general behavior although the strong deficiency of the Co position leads to a small positional disorder of a neighboring Sn site. This disorder does not affect the occupation but leads to the optimization of the interatomic contacts in the area (Fig. 6, dashed lines). On first sight, the atomic arrangement has a lot in common with binary Sn_2Pr,[55] including symmetry and unit cell proportions.

The crystal structure of (**12**) appears as a layered structure, while the layers can hardly be considered as separated. The anionic (Co/Sn) substructure is built of empty {Sn_5} and {$CoSn_5$} tetragonal pyramids forming an up and down checkered pattern. Two such slabs are mirrored through the common vertices of the empty pyramids and can be considered as a pseudo-two-dimensional motif in the *ac* plane. The slabs are connected through rather weak Sn−Sn interactions of 3.053 Å which are pretty short taking the situation in $CoSn_3Pr_{1-x}$ into account. In contrast, the checkered pattern in the related Sn_2Pr (=Sn_6Pr_3) is formed of overlapping up and down pyramids (resulting in empty octahedra), empty slots between them, and consequently vertex-sharing as the layer forming tool. Both structures contain zigzag chains along the *a* direction, while (**12**) contains additional planes of Pr rectangles. Nevertheless, in all cases Pr−Pr distances exceed 4 Å and can hardly be considered important in bonding schemes. Two different

Pr polyhedra are observed in the structure, within and between the slabs. The former are cuboctahedra filling the space between empty $\{Sn_5\}$ pyramids, while the latter are slightly irregular $\{Sn_8\}$ square prisms capped by two extra Sn and two Pr atoms over the larger square faces. These polyhedra together with the centered $\{CoSn_5\}$ pyramids form the connecting slabs.

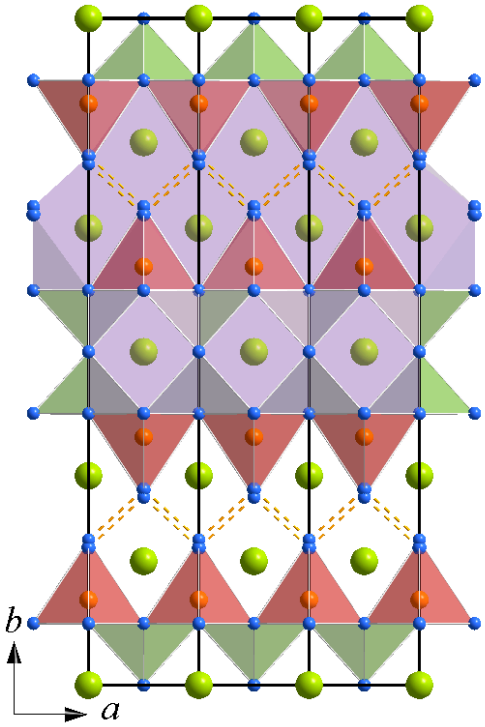

Figure 5. $\{CoSn_5\}$ square pyramidal network and $\{PrSn_{12}\}$ cuboctahedra in the crystal structure of $Co_{2-x}Sn_7Pr_3$.

Electronic structure calculations have been performed for Co_7Pr_{17} (**10**), Co_2Pr_5 (**2**) and $CoSn_3Pr$ (**11**). For $CoSn_3Pr$ fully occupied Pr positions were assumed. The electronic densities of states (DOS) curves for Co_7Pr_{17} (**10**) and $CoSn_3Pr$ (**11**) (Figure 6) differ due to the presence of the *p* component (Sn) in the ternary compound and, accordingly, more extended bands until −11 eV. However, they are qualitatively similar down to -5 eV from E_F where Pr 5*d* and Co 3*d* contributions are dominant. Figure 7 shows the site projected DOS curves for both compounds. The DOS curve for $CoSn_3Pr$ exhibits a maximum in the range of −0.5 to −2.5 eV which is

significantly closer to the Fermi level than in corresponding palladides, platinides or aurides.[27,29,56,38] The close vicinity of the Co 3*d* orbitals to the Fermi level suggests that their role must be more important in valence electron count while the transition metals are usually assumed to not provide valence electrons. Such a narrow distribution of the *d* orbitals is typical for some ionic platinides where relativistic effects play a crucial role,[57,58] while the *p*-element containing compounds usually show considerably higher dispersion.[59-61] Pr 6*s* and Co 4*s* orbitals in (**10**) are located between -2 and -4 eV from E_F, whereas the presence of Sn in (**11**) shifts them into the area below –4 eV with second maxima around –8 eV. Sn 5*s* contributions are dominant in the range between –6 and –11 eV, while Sn 5*p* are significant down to –5 eV. Being less visible, both Pr 6*s* and 6*p* orbitals provide quite decent contributions particularly at the Fermi level.[42]

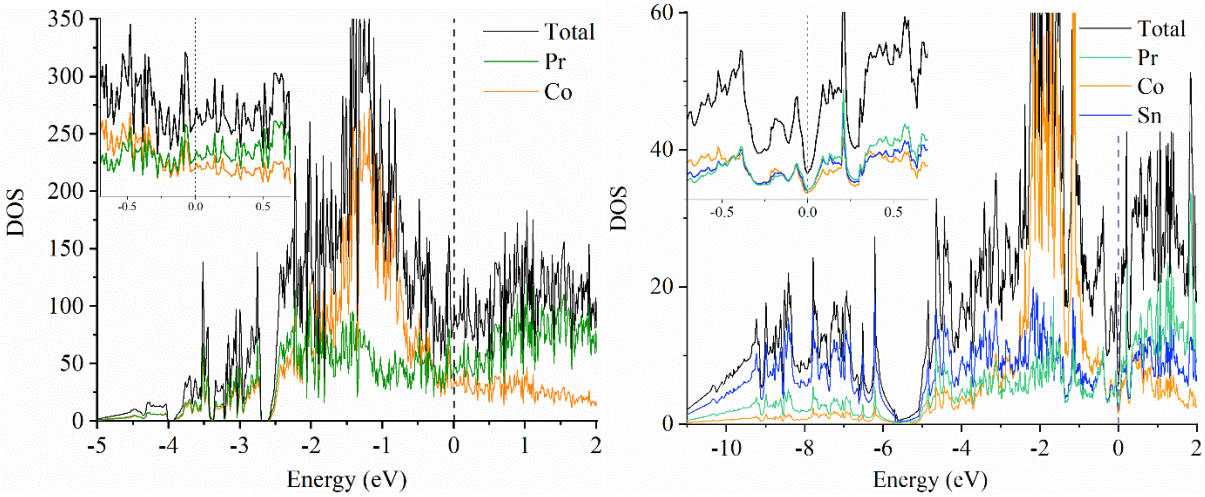

Figure 6. Total and element projected DOS curves for Co_7Pr_{17} (left) and $CoSn_3Pr$ (right).

Co_7Pr_{17} demonstrates significant DOS values at the Fermi level with the latter being located in a small local minimum. Due to structural complexity and the large unit cell it is hard to observe any clear pseudogap. However, the Pr and Co curves cross around that point with the former starting to increase and the latter continuing to drop. A significantly different picture is

observed for $CoSn_3Pr$ where E_F falls into a narrow but very deep pseudogap indicating the importance of a certain valence electron count for the structural stability.

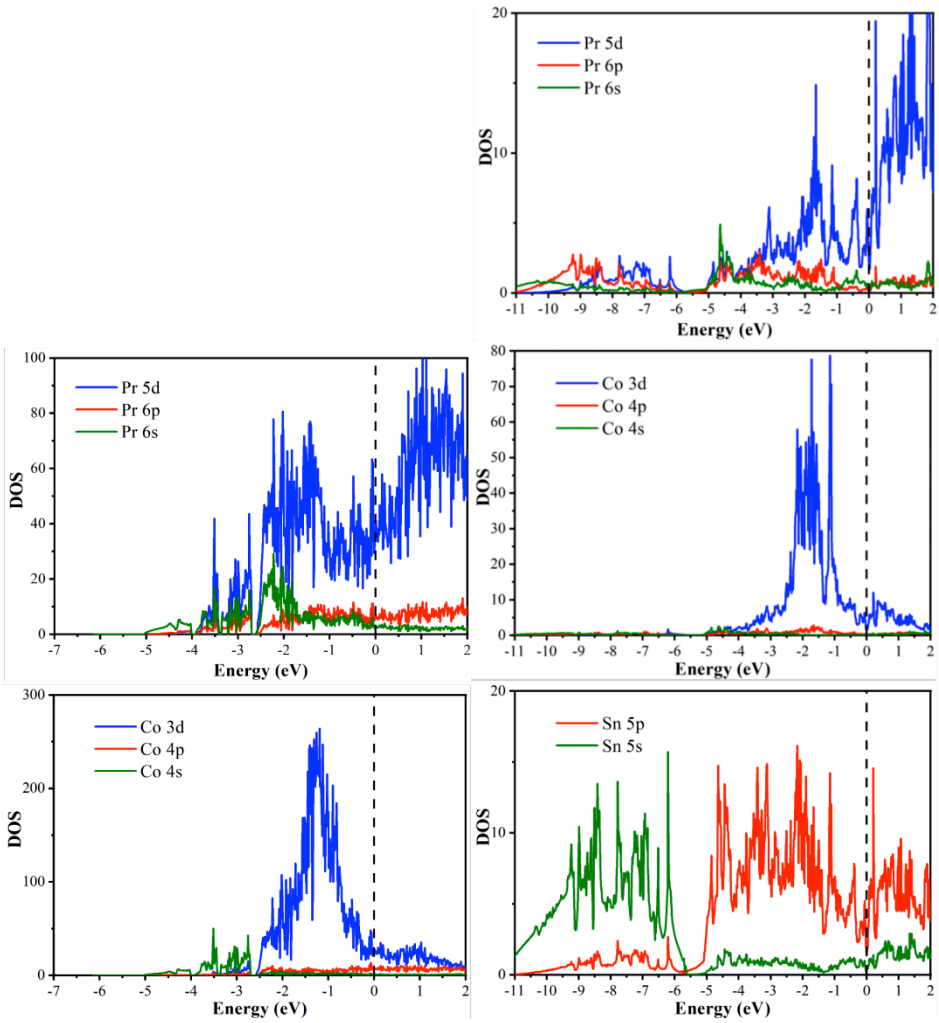

Figure 7. Site projected DOS curves (PDOS) for Co_7Pr_{17} (left) and $CoSn_3Pr$ (right).

This situation has been observed in a number of Ga rich polar intermetallics with active metals.[62,63] $Na_{17}Au_{5.87}Ga_{46.63}$ for example contains an extended network of separate or fused empty icosahedra almost opening a gap at the Fermi level. In that case Au is acting as the doping atom for the *vec* (valence electron concentration) adjustment, while Na is a nearly a pure electron donor. It has already been shown on the example of $RuSn_3Eu$ that the *vec* is not the least important factor for the stability of the $Rh_4Sn_{13}Pr_3$ structure type so it may even be responsible for the oxidation state of Eu in the mixed-valent systems.[49]

The same conclusion may be derived from the DOS curves of (**11**) with the potential replacement of two Pr for Sn leading to significantly higher values at the Fermi level as well as moving some interatomic interactions into the strongly antibonding regions (Figure 8). On the other hand, this concept supports the possibility of the second tin position with divalent metals e.g. Ca or Sr.

From a structural point of view Co_2Pr_5 contains Co-centered trigonal prisms of Pr, $\{CoPr_6\}$, exclusively, while in Co_7Pr_{17} higher coordinated Co atoms are evident, although the $\{CoPr_6\}$, prisms are still basic, all with varying connection principles. The analysis of the bonding aspects may shed more light on composition/bonding interplay as a main factor leading to two phases with such a close composition and, in the end, rather different structures. Co−Pr distances in both compounds are in the ranges 2.81−3.68 Å and 2.72−3.59 Å, respectively, showing an insignificant shortage in the latter case that is compensated through Pr−Pr separations, 3.35−3.77 Å and 3.55−3.94 Å, showing an identical degree of dispersion. This distribution is also quantitatively expressed in the contribution to the total bonding in both compounds (Table 4). Heteroatomic Co−Pr contributions, dominating in both structures, increase significantly from 72.4 (Co_7Pr_{17}) to 87.9% (Co_2Pr_5) while Pr−Pr contributions are reduced by ~50% from 25.7 to 12.1%.

The situation within the Co-Sn clusters in both Co_7Pr_{17} (**11**) and Co_2Pr_5 (**2**) is almost identical with 1.12−0.92 and 1.12−0.86 eV/bond, respectively. Pr−Pr contributions are unsurprisingly less populated, they provide up to 0.35 eV/bond, though the average contribution is much lower, especially in (**2**), see Table 4. Co−Co populations are also not negligible in Co_7Pr_{17} (**11**), not at least due to *d* orbital contributions at lower energies and are, on the average, equal to those of Pr−Pr. In Co_2Pr_5 (**2**), Co−Co interactions are located beyond any reasonable limits and do not participate in bonding schemes. Co−Pr and Pr−Pr −COHP curves show bonding

interactions at all energies; those of (**2**) exhibit a strong maximum of bonding interactions at the Fermi level, which is assumed to be an important hint at the higher thermodynamic stability of Co_2Pr_5 compared with Co_7Pr_{17}.

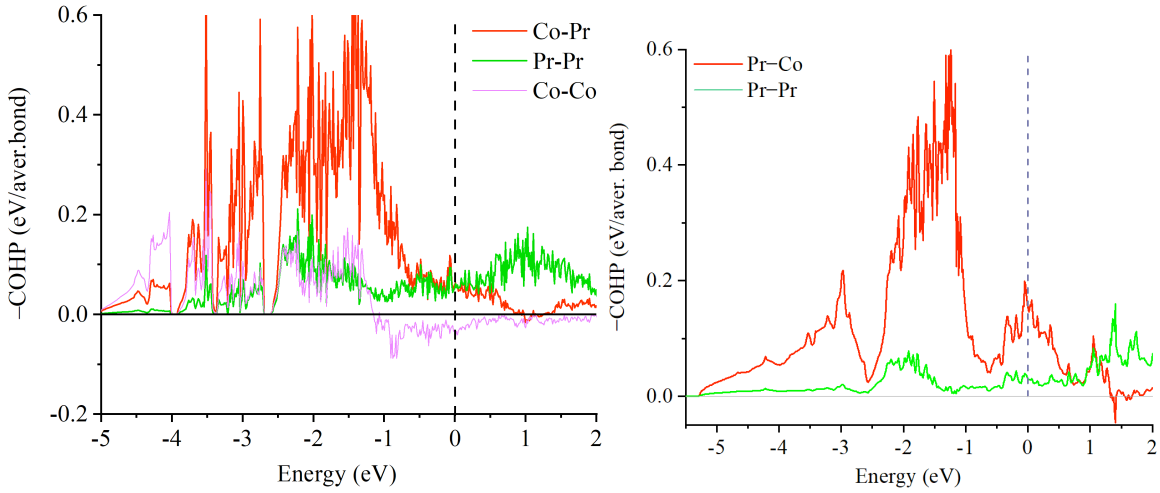

Figure 8. Average –COHP curves for interatomic interactions in the crystal structures of Co_7Pr_{17} (left) and Co_2Pr_5 (right).

Bonding analysis for the ternaries is based on $CoSn_3Pr$ (**11**) alone subject to heavy disorder in (**12**) that does not allow a precise examination of its electronic structure. Heteroatomic bonding dominates quantitatively also in $CoSn_3Pr$, though the main contributors are slightly redistributed. Co−Sn and Sn−Pr interactions provide 82.4% in the total bonding with very similar fractions, with little contribution from Co-Pr interactions (5.6%), although the individual –ICOHP is still 0.49 eV/bond, larger than for homoatomic Sn-Sn interactions (0.30 eV/bond). As their number per unit cell is much larger, the overall contribution of Sn-Sn bonding is 12.0 %. Co−Sn only interactions in the structure of $CoSn_3Pr$ (**11**) are limited to $\{CoSn_6\}$ trigonal prisms alone (as in Co_2Pr_5) and are represented by one bond length of 2.608 Å. This picture is a specific anti-type analogy to the Au-rich rare earth stannides $Au_7Sn_3R_3$,[64,65] where all T−Sn contacts are restricted to $\{SnT_6\}$ trigonal antiprisms. The corresponding −COHP plot shows that these interactions are significantly populated at lower energies but are rather nonbonding at the E_F,

while the addition of more electrons shifts them into strongly antibonding regions. Pr−Sn bonds in the structure of $CoSn_3Pr$ are present in two polyhedra, $\{PrSn_{12}\}$ icosahedra and the larger $\{PrSn_{12}\}Co_4$ units in a pretty narrow range from 3.27 to 3.40 Å. All these interactions are highly populated and strongly bonding at the Fermi level. Although the Co atoms in $\{PrSn_{12}\}Co_4$ may be considered as in the first coordination sphere of Pr (3.390 Å) but their smaller atomic size indicates weaker bonding. Co−Pr interactions are optimized well below the Fermi level and remain nonbonding uo to the Fermi level. Sn−Sn interatomic contacts are widely spread between 3.00 and 3.77 Å. Their interaction can be characterized as antibonding; however, strong maxima (antibonding minima) at E_F point to some electronic stabilization. Adding more electrons, e.g. replacing Pr in the 2*a* position with Sn, again pushes the interaction to a strongly antibonding regime. This is in line with the DOS curves and the conclusions from the $RuSn_3Eu$ work about strict *vec* requirements for the structure type. Na−Au−*E* (*E* = Ga, Ge, Sn) Bergman type approximants may serve as an additional example for the occupation of icosahedral centers based on the total *vec*. Strictly, within one Na−Au−Ga system, icosahedra in the Ga rich phases are always empty, while those in the Au rich part are occupied by extra Ga to compensate valence electron loss.[66,67]

The bonding picture in $Co_{2-x}Sn_7Pr_3$ (**12**) is qualitatively similar in many aspects: Co−Co and Pr−Pr interactions are practically absent and do not play any visible role in the bonding, Pr and Co are separated from each other as much as possible, Co is surrounded strictly by Sn atoms, although in the form of square pyramids. Thus, heteroatomic Co-Sn, Sn-Pr and Co−Pr with some contribution from homoatomic Sn−Sn bonding provide to total bonding. Due to significant positional disorder, an exact analysis of the interatomic contacts cannot be drawn.

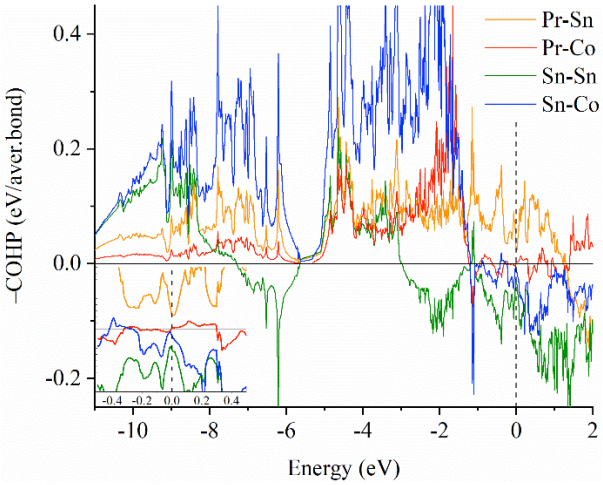

Figure 9. Average –COHP curves for interatomic interactions in the crystal structure of $CoSn_3Pr$.

Conclusions

With this study, we have added a new binary polar intermetallic, Co_7Pr_{17}, and two ternaries, $CoSn_3Pr_{1-x}$ (x = 0.04) and $Co_{2-x}Sn_7Pr_3$ (x = 0.78), to the Co-Sn-Pr system. Co_7Pr_{17} ($CoPr_{2.43}$) is either nonexistent in the sense that is thermodynamically unstable or it is obscured in the equilibrium phase diagram subject to its close neighbor, Co_2Pr_5 ($CoPr_{2.5}$). The structures of the four compounds were determined by single-crystal X-ray diffraction. {$CoPr_6$} trigonal-prismatic clusters are an important structural unit in the binaries, exclusively in Co_2Pr_5, complemented by additional Pr atoms to enhanced coordination numbers of 8 and 9, respectively. In the ternaries, Sn takes over the first coordination sphere of Co atoms; trigonal-prismatic {$CoSn_6$} clusters and {$Pr1Sn_{12}$} icosahedra, partially complemented by Co "ligands" are important structural features in $CoSn_3Pr_{1-x}$ (x = 0.04, $RuSn_3La$ type) as well as square pyramidal {$CoSn_5$} clusters and {$PrSn_{12}$} cuboctahedra are highlighting the crystal structure of $Co_{2-x}Sn_7Pr_3$ ($Ni_{2-x}Sn_{7-y}Ce_3$ type). The electronic structures are dominated by extensive heteroatomic Co-Pr interactions in the binaries (72.4 % and 89.7% contribution to the total bonding in Co_7Pr_{17} and Co_2Pr_5, respectively, with little homoatomic contributions, none for Co-Co in Co_2Pr_5. Introducing tin as a third component in the ternaries, heteroatomic Co–Sn (45.0%) and Sn–Pr (37.4%)

bonding interactions are dominant in $CoSn_3Pr$, with a small contribution from Co-Pr interactions, subject to the long distances between these atoms (3.390 Å). Homoatomic Sn-Sn interactions play a surprising role, 12.0%. The electronic structures very nicely mimic the atomic arrangements in the four compounds of this study.

Table 1. Crystallographic details and refinement parameters for Co_7Pr_{17}, Co_2Pr_5, $CoSn_3Pr_{1-x}$, $(Co_xSn_{1-x})_2$ Pr and $Co_{2-x}Sn_7Pr_3$.

Formula	Co_7Pr_{17}	Co_2Pr_5	$CoSn_3Pr_{0.96}$	$Co_{1.22}Sn_7Pr_3$
CCDC	1836697	1836695	1836694	1836696
Structure type	Own	C_2Mn_5	$Rh_4Sn_{13}Pr_3$	$Ni_{2-x}Sn_{7-y}Ce_3$
Form. wt., g/mol	2807.98	822.41	549.75	1325.28
Space group, *Z*	$P2_13$ (no. 198), 4	$C2/c$ (no. 15), 4	$Pm\bar{3}n$ (no. 223), 8	$Cmmm$ (65), 2
a, Å	13.4147(8)	16.5471(7)	9.587(3)	4.5043(4)
b, Å		6.5107(3)		27.227(2)
c, Å		7.1067(3)		4.5444(3)
β, º		96.230(3)		
V [Å^3]	2414.0(2)	761.11(7)	881.2(9)	557.32(8)
Temperature, K	293(2)	293(2)	293(2)	293(2)
Density (calculated), g/cm^3	7.726	7.149	8.288	7.897
Absorption coefficient, μ, mm^{-1}	38.172	35.345	30.612	29.911
F (000)	4768	1396	1867	1120
θ range for data collection, °	1.52 to 27.26	2.47 to 32.12	3.00 to 33.18	3.00 to 29.95
Index ranges	-17 < h < 17	-24 < h < 22	-7 < h < 13	-6 < h < 6
	-17 < k < 17	-9 < k < 9	-11 < k < 14	-38 < k < 38
	-17 < l < 17	-10 < l < 10	-14 < l < 14	-6 < l < 6
Intensity data collected	37916	6828	8089	3058
Number of independent reflections	1804 [R_{int} = 0.0979]	1278 [R_{int} = 0.0682]	330 [R_{int} = 0.0615]	515 [R_{int} = 0.0979]
Completeness, %	99.1	99.9	100	99.1
Flack parameter	0.00(1)	–	–	–
Data/ Restraints/ Parameters	1804/0/77	1278/0/33	330/0/14	515/0/32
Goodness-of-fit (F^2)	1.194	0.985	1.118	1.135
R_1, ωR_2 [$I_0>2\sigma$ (I)]	0.0444; 0.1346	0.0381; 0.0648	0.0199; 0.0408	0.0208; 0.0454
R_1, ωR_2 (all data)	0.0462; 0.1361	0.0591; 0.0697	0.0262; 0.0425	0.0226; 0.0461
Largest diff. peak and hole [e/Å^{-3}]	5.076 and –2.097	1.820 and –1.993	1.230 and –1.183	1.823 and –1.291

Table 2. Atomic positions and equivalent thermal parameters for Co_7Pr_{17} and Co_2Pr_5.

Atomic parameters					
Atom	Wyck.	*x*	*y*	*z*	U_{eq}
Co_7Pr_{17}					
Co1	12*b*	0.1887(3)	0.3598(3)	0.3610(3)	0.0098(8)
Co2	12*b*	0.0950(3)	0.5826(4)	0.1188(3)	0.0118(9)
Co3	4*a*	0.1384(3)	x	x	0.0102(14)
Pr1	12*b*	0.0109(2)	0.4928(2)	0.3168(2)	0.0247(5)
Pr2	12*b*	0.0133(2)	0.3092(2)	0.4933(2)	0.0245(5)
Pr3	12*b*	0.0661(2)	0.7441(2)	0.2552(2)	0.0260(6)
Pr4	12*b*	0.1512(2)	0.1527(2)	0.3471(2)	0.0293(6)
Pr5	12*b*	0.2576(2)	0.5630(2)	0.2600(2)	0.0244(5)
Pr6	4a	0.5561(2)	x	x	0.0297(9)
Pr7	4*a*	0.4019(2)	x	x	0.0308(9)
Co_2Pr_5					
Co	8*f*	0.11003(9)	0.2080(2)	0.5749(2)	0.0238(3)
Pr1	8*f*	0.21589(3)	0.06988(8)	0.31833(7)	0.0178(1)
Pr2	8*f*	0.40637(3)	0.11154(8)	0.08556(7)	0.0186(1)
Pr3	4*e*	0	0.0758(1)	¼	0.0171(2)

Table 3. Atomic positions and equivalent thermal parameters for $CoSn_3Pr_{1-x}$ and $Co_{2-x}Sn_7Pr_3$.

Atomic parameters						
Atom	Wyckoff	*x*	*y*	*z*	U_{eq}	*SOF*
$CoSn_3Pr_{1-x}$ (x = 0.044)						
Co	8*e*	¼	¼	¼	0.0073(2)	1
Sn	24*k*	0	0.15689(4)	0.30330(4)	0.0134(1)	1
Pr1	2*a*	0	0	0	0.0147(4)	0.825(5)
Pr2	6*c*	¼	0	½	0.0100(1)	1
$Co_{2-x}Sn_7Pr_3$ (x = 0.782)						
Co	4*i*	0	0.12779(6)	0	0.0113(5)	0.609(6)
Sn1	4*j*	0	0.09222(2)	½	0.0141(1)	1
Sn2	4*i*	0	0.40742(2)	0	0.0163(1)	1
Sn3	4*i*	0	0.2182(2)	0	0.0116(5)	0.79(2)
Sn4	4*i*	0	0.2061(5)	0	0.0116(5)	0.21(2)
Sn5	2*c*	½	0	½	0.0151(2)	1
Pr1	4*j*	0	0.31416(2)	½	0.0096(1)	1
Pr2	2*a*	0	0	0	0.0087(1)	1

Table 4. Bond length ranges and average −ICOHP values as well as total contributions to bonding interactions in Co_7Pr_{17}, Co_2Pr_5 and $CoSn_3Pr$.

Bond type	Length (Å)	Average length (Å)	−ICOHP (eV/bond)	no./cell	−ICOHP (eV/cell)	Contribution (%)
			Co_7Pr_{17}			
Co−Co	2.257−3.944	3.601	0.24	24	5.705	1.9
Co−Pr	2.811−3.689	3.039	0.83	256	212.5	72.4
Pr−Pr	3.340−3.763	3.548	0.22	340	75.39	25.7
			Co_2Pr_5			
Co−Pr	2.727−3.586	3.008	1.16	76	57.44	87.9
Pr−Pr	3.540−3.945	3.703	0.12	102	7.90	12.1
			$CoSn_3Pr$			
Co−Sn	2.608	2.608	1.97	48	94.56	45.0
Sn−Sn	3.008−3.772	3.431	0.30	84	25.14	12.0
Sn−Pr	3.274−3.400	3.351	0.82	96	78.72	37.4
Co–Pr	3.390	3.390	0.49	24	11.76	5.6

Associated content

Supporting Information

Structural data as CIF files.

Accession Codes CCDC 1836694−1836697 contain the supplementary crystallographic data for this paper. These data can be obtained free of charge via www.ccdc.cam.ac.uk/data_request/cif, or by emailing data_request@ccdc.cam.ac.uk, or by contacting The Cambridge Crystallographic Data Centre, 12 Union Road, Cambridge CB2 1EZ, UK; fax: +44 1223 336033.

Author Information

Corresponding Author

*E-mail for GHM: ghmeyer@iastate.edu

ORCID

Volodymyr Smetana: 0000-0003-0763-1457

Anja-Verena Mudring: 0000-0002-2800-1684

Gerd H. Meyer: 0000-0003-1000-9001

Notes

The authors declare no competing financial interest.

Acknowledgments

Initial research by T. B. was supported by direct funds from the University of Cologne, Cologne, Germany. More recent research was supported by the Office of the Basic Energy Sciences, Materials Sciences Division, U. S. Department of Energy (DOE), and the Department of Chemistry at Iowa State University (ISU). Ames Laboratory is operated for DOE by ISU under contract No. DE-AC02-07CH11358.

References

(1) Villars, P. (editor-in-chief), ASM Alloys Phase Diagram Center, Okamoto, H., Cenzual, K. (section editors), ASM International, Materials Park, Ohio, U.S.A., 2006-2015. http://www1.asminternational.org/AsmEnterprise/APD.

(2) Dasent, W. E. *J. Chem. Educ.* Non-existent compounds **1963**, *40*, 130.

(3) Dasent, W. E. *Nonexistent compounds: compounds of low stability*; Dekker, M., Ed.; Marcel Dekker Inc.: New York, 1965.

(4) Canepa, F.; Cirafici, S.; Fornasini, M. L.; Manfrinetti, P.; Merlo, F.; Palenzona, A.; Pani, M. *J. Alloys Compd.* Crystal structure of $R_3Co_8Sn_4$ compounds (R=Pr, Nd, Sm, Gd, Tb, Dy, Ho, Er, Tm, Yb, Lu, Y) **2000**, *297*, 109-113.

(5) He, W.; Zhang, J.; Yan, J.; Fu, Y.; Zeng, L. *J. Alloys Compd.* Crystal-structure and magnetic properties of the new ternary compound $Pr_{117}Co_{57}Sn_{112}$ **2010**, *491*, 49-52.

(6) Mudryk, Y.; Manfrinetti, P.; Smetana, V.; Liu, J.; Fornasini, M. L.; Provino, A.; Pecharsky, V. K.; Miller, G. J.; Gschneidner, K. A. *J. Alloys Compd.* Structural disorder and magnetism in rare-earth (*R*) $R_{117}Co_{54+x}Sn_{112\pm y}$ **2013**, *557*, 252-260.

(7) Skolozdra, R.; IV, Y.; OE, K.; Aksel'rud, L. *Dop. Akad. Nauk Ukrain RSR, Seriya B* Crystallographic structure of *R*Co1.33Sn4.33 (*R* = La, Ce, Pr, Nd, Sm, Gd, Tb). **1983**, *6*, 43-45.

(8) François, M.; Venturini, G.; Malaman, B.; Roques, B. *J. Less Common Met.* Nouveaux isotypes de $CeNiSi_2$ dans les systemes R-M-X (R ≡ La-Lu, M ≡ metaux des groupes 7 A 11 ET X ≡ Ge, Sn). I Compositions et parametres cristallins **1990**, *160*, 197-213.

(9) Pearson's Handbook, Crystallographic Data for Intermetallic Phases, Desk edition, P. Villars, ASM International, The Materials Information Society, Materials Park, OH, 1997.

(10) Skolozdra, R.; Gorelenko, Y. K.; YE, T.; Tkachuk, V. *Phys. Met. Metallogr.* Influence of components on magnetic and electrokinetic properties and composition of compounds $RMe_{1-x}Sn_{2-y}$ **1988**, *66*, 26-33.

(11) Meyer, G.; Dötsch, S.; Staffel, T. *J. Less Common Met.* The ammonium-bromide route to anhydrous rare earth bromides MBr_3 **1987**, *127*, 155-160.

(12) WinXPow. Stoe & Cie GmbH, Darmstadt, Germany. **2004**.

(13) *APEX3 and SAINT. Bruker AXS Inc., Madison, Wisconsin, USA.*

(14) Krause, L.; Herbst-Irmer, R.; Sheldrick, G. M.; Stalke, D. *J. Appl. Crystallogr.* Comparison of silver and molybdenum microfocus X-ray sources for single-crystal structure determination **2015**, *48*, 3-10.

(15) Sheldrick, G. *Acta Crystallogr. Sect. A* SHELXT - Integrated space-group and crystal-structure determination **2015**, *71*, 3-8.

(16) Sheldrick, G. *Acta Crystallogr. Sect. C: Struct. Chem.* Crystal structure refinement with SHELXL **2015**, *71*, 3-8.

(17) Tank, R.; Jepsen, O.; Burkhardt, A.; Andersen, O. K. *TB-LMTO-ASA Program, Max-Planck-Institut für Festkörperforschung, Stuttgart, Germany, 1994*

(18) Andersen, O. K.; Jepsen, O. *Phys. Rev. Lett.* Explicit, First-Principles Tight-Binding Theory **1984**, *53*, 2571-2574.

(19) Lambrecht, W. R. L.; Andersen, O. K. *Phys. Rev. B* Minimal basis sets in the linear muffin-tin orbital method: Application to the diamond-structure crystals C, Si, and Ge **1986**, *34*, 2439-2449.

(20) Dronskowski, R.; Bloechl, P. E. *J. Phys. Chem.* Crystal orbital Hamilton populations (COHP): energy-resolved visualization of chemical bonding in solids based on density-functional calculations **1993**, *97*, 8617-8624.

(21) Andriy, P.; Ingo, P.; Gerd, M. *Z. Anorg. Allg. Chem.* A Section Through the Compositional Triangle Pr-Co-I at 600 °C: Pr_7CoI_{12} and Pr_2Co_2I **2006**, *632*, 1969-1971.

(22) Meyer, G. Symbiosis of Intermetallic and Salt: Rare-Earth Metal Cluster Complexes with Endohedral Transition Metal Atoms. Handbook on the Physics and Chemistry of Rare Earths. Elsevier, 2014, vol. 45, chapter 264, p. 111-178.

(23) Llusar, R.; Corbett, J. D. *Inorg. Chem.* Reduced Praseodymium Cluster Bromides Stabilized by Transition Metals **1994**, *33*, 849-853.

(24) Warkentin, E.; Simon, A. *Rev. Chim. Miner.* Gd_3CCl_3, ein metallisches Gadoliniumcarbidhalogenid **1983**, *20*, 488-495.

(25) Fornasini, M. L.; Palenzona, A. *J. Less Common Met.* Crystal structure of the so-called $R.E._5Pd_2$ compounds **1974**, *38*, 77-82.

(26) Yurko, G. A.; Barton, J. W.; Parr, J. G. *Acta Crystallogr.* The crystal structure of Ti_2Ni **1959**, *12*, 909-911.

(27) Bell, T.; Rhodehouse, M.; Smetana, V.; Mudring, A.-V.; Meyer, G. *CGD* The Hidden Island of Rare Earth rich intermetallics: Finding Access to ”Unexisting Polymorphs” **2018**, *manuscript in preparation*.

(28) Bradley, A. J.; Gregory, C. H. *The London, Edinburgh, and Dublin Philosophical Magazine and Journal of Science* A comparison of the crystal structures of Cu_5Zn_8 and Cu_5Cd_8 **1931**, *12*, 143-162.

(29) Rhodehouse, M.; Bell, T.; Smetana, V.; Mudring, A.-V.; Meyer, G. *Inorg. Chem.* From the “non-existent” polar intermetallic Pt_3Pr_4 via $Pt_{2-x}Pr_3$ to some insight into Pt/Sn/Pr ternaries **2018**, *Submitted*.

(30) Le Roy, J.; Moreau, J.-M.; Paccard, D.; Parthe, E. *Acta Crystallogr. Sect. B: Struct. Sci.* R_3T_2 compounds (R = rare earth or Y; T = Rh, Pd, Pt) with the rhombohedral Er_3Ni_2 structure type **1977**, *33*, 2414-2417.

(31) Olcese, G. L. *J. Less Common Met.* Crystal structure and magnetic properties of some 7:3 binary phases between lanthanides and metals of the 8th group **1973**, *33*, 71-81.

(32) Moreau, J. M.; Parthé, E. *J. Less Common Met.* Ferromagnetic Gd_7Pd_3 and other rare-earth-palladium compounds with non-centrosymmetric Th_7Fe_3 structure **1973**, *32*, 91-96.

(33) Sologub, O.; Rogl, P.; Salamakha, L.; Bauer, E.; Hilscher, G.; Michor, H.; Giester, G. *J. Solid State Chem.* On phase equilibria and crystal structures in the systems Ce–Pd–B and Yb–Pd–B. Physical properties of R2Pd13.6B5 (R=Yb, Lu) **2010**, *183*, 1013-1037.

(34) Iandelli, A.; Palenzona, A. *J. Less Common Met.* The europium-palladium system **1974**, *38*, 1-7.

(35) Moreau, J.-M.; Paccard, D. *Acta Crystallogr. Sect. B: Struct. Sci.* The monoclinic crystal structure of R_5Co_2 (R = Pr, Nd, Sm) with the Mn_5C_2 structure type **1976**, *32*, 1654-1657.

(36) P. K. Doye, J.; J. Wales, D. *J. Chem. Soc., Faraday Trans.* Structural consequences of the range of the interatomic potential A menagerie of clusters **1997**, *93*, 4233-4243.

(37) Brandon, J. K.; Brizard, R. Y.; Chieh, P. C.; McMillan, R. K.; Pearson, W. B. *Acta Crystallogr. B* New refinements of the [gamma] brass type structures Cu_5Zn_8, Cu_5Cd_8 and Fe_3Zn_{10} **1974**, *30*, 1412-1417.

(38) Smetana, V.; Babizhetskyy, V.; Vajenine, G. V.; Hoch, C.; Simon, A. *Inorg. Chem.* Double-Icosahedral Li Clusters in a New Binary Compound $Ba_{19}Li_{44}$: A Reinvestigation of the Ba−Li Phase Diagram **2007**, *46*, 5425-5428.

(39) Smetana, V.; Babizhetskyy, V.; Hoch, C.; Simon, A. *J. Solid State Chem.* Icosahedral Li clusters in the structures of $Li_{33.3}Ba_{13.1}Ca_3$ and $Li_{18.9}Na_{8.3}Ba_{15.3}$ **2007**, *180*, 3302-3309.

(40) Smetana, V.; Kienle, L.; Duppel, V.; Simon, A. *Inorg. Chem.* Synthesis, Crystal Structure, and TEM Analysis of $Sr_{19}Li_{44}$ and Sr_3Li_2: A Reinvestigation of the Sr–Li Phase Diagram **2015**, *54*, 733-739.

(41) Smetana, V.; Babizhetskyy, V.; Vajenine, G. V.; Simon, A. *Angew. Chem. Int. Ed.* Li_{26} Clusters in the Compound $Li_{13}Na_{29}Ba_{19}$ **2006**, *45*, 6051-6053.

(42) Taylor, M. *Acta Crystallogr.* The crystal structure of Mn_3Al_{10} **1959**, *12*, 393-396.

(43) Solokha, P.; De Negri, S.; Pavlyuk, V.; Saccone, A. *Inorg. Chem.* Anti-Mackay Polyicosahedral Clusters in La−Ni−Mg Ternary Compounds: Synthesis and Crystal Structure of the $La_{43}Ni_{17}Mg_5$ New Intermetallic Phase **2009**, *48*, 11586-11593.

(44) Bergman, G.; Waugh, J. L. T.; Pauling, L. *Acta Crystallogr.* The crystal structure of the metallic phase $Mg_{32}(Al, Zn)_{49}$ **1957**, *10*, 254-259.

(45) Puselj, M.; Ban, Z. *Croat. Chem. Acta* The crystal structure of $TiCuHg_2$ **1969**, *41*, 79-83.

(46) Heusler, O. *Annalen der Physik* Kristallstruktur und Ferromagnetismus der Mangan-Aluminium-Kupferlegierungen **1934**, *411*, 155-201.

(47) Sprenger, H. *J. Less Common Met.* Die ternären systeme (Titan, Zirkonium, Hafnium)-kupfer-Silizium **1974**, *34*, 39-71.

(48) Eisenmann, B.; Schäfer, H. *J. Less Common Met.* Käfigstrukturen in intermetallischen Verbindungen: zur Kenntnis von $LaRuSn_3$, $CeRuSn_3$, $PrRuSn_3$ und $NdRuSn_3$ **1986**, *123*, 89-94.

(49) Harmening, T.; Hermes, W.; Eul, M.; Pöttgen, R. *Solid State Sci.* Mixed valent stannide $EuRuSn_3$ – Structure, magnetic properties, and Mössbauer spectroscopic investigation **2010**, *12*, 284-290.

(50) Zhuravleva, M. A.; Bilc, D.; Mahanti, S. D.; Kanatzidis, M. G. *Z. Anorg. Allg. Chem.* Single Crystal X-ray Structure Investigation and Electronic Structure Studies of La-Deficient Nickel Stannide $La_{4.87}Ni_{12}Sn_{24}$ Grown from Sn Flux **2003**, *629*, 327-334.

(51) Komarovskaya, L.; Skolozdra, R. *Dop. Akad. Nauk Ukrain RSR, Seriya A* The crystal structure of $Gd_3Ni_8Sn_{16}$ and RNi_3Sn_2 (R = rare-earth element) compounds **1985**, *47*, 81-83.

(52) Romaka, V. V.; Hlil, E. K.; Romaka, L.; Gignoux, D.; Fruchart, D.; Horyn, A.; Miraglia, S. *J. Alloys Compd.* Crystallographic, magnetic and electrical characteristics of some $R_{5-x}Ni_{12}Sn_{24+x}$ intermetallics **2010**, *493*, 35-40.

(53) Schreyer, M.; Fässler, T. F. *Solid State Sci.* $Ca_7Co_8Sn_{25}$–$Ca_3Co_4Sn_{13}$ revised **2006**, *8*, 793-797.

(54) Mudryk, Y.; Grytsiv, A.; Rogl, P.; Dusek, C.; Galatanu, A.; Idl, E.; Michor, H.; Bauer, E.; Godart, C.; Kaczorowski, D.et al. *J. Phys.-Condens. Matter* Physical properties and superconductivity of skutterudite-related $Yb_3Co_{4.3}Sn_{12.7}$ and $Yb_3Co_4Ge_{13}$ **2001**, *13*, 7391.

(55) Weitzer, F.; Hiebl, K.; Rogl, P. *J. Solid State Chem.* Crystal chemistry and magnetism of neodymium stannides including compounds of the structural series RE_nSn_{3n-2} **1992**, *98*, 291-300.

(56) Smetana, V.; Rhodehouse, M.; Meyer, G.; Mudring, A.-V. *Acc. Chem. Res.* Gold polar intermetallics: structural versatility through exclusive bonding motifs **2017**, *50*, 2633-2641.

(57) Karpov, A.; Nuss, J.; Wedig, U.; Jansen, M. *Angew. Chem. Int. Ed.* Cs2Pt: A Platinide(-II) Exhibiting Complete Charge Separation **2003**, *42*, 4818-4821.

(58) Smetana, V.; Mudring, A.-V. *Angew. Chem. Int. Ed.* Cesium platinide hydride $4Cs_2Pt{\cdot}CsH$: an intermetallic double salt featuring metal anions **2016**, *55*, 14838-14841.

(59) Samal, S. L.; Corbett, J. D. *Z. Anorg. Allg. Chem.* Synthesis, structure, and bonding analysis of the polar Intermetallic phase Ca_2Pt_2Cd **2012**, *638*, 1963-1969.

(60) Gulo, F.; Samal, S. L.; Corbett, J. D. *Inorg. Chem.* Substantial Cd–Cd bonding in Ca_6PtCd_{11}: a condensed intermetallic phase built of pentagonal Cd_7 and rectangular $Cd_{4/2}Pt$ Pyramids **2013**, *52*, 10112-10118.

(61) Samal, S. L.; Gulo, F.; Corbett, J. D. *Inorg. Chem.* Cluster chemistry in electron-poor Ae–Pt–Cd systems (Ae = Ca, Sr, Ba): $(Sr,Ba)Pt_2Cd_4$, $Ca_6Pt_8Cd_{16}$, and its known antitype $Er_6Pd_{16}Sb_8$ **2013**, *52*, 2697-2704.

(62) Smetana, V.; Steinberg, S.; Mudring, A.-V. *Cryst. Growth Des.* Layered Structures and Disordered Polyanionic Nets in the Cation-Poor Polar Intermetallics $CsAu_{1.4}Ga_{2.8}$ and $CsAu_2Ga_{2.6}$ **2017**, *17*, 693-700.

(63) Smetana, V.; Corbett, J. D.; Miller, G. J. *J. Solid State Chem.* $Na_8Au_{9.8(4)}Ga_{7.2}$ and $Na_{17}Au_{5.87(2)}Ga_{46.63}$: The diversity of pseudo 5-fold symmetries in the Na–Au–Ga system **2013**, *207*, 21-28.

(64) Provino, A.; Steinberg, S.; Smetana, V.; Kulkarni, R.; Dhar, S. K.; Manfrinetti, P.; Mudring, A.-V. *J. Mat. Chem. C* Gold-rich $R_3Au_7Sn_3$: establishing the interdependence between electronic features and physical properties **2015**, *3*, 8311-8321.

(65) Provino, A.; Steinberg, S.; Smetana, V.; Paramanik, U.; Manfrinetti, P.; Dhar, S. K.; Mudring, A.-V. *Cryst. Growth Des.* Gold in the layered structures of $R_3Au_7Sn_3$: from relativity to versatility **2016**, *16*, 5657-5668.

(66) Lin, Q.; Smetana, V.; Miller, G. J.; Corbett, J. D. *Inorg. Chem.* Conventional and Stuffed Bergman-Type Phases in the Na–Au–T (T = Ga, Ge, Sn) Systems: Syntheses, Structures, Coloring of Cluster Centers, and Fermi Sphere–Brillouin Zone Interactions **2012**, *51*, 8882-8889.

(67) Smetana, V.; Lin, Q.; Pratt Daniel, K.; Kreyssig, A.; Ramazanoglu, M.; Corbett John, D.; Goldman Alan, I.; Miller Gordon, J. *Angew. Chem. Int. Ed.* A Sodium-Containing Quasicrystal: Using Gold To Enhance Sodium's Covalency in Intermetallic Compounds **2012**, *51*, 12699-12702.

CHAPTER 6. CONCLUSIONS

Conclusion

In this work we have added three new binary compounds, Pt_3Pr_4, $Pt_{2-x}Pr_3$, and Co_7Pr_{17} in the R/Pr phase diagrams. These phases have been synthesized via high temperature using $PrCl_3$ or NaCl fluxes. Both Pt_3Pr_4 and Co_7Pr_{17} crystallize in new structure types: the first a monoclinic structure with six crystallographically independent Pt positions and the later a cubic structure containing Co atoms with coordination numbers of eight and nine. In the case of $Pt_{2-x}Pr_3$, calculations of total energy of the tetragonal Pt_2Pr_3 are higher than the previously reported rhombohedral Pt_2Pr_3 making the tetragonal phase thermodynamically unstable. Co_7Pr_{17} also exhibits thermodynamic instability as it is also not shown in the phase diagram. The reported Co_2Pr_5 is very close in composition (~6% increase in Pr), however crystallizes in a different structure.

With the introduction of a reactive tin flux the series $Pt_4Sn_6R_3$ was formed for R = La–Nd, along with $Pt_4Sn_6Pr_{2.91}$, $Pt_{12}Sn_{24}Pr_{4.84}$ and two ternaries, $CoSn_3Pr_{1-x}$ (x = 0.04) and $Co_{2-x}Sn_7Pr_3$ (x = 0.78), in the Co-Sn-Pr system. The Pt compounds crystallize in the $Pt_4Ge_6R_3$ (*R* = Pr–Dy) structure type with the Pr and Nd analogs also forming a high temperature modification, $Pt_4Sn_6R_{3-x}$. The modification crystallizes in same space group (Pnma) and cell volume but one elongated cell axis and reduced rare earth content, x = 0.09 for Pr and x = 0.11 for Nd. Additionally, disorder on Pr and Sn sites is observed. In both modifications 5 and 6 membered rings of Pt and Sn form nets along one plane. In an attempt to expand the $Pt_4Sn_6R_3$ family further $Pt_7Sn_9Sm_5$ was formed and characterized as the rare $Zr_5Pd_9P_7$ structure type.

In the ternaries, the first coordination sphere of Co atoms is Sn. Trigonal prisms of Sn surrounded Co, {$CoSn_6$}, and {$Pr1Sn_{12}$} icosahedra are observed in the $RuSn_3La$-type $CoSn_3Pr_{1-x}$ (x = 0.04,). Square pyramids, also of Sn surrounded Co, {$CoSn_5$}, and {$PrSn_{12}$} cuboctahedra define the crystal structure of $Co_{2-x}Sn_7Pr_3$ ($Ni_{2-x}Sn_{7-y}Ce_3$ type). Homoatomic bonding in these binaries contributes little to the total while Sn-Sn interactions contribute a surprising 12% in the ternary compounds. The dominant heteroatomic bonding interactions are Co–Sn (45.0%) and Sn–Pr (37.4%) in $CoSn_3Pr$.

Future work

During this work ternary compounds of non-targeted compositions were found. One example is that of $Co_3Pr_4Sn_5$ = $Pr(Co,Sn)_2$ (cP12, Pa, a = 6.678(3) Å, Z = 4). Initial findings show this compound to belong to the FeS_2 family: the first intermetallic representative. The structure can be described as octahedra of Sn and Co around the Pr atoms. Each of the octahedra share all vertices with neighboring polyhedra in a canted pattern. Unlike that seen in the other reported ternary Co/Pr/Sn phases, the structure of $Co_3Pr_4Sn_5$ contains a mixed position occupied by both Co and Sn. With only six ternaries reported there appears to be the possibility for further exploration of this system.

REFERENCES

(1) Meyer, G. Symbiosis of Intermetallic and Salt: Rare-Earth Metal Cluster Complexes with Endohedral Transition Metal Atoms, *Handbook on the Physics and Chemistry of Rare Earths*, Vol. 45, Chapter 264, Elsevier, 2014.

(2) Corbett, J.D. *J. Alloys and Comp.* Exploratory synthesis of reduced rare-earth-metal halides, chalcogenides, intermetallics: New compounds, structures, and properties. 2006, 418, 1-20.

(3) Lokken, D. A.; Corbett, J. D. *Inorg. Chem.* Rare earth metal-metal halide systems. XV. Crystal structure of gadolinium sesquichloride. Phase with unique metal chains **1973**, *12*, 556-559.

(4) Simon, A.; Holzer, N.; Mattausch, H. *Z. Anorg. Allg. Chem.* Metallreiche Verbindungen der Seltenen Erden Gd_2Cl_3, Gd_2Br_3 und Tb_2Cl_3 **1979**, *456*, 207-216.

(5) Meyer, G. *Z. Anorg. Allg. Chem.* Cluster Complexes as anti-Werner Complexes **2008**, *634*, 2729-2736.

(6) Meyer, G. In *The rare earth elements: fundamentals and applications*; Arwood, D. A., Ed.; John Wiley & Sons, Inc., 2012.

(7) Meyer, G. In *Handbook on the Physics and Chemistry of Rare Earths*; Bünzli, J.-C. G.;Pecharsky, V. K., Eds.; Elsevier, 2014.

(8) Payne, M. W.; Corbett, J. D. *Inorg. Chem.* Encapsulation of the platinum and neighboring metals within cluster iodides of rare-earth elements **1990**, *29*, 2246-2251.

(9) Dorhout, P. K.; Payne, M. W.; Corbett, J. D. *Inorg. Chem.* Condensed metal cluster iodides centered by noble metals. Six examples of cubic R_3I_3Z phases (R = La, Pr; Z = Os, Ir, Pt) **1991**, *30*, 4960-4962.

(10) Llusar, R.; Corbett, J. D. *Inorg. Chem.* Reduced Praseodymium Cluster Bromides Stabilized by Transition Metals **1994**, *33*, 849-853.

(11) Massalski, T.; Okamoto, H.; Subramanian, P.; Kacprzak, L. Binary Alloy Phase Diagrams, ASM International, Materials Park, OH, 1990.

(12) Kanatzidis, M.G.; Pottgen, R.; Jeitschko, W.; The metal flux: A preparative tool for the exploration of intermetallic compounds, *Angew. Chem. Int. Ed.*, **2005**, 44, 6996-7023.

(13) Rhodehouse, M. L.; Bell, T.; Smetana, V.; Mudring, A.-V.; Meyer, G. H. From the non-existent polar intermetallic Pt_3Pr_4 via $Pt_{2-x}Pr_3$ to novel Pt/Sn/Pr ternaries, *Inorg. Chem*. **2018**, revised.

(14) Dwight, A. E.; Harper, W. C.; Kimball, C. W. HoPtSn and other intermetallic compounds with the Fe_2P-type structure. *J. Less-Common Met.* **1973**, *30*, 1-8.

(15) Venturini, G.; Malaman, B. Crystal structure of $Y_3Pt_4Ge_6$: An intergrowth of $BaAl_4$ and $YIrGe_2$ slabs. *J. Less-Common Met.* **1990**, *167*, 45-52.

(16) Gribanov, A.; Rogl, P.; Grytsiv, A.; Seropegin, Y.; Giester, G. Novel intermetallic $Yb_{\sim 3}Pt_{\sim 4}Si_{6-x}$ (x = 0.3) – A disordered variant of the $Y_3Pt_4Ge_6$-type. *J. Alloys Compd.* **2013**, *571*, 93-97.

(17) Gribanov, A.V.; Sologub, O. L.; Salamakha, P. S.; Bodak, O. I.; Seropegin, Y. D.; Pecharsky, V. K. Crystal structure of the compound $Ce_3Pt_4Ge_6$. *J. Alloys Compd.* **1992**, *179*, L7–L11.

(18) Imre, A.; Hellmann, A.; Mewis, A. New Germanides with an Ordered Variant of the $Ce_3Pt_4Ge_6$ Type of Structure – The Compounds $Ln_3Pt_4Ge_6$ (Ln: Pr–Dy). *Z. Anorg. Allg. Chem.* **2006**, *632*, 1145–1149.

(19) Niepmann, D.; Pöttgen, R.; Künnen, B.; Kotzyba, G.; Mosel, B. D. The Stannides $La_3Pd_4Sn_6$, $Ce_3Pd_4Sn_6$, and $Pr_3Pd_4Sn_6$: A New Structure Type with a Complex Three-Dimensional $[Pd_4Sn_6]$ Polyanion. *Chem. Mater.* **2000**, *12*, 533–539.

(20) Tursina, A. I.; Gribanov, A.V.; Bukhan'ko, N.G.; Rogl, P.; Seropegin, Y.D. Crystal structure of the novel compound $Ce_3Pt_4Al_6$. *Chem Met. Alloys* **2008**, *1*, 62–66.

(21) Villars, P. (editor-in-chief), ASM Alloys Phase Diagram Center, Okamoto, H., Cenzual, K. (section editors), ASM International, Materials Park, Ohio, U.S.A., 2006-2015. http://www1.asminternational.org/AsmEnterprise/APD.

(22) Dasent, W. E. *J. Chem. Educ.* Non-existent compounds **1963**, *40*, 130.

(23) Dasent, W. E. *Nonexistent compounds: compounds of low stability*; Dekker, M., Ed.; Marcel Dekker Inc.: New York, 1965.

(24) Canepa, F.; Cirafici, S.; Fornasini, M. L.; Manfrinetti, P.; Merlo, F.; Palenzona, A.; Pani, M. *J. Alloys Compd.* Crystal structure of $R_3Co_8Sn_4$ compounds (R=Pr, Nd, Sm, Gd, Tb, Dy, Ho, Er, Tm, Yb, Lu, Y) **2000**, *297*, 109-113.

(25) He, W.; Zhang, J.; Yan, J.; Fu, Y.; Zeng, L. *J. Alloys Compd.* Crystal-structure and magnetic properties of the new ternary compound $Pr_{117}Co_{57}Sn_{112}$ **2010**, *491*, 49-52.

(26) Mudryk, Y.; Manfrinetti, P.; Smetana, V.; Liu, J.; Fornasini, M. L.; Provino, A.; Pecharsky, V. K.; Miller, G. J.; Gschneidner, K. A. *J. Alloys Compd.* Structural disorder and magnetism in rare-earth (*R*) $R_{117}Co_{54+x}Sn_{112\pm y}$ **2013**, *557*, 252-260.

(27) Skolozdra, R.; IV, Y.; OE, K.; Aksel'rud, L. *Dop. Akad. Nauk Ukrain RSR, Seriya B* Crystallographic structure of *R*Co1.33Sn4.33 (*R* = La, Ce, Pr, Nd, Sm, Gd, Tb). **1983**, *6*, 43-45.

(28) François, M.; Venturini, G.; Malaman, B.; Roques, B. *J. Less Common Met.* Nouveaux isotypes de $CeNiSi_2$ dans les systemes R-M-X (R ≡ La-Lu, M ≡ metaux des groupes 7 A 11 ET X ≡ Ge, Sn). I Compositions et parametres cristallins **1990**, *160*, 197-213.

(29) Pearson's Handbook, Crystallographic Data for Intermetallic Phases, Desk edition, P. Villars, ASM International, The Materials Information Society, Materials Park, OH, 1997.

(30) Skolozdra, R.; Gorelenko, Y. K.; YE, T.; Tkachuk, V. *Phys. Met. Metallogr.* Influence of components on magnetic and electrokinetic properties and composition of compounds $RMe_{1-x}Sn_{2-y}$ **1988**, *66*, 26-33.

(31) Meyer, G.; Dötsch, S.; Staffel, T. *J. Less Common Met.* The ammonium-bromide route to anhydrous rare earth bromides MBr_3 **1987**, *127*, 155-160.

(33) Stoe & Cie GmbH, Darmstadt, Germany, 2004.

(32) I. Bruker AXS, Madison, Wisconsin, 1996.

(34) R. Blessing, *Acta Crystallographica Section a*, 1995, **51**, 33-38.

(35) G. Sheldrick, *Acta Crystallographica Section a*, 2008, **64**, 112-122.

(36) Y. Mozharivskyj and H. Franzen, *Journal of Alloys and Compounds*, 2001, **327**, 78-81.

APPENDIX: SUPPLEMENTARY TABLES AND FIGURES

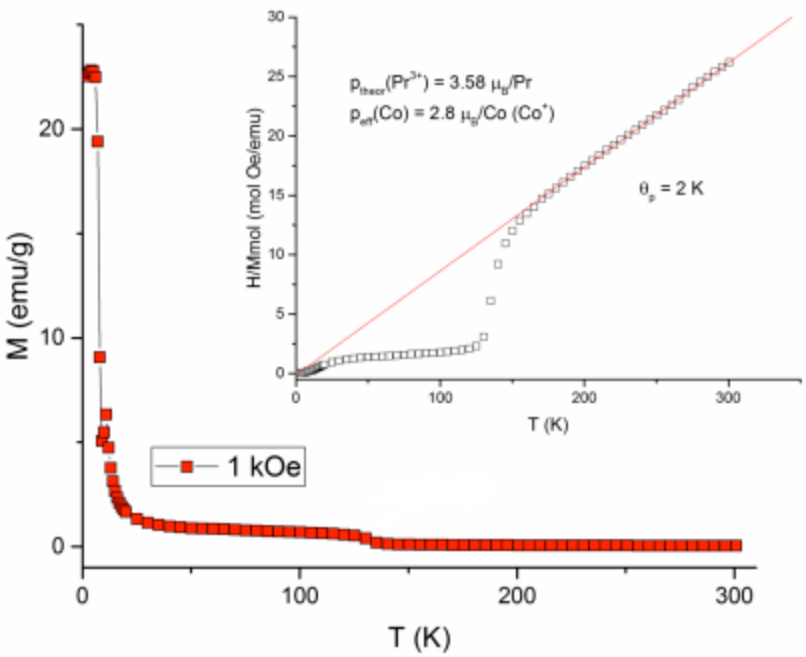

Figure 1. Magnetization *versus* temperature for Co_2Pr_5 measured in an applied magnetic field of 1 kOe between 2 and 250 K. Curie-Weiss fitting (top right inset) of magnetic field over magnetization curve *versus* 2-300 K temperature range.

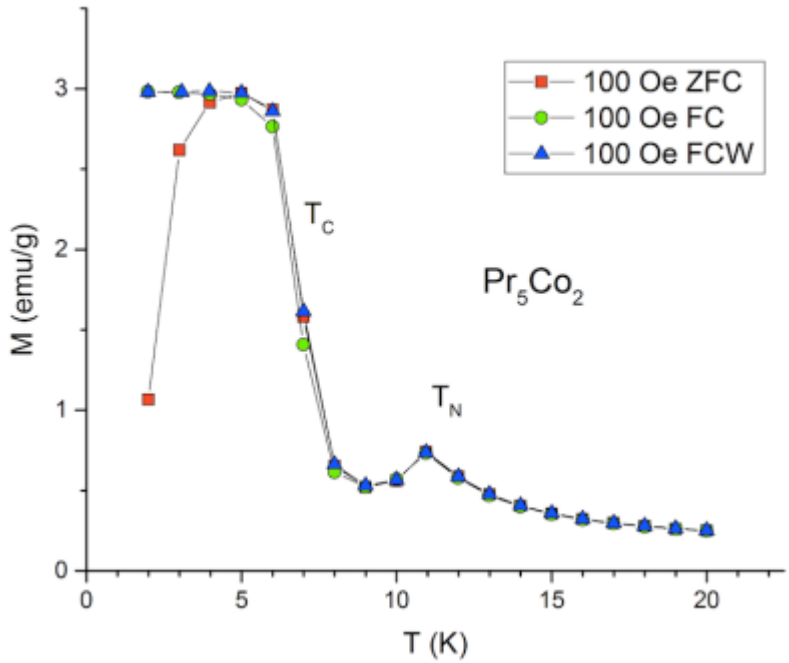

Figure 2. Magnetization *versus* temperature for Co_2Pr_5 measured in an applied magnetic field of 1 kOe between 2 and 20 K.